Physics – Uspekhi **39** (3) 231 – 260 (1996)

REVIEWS OF TOPICAL PROBLEMS PACS number: 42.25.Gy, 42.25.Fx, **42.30.–d**, 71.55.Jv

Coherent phenomena in light scattering from disordered systems

V L Kuz'min, V P Romanov

Contents

Abstract. The current status of research on coherent phenomena in multiple light scattering from disordered systems is reviewed. The coherent light backscattering, temporal and spatial correlations of intensity of light propagating through a randomly inhomogeneous medium, and coherent effects due to the multiple scattering from very rough surfaces are considered. The present-day theories as well as methods and results of experimental studies are outlined. Almost all theoretical predictions are found to be illustrated well by respective experimental data.

1. Introduction

Recently the propagation and scattering of light in highly turbid media have raised considerable interest. On passing through a highly heterogeneous medium, coherent light is generally to become incoherent due to multiple scattering. However despite the multiple scattering which randomises the wave phase distribution, a whole series of phenomena appears to exist wherein the coherence and interference properties of radiation manifest themselves strongly. Most remarkable among these are the coherent backscattering, spatial and temporal correlations of light intensity, and enhancement of backscattering from rough surfaces. The search [1, 2] for these effects has been significantly facilitated since they turned to be classical analogues of respective quantum phenomena discovered previously in the physics of disordered metals (see Refs [3 – 6]).

V L Kuz'min Department of Higher Mathematics, Institute of Trade and Economics, 194018 St. Petersburg, Russia
Fax (7-812) 247-43 42
V P Romanov Faculty of Physics, St. Petersburg State University 198904 Petrodvorets, St. Petersburg, Russia
Fax (7-812) 427-72 40
E-mail: apver@onti.niif.spb.su

Received 20 January 1995, revised 26 October 1995
Uspekhi Fizicheskikh Nauk **166** (3) 247–278 (1996)
Translated by authors, edited by S D Danilov

The coherent backscattering phenomenon manifests itself as a sharp enhancement of light intensity scattered within a narrow angular range around the direction opposite to direction of incidence. The physical picture of coherent backscattering is quite simple. Let a coherent plane wave fall upon a system. The direction and phase of the wave change during the elastic scattering events. The light beam scattered from random inhomogeneities becomes totally incoherent. However, for every sequence of scattering events there are two waves which can be coherent passing the scatterers in opposite directions. Even for such a pair of waves the effect of interference disappears due to the randomised distribution of scatterers except for scattering backward when the paths and phase-shifts for both waves are exactly the same. Such an effect has a general wave nature and occurs in any wave process. It was first studied in detail in disordered metals and is known as electron weak localisation, which is caused by the quantum interference of conduction electrons during the multiple scattering from impurities at low temperature, when the mean elastic scattering free path is essentially less than the inelastic one. The theoretically anticipated effect of weak localisation was discovered at the beginning of the Eighties in numerous experiments on measuring electroconductivity and magnetoresistance of restricted size metallic patterns which can be considered as 1D-, 2D- or 3D- systems [3 – 6].

The coherent light backscattering was observed for the first time as an analogue of the electron weak localisation simultaneously by van Albada and Lagendijk [1] and Wolf and Maret [2] in concentrated latex mixtures, and later on by Etemad et al. [7], and Kaveh et al. [8]. The main peculiarities of the coherent backscattering have been detected [1, 2]: the nearly two-fold increase of scattering intensity in the backward direction, the triangle form of angular scattering indicatrix, and significant dependence on the light polarisation and scatterer size. A moderate backscattering enhancement of the order of 15% had been reported earlier by Kuga and Ishimaru [9, 10] who interpreted it as a result of interference within the framework of

the double-scattering [11] and multiple scattering [12] approaches.

The theory of coherent backscattering in a medium occupying half-space, was developed by Golubentsev [13] and Akkermans et al. [14] for a scalar field. The triangular form of backscattering peak was explained [14] in the framework of the diffusion approximation. Stephen and Cwilich [15] took into account rigorously the light polarisation for point-like scatterers. Akkermans et al. [16] and Barabanenkov and Ozrin [17] have shown within the diffusion approximation for the radiation transfer equation that with account for finite size of scatterers the extinction length should be replaced by a transport length.

The temporal auto-correlation function in coherent backscattering was first measured by Maret and Wolf [18], and Pine et al. [19] and calculated theoretically by Stephen [20].

When studying the multiple light scattering large correlated fluctuations of the scattered light intensity are observed. Works on the conductance fluctuations in disordered metals appeared to be theoretical as well as experimental impulses for discovery of light intensity correlations. The correlation properties of intensity fluctuations turn out to be similar to the universal conductance fluctuations found previously [21 – 25]. Namely, the value of mean square deviation of the conductance for a cube pattern in $e^2/\hbar$ units was found to be of unity order and universally independent of cube size due to fluctuations of different modes being correlated. The similar correlations were recently found and intensively investigated in optics of highly heterogeneous systems.

The theory of intensity fluctuations was developed by Shapiro [26] who described the short-range correlations of dispersed intensities. Stephen and Cwilich [27] and Feng et al. [28] found the long-range asymptotics of the spatial, frequency, and angular correlation functions of scattered light using the Hikami diagram method [29]. The intensity correlation function of light transmitted through a finite thickness slab was presented in Ref. [28] as sum of three terms of different order. The first, short-range term corresponds to Shapiro's factorisation approximation [26], the weaker second one exhibits a long-range behaviour, and the third term does not depend on the mutual remoteness of modes and corresponds to the universal conductance fluctuations of the disordered metal electron conductivity theory. A novel effect, labelled as the memory effect, was shown to exist [28]. In short, the effect may be described as follows: two outgoing beams, transmitted through a thick turbid slab, appear to be strongly correlated despite the multiple scattering if their wave vector difference is equal to that of incident beams.

The intensity correlation functions have been studied in detail experimentally. The temporal correlation functions have been measured by Pine et al. [19] and Rimberg and Westervelt [30]. Freund et al. [31] have studied the angular correlation functions and, in particular, the memory effect. Genack and Drake [32] have investigated the frequency correlation function. The main short-range part of correlation function is investigated in these works. Garcia and Genack [33] and van Albada et al. [34] have measured the long-range part of correlation function, while Van Albada et al. [35] have studied the velocity of the radiation energy transfer in a highly heterogeneous medium. They found that a parameter with dimension of velocity which enters the classical definition of the light diffusion coefficient, can be one order of magnitude less than the light velocity.

Along with studies on coherent effects in multiple scattering from the bulk systems, in recent years an enhancement of backscattering from very rough surfaces caused by the similar mechanism has been discovered and studied intensively. This effect was first measured by Mendez and O'Donnell [36, 37]. Practically all measurements were performed using metallic surfaces to exclude the bulk scattering. The coherence effect manifests itself as a distinctive peak in the backward direction in the angular distribution of reflected light.

Describing this effect Ishimaru and Chen [38, 39] used the modified Kirchhoff approximation. Separating the single- and double- scattering contributions they showed that the cyclic diagram of double-scattering is responsible for the enhancement of backscattering from a rough surface. Maradudin et al. [40] developed the successive theory of multiple scattering from surface fluctuations.

As in the case of bulk scattering, besides backscattering enhancement, intensity correlations are also observed. The angular correlation functions of light scattered from rough surfaces were measured for the first time by Knotts et al. [41] and Nieto-Vesperinas and Sanchez-Gil [42].

The problems of propagation and scattering of light in highly inhomogeneous media in the multiple scattering regime, coherent backscattering included, were studied theoretically for many years by Barabanenkov, Kravtsov et al. In particular, describing the effects of coherence, they used diffusion approximation for the first time. Their results are outlined systematically in Ref. [43].

The contents of the present review is as follows. Coherent backscattering is considered in Section 2. Fundamentals of the multiple scattering theory are presented and the physical mechanism of the phenomenon is discussed. The theory of the effect is outlined in detail within the point-like scatterer approximation. Numerous experimental results are presented. We set forth the results obtained within the framework of the diffusion approximation for the radiation transfer equation permitting one to describe the effect in the case of finite size scatterers. The findings of investigation of the temporal correlation function are also discussed in detail.

In Section 3 the general approach is expounded for calculation of the intensity correlation functions. The derivation of the angular as well as frequency correlation functions is given for the light transmitted through a finite thickness slab. The experimental results on the correlation function measurements are discussed. The problem of determining the radiation energy transfer velocity in highly inhomogeneous medium is considered.

Section 4 is devoted to the theoretical and experimental studies of the multiple light scattering from very rough surfaces.

2. Coherent light backscattering

2.1 Multiple light scattering

Light is scattered propagating through a medium with strongly developed inhomogeneities of permittivity. If the photon free path, or extinction length, is significantly less than a linear size of the system the light propagation occurs in the multiple scattering regime. Developing the theory of multiple scattering, one starts from the wave equation for the electromagnetic field in a random medium. To avoid cumbersome description one uses as a rule the Helmholtz

wave equation for a scalar field. Being immediately appropriate for acoustic problems the Helmholtz equation applies also to optical problems since it allows one to treat the main effects due to the multiple character of scattering.

We restrict ourselves to a static case when one can neglect displacements of particles during the wave propagation. We present the wave equation describing the monochromatic electromagnetic wave in a nonmagnetic dielectric with the random permittivity $\epsilon(\mathbf{r})$ in the form

$$(\mathrm{rot}\,\mathrm{rot} - k^2)\,\mathbf{E}_{\mathrm{fl}}(\mathbf{r}) = k^2 \Delta\epsilon(\mathbf{r})\,\mathbf{E}_{\mathrm{fl}}(\mathbf{r})\,, \tag{2.1}$$

where $\mathbf{E}_{\mathrm{fl}}(\mathbf{r})$ is the electric field in the fluctuating random medium, $k = \omega n/c$ is the wavenumber, ω is the circular frequency, n is the average refractive index, and c is the light velocity in vacuum. We omit factor $\exp(\mathrm{i}\omega t)$ describing the temporal dependence of the field due to the static character of the $\epsilon(\mathbf{r})$. The difference $\Delta\epsilon(\mathbf{r}) = \epsilon(\mathbf{r}) - \epsilon$ describes the permittivity fluctuations with respect to the mean value $\epsilon = \langle\epsilon(\mathbf{r})\rangle$.

The wave equation (2.1) can be presented in the integral form

$$\mathbf{E}_{\mathrm{fl}}(\mathbf{r}) = \mathbf{E}(\mathbf{r}) + \int \mathrm{d}\mathbf{r}_1\,\hat{\mathbf{T}}(\mathbf{r} - \mathbf{r}_1)\,\frac{\Delta\epsilon(\mathbf{r}_1)}{4\pi}\,\mathbf{E}_{\mathrm{fl}}(\mathbf{r}_1)\,, \tag{2.2}$$

where $\mathbf{E}(\mathbf{r})$ is the mean field in a homogeneous medium with permittivity ϵ, $\hat{\mathbf{T}}(\mathbf{r})$ is the electromagnetic field propagator,

$$\hat{\mathbf{T}}(\mathbf{r}) = (\hat{\mathbf{I}}\,k^2 + \nabla\nabla)\,\frac{\exp(\mathrm{i}kr)}{\epsilon r}\,, \tag{2.3}$$

coinciding up to the factor 4π with Green's function of Eqn (2.1), and $\hat{\mathbf{I}}$ is the unit tensor.

For the problems of electromagnetic radiation transfer considered in the present review one can use the far zone approximation which is valid for spatial scales far exceeding the light wavelength λ. In this approximation

$$\hat{\mathbf{T}}(\mathbf{r}) = \frac{k^2}{\epsilon r}\left(\hat{\mathbf{I}} - \frac{\mathbf{r}\cdot\mathbf{r}}{r^2}\right)\exp(\mathrm{i}kr)\,. \tag{2.4}$$

The integral light scattering intensity is defined as the quadratic form of the electric field

$$I = \langle\mathbf{E}_{\mathrm{fl}}\cdot\mathbf{E}_{\mathrm{fl}}^*\rangle - \mathbf{E}\cdot\mathbf{E}^*\,. \tag{2.5}$$

The subtracted term in Eqn (2.5) removes from the scattering intensity the contribution of the mean field. Definition (2.5) differs from the physical definition of intensity as a specific energy flow by a constant factor.

Eqn (2.2) is solved by iterations. Substituting the iterative series into Eqn (2.5) one finds the expansion in orders of $\Delta\epsilon$ fluctuations. The resultant series describes the multiple scattering. In particular, one presents the single-scattering intensity as

$$I_1 = (4\pi)^{-2}\int \mathrm{d}\mathbf{r}_1\,\mathrm{d}\mathbf{r}_1'\,T_{\alpha(0)\beta}(\mathbf{r}_0 - \mathbf{r}_1)\,T^*_{\alpha(0)\gamma}(\mathbf{r}_0 - \mathbf{r}_1') \times \langle\Delta\epsilon\,(\mathbf{r}_1)\,\Delta\epsilon\,(\mathbf{r}_1')\rangle E_\beta(\mathbf{r}_1)\,E^*_\gamma(\mathbf{r}_1')\,, \tag{2.6}$$

the double-scattering as

$$I_2 = (4\pi)^{-4}\int \mathrm{d}\mathbf{r}_1\,\mathrm{d}\mathbf{r}_2\,\mathrm{d}\mathbf{r}_1'\,\mathrm{d}\mathbf{r}_2'\,T_{\alpha(0)\beta}(\mathbf{r}_0 - \mathbf{r}_1) \times T_{\beta\gamma}(\mathbf{r}_1 - \mathbf{r}_2)\,T^*_{\alpha(0)\delta}(\mathbf{r}_0 - \mathbf{r}_1')\,T^*_{\delta\mu}(\mathbf{r}_1' - \mathbf{r}_2') \times \big[\langle\Delta\epsilon(\mathbf{r}_1)\,\Delta\epsilon(\mathbf{r}_2)\,\Delta\epsilon(\mathbf{r}_1')\,\Delta\epsilon(\mathbf{r}_2')\rangle - \langle\Delta\epsilon(\mathbf{r}_1)\,\Delta\epsilon(\mathbf{r}_2)\rangle\,\langle\Delta\epsilon(\mathbf{r}_1')\,\Delta\epsilon(\mathbf{r}_2')\rangle\big]\,E_\gamma(\mathbf{r}_2)\,E^*_\mu(\mathbf{r}_2') \tag{2.7}$$

and so on, where $\mathbf{r}_0$ is the observation point. One assumes the summation to be done over the repeating indices except for index α_0, which determines the polarisation of the scattered light. Since, as usual, the distance from the system to the observation point exceeds significantly the linear size of the illuminated volume, one extracts the factor describing the plane wave vector $\mathbf{k}_s = (\mathbf{r}_0/r_0)\,k$ directed to the observation point

$$T_{\alpha(0)\beta}(\mathbf{r}_0 - \mathbf{r}) = \frac{k^2}{\epsilon r_0}\left(\delta_{\alpha(0)\beta} - \frac{k_{s\alpha(0)}k_{s\beta}}{k^2}\right)\exp(\mathrm{i}kr_0 - \mathrm{i}\mathbf{k}_s\cdot\mathbf{r}) \equiv T_{\alpha(0)\beta}\exp(\mathrm{i}kr_0 - \mathrm{i}\mathbf{k}_s\cdot\mathbf{r})\,. \tag{2.8}$$

In the general case the $2n$-point average $\langle\Delta\epsilon(\mathbf{r}_1)\ldots\Delta\epsilon(\mathbf{r}_{2n})\rangle$ determines the n-fold scattering. This average can be presented within the Gaussian approximation as all possible combinations of pair correlators

$$G\,(\mathbf{r}_1 - \mathbf{r}_2) = \langle\Delta\epsilon(\mathbf{r}_1)\,\Delta\epsilon(\mathbf{r}_2)\rangle\,. \tag{2.9}$$

The separate terms of iterative series for intensity are illustrated by diagrams. The diagrams describing single-, double-, and triple-scattering are shown in Fig. 1. The expression corresponding to each diagram turns out to be the fourth rank tensor. To obtain the scattering intensity one has to contract this tensor with the product of amplitudes of incident field in the right side and with the complex-conjugated pair of propagators (2.8) in the left side.

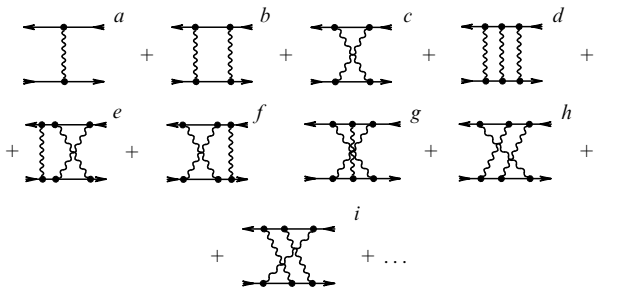

Figure 1. Diagrams, representing the single-scattering (*a*), double-scattering (*b*) and (*c*), and triple-scattering (*d*)–(*i*); (*a*), (*b*) and (*d*) are the ladder diagrams and (*c*), (*g*) are the cyclic ones. The arrows presents either the incident plane wave $\exp(\mathrm{i}\mathbf{k}_i\cdot\mathbf{r})$ with the wave vector $\mathbf{k}_i$ or the scattering, outgoing wave $\exp(-\mathrm{i}\mathbf{k}_s\cdot\mathbf{r})$ with the wave vector $\mathbf{k}_s$. The straight line segments presents propagator $\hat{\mathbf{T}}(\mathbf{r}_i - \mathbf{r}_j)$. The quantities presented in the lower lines are assumed to be complex conjugated implying that the direction of arrows is changed to opposite and propagator $\hat{\mathbf{T}}$ to $\hat{\mathbf{T}}^*$. The correlation function $(4\pi)^{-2}\langle\Delta\epsilon(\mathbf{r}_i)\,\Delta\epsilon(\mathbf{r}_j')\rangle$ is presented by the wavy line connecting vertexes $\mathbf{r}_i$ and $\mathbf{r}_j'$. The integration over the illuminated volume and summation over polarisations are assumed to be done in every vertex. The subtraction in Eqn (2.5) guarantees that the intensity series does not contain unconnected diagrams wherein wavy lines connect either upper vertexes or lower ones only.

2.2 Ladder and cyclic diagrams

The range of convergence of spatial integrals in diagrams is determined generally by the wavelength. However for the so-called ladder diagrams (diagrams *b* and *d* in Fig. 1) the oscillating factors in the complex-conjugated pairs $\hat{\mathbf{T}}(\mathbf{r}_i - \mathbf{r}_j)\,\hat{\mathbf{T}}^*(\mathbf{r}_i' - \mathbf{r}_j')$ cancel each other out, and the conver-

gence is determined by the extinction length

$$\exp\bigl(\mathrm{i}k|\mathbf{r}_i-\mathbf{r}_j|-\mathrm{i}k^*|\mathbf{r}'_i-\mathbf{r}'_j|\bigr)=\exp\bigl(-\sigma|\mathbf{r}_i-\mathbf{r}_j|\bigr) \qquad (2.10)$$

for $|\mathbf{r}_i-\mathbf{r}_j|\gg|\mathbf{r}_i-\mathbf{r}'_i|$, $|\mathbf{r}_j-\mathbf{r}'_j|$, where $\sigma=2n_2k_0$ is the extinction coefficient, $\sigma=l_{\mathrm{ext}}^{-1}$, $k_0=2\pi/\lambda$, and n_2 is the imaginary part of the refractive index. That is why the sum of the ladder diagrams determines as a rule the multiple scattering series.

However, as is seen from Fig. 1, diagrams *c* and *g* coincide exactly with ladder diagrams *b* and *d*, respectively, for $\mathbf{k}_s=-\mathbf{k}_i$ i.e. for scattering strictly backward. The same is true for all such diagrams known as the cyclic ones. Graphically the cyclic diagrams are the maximally crossed ones. One illustrates schematically the identity of the ladder and cyclic diagrams by means of following graphic rearrangements [16]. Rotating the lower lines to 180° and changing additionally the direction of the wave vectors of the lower lines to opposite direction one transforms cyclic diagrams *c* and *g* to the ladder ones. The arising diagrams coincide with the respective ladder diagrams at $\mathbf{k}_s=-\mathbf{k}_i$.

The equality of ladder and cyclic diagrams at $\mathbf{k}_s=-\mathbf{k}_i$ was first found in 1966 [44]. Namely this equality underlies the effect of the coherent backscattering.

To clarify it we consider physical scattering processes corresponding to the respective diagrams [45] (Fig. 2). As is seen the ladder diagrams describe the scattering processes wherein two waves propagating parallel one to another remain coherent passing the same paths. The cyclic diagrams describe the same processes in which the second wave passes the same inhomogeneities in reverse order. Being averaged over the scatterer positions these two beams become incoherent except for the case of backward scattering. Another example is the triple-scattering diagram with intermediate number of intersections of the wavy lines. As seen from the physical scheme, the process corresponding to this diagram can never be coherent since the paths of two waves are always different.

The physical picture of coherent backscattering is easily described in terms of wave vectors [2, 4]. We consider the plane wave with the wave vector $\mathbf{k}_i$, experiencing some sequence of elastic scattering events. These scatterings are determined by the wave vectors $\mathbf{k}_i$, $\mathbf{k}_1$, $\mathbf{k}_2$, ..., $\mathbf{k}_n$ where $\mathbf{k}_j$ is the wave vector emerging after the *j*-th scattering event and $\mathbf{k}_n=\mathbf{k}_s$. For the every such scattering sequence there is the inverse one determined by the set of wave vectors $\mathbf{k}_i$, $-\mathbf{k}_{n-1}$, $-\mathbf{k}_{n-2}$, ..., $-\mathbf{k}_1$, $\mathbf{k}_s$. In case of the backward scattering, ($\mathbf{k}_s=-\mathbf{k}_i$), two waves arising from these two scattering sequences appear to be in phase leaving the system and enhance one another by interference. For scattering angle not equal strictly to 180°, the phase difference of these two waves is of the order of $(\mathbf{k}_i+\mathbf{k}_s)\cdot(\mathbf{r}_1-\mathbf{r}_n)$ where $\mathbf{r}_1$ and $\mathbf{r}_n$ are the coordinates of the first and the last scattering events. Thus, the width θ of the interference maximum can be evaluated from the relationship

$$|\,\mathbf{k}_s+\mathbf{k}_i\,|\langle|\,\mathbf{r}_1-\mathbf{r}_2\,|\rangle\sim|\,\mathbf{k}_s+\mathbf{k}_i\,|\,l_{\mathrm{ext}}<1\,. \qquad (2.11)$$

Since for small scattering angle one has $|\,\mathbf{k}_s+\mathbf{k}_i\,|\approx k\theta$, the coherent backscattering peak is to be a cone with the axis directed backward and the angular width of order of λ/l_{ext}.

Thus neglecting the single-scattering the cyclic diagram contribution doubles the scattering intensity in the backward direction. Previously the effect of the same physical nature was discovered in disordered metals and became known as the electron weak localisation [3 – 6]. It is caused by the quantum interference of the conduction electrons which appears as a result of multiple scattering from defects in metals. This interference occurs at sufficiently low temperature, when the inelastic lifetime τ_i is several orders greater than the elastic lifetime τ_0. As a result, electron experiences multiple scattering from defects without loss of energy.

An electron in an initial eigenstate of wave vector $\mathbf{k}_i$ transits to a final state of wave vector $\mathbf{k}_s=-\mathbf{k}_i$ experiencing the multiple scattering through two sequences of states determined either by the wave vector transfers $\Delta\mathbf{k}_1$, $\Delta\mathbf{k}_2$, ..., $\Delta\mathbf{k}_n$, or by the same wave vector transfers $\Delta\mathbf{k}_n$, $\Delta\mathbf{k}_{n-1}$, ..., $\Delta\mathbf{k}_1$ in reverse order. Since the absolute value of the wave vector is preserved during elastic scattering both waves amplify one another by interference. They are assumed to be coherent during the time not exceeding the inelastic lifetime τ_i. Physically this effect is observed as an anomalous conductance dependence on temperature in the low temperature region [46, 47].

A short electric field pulse generates a short current pulse, decaying exponentially with the characteristic time τ_0 due to the elastic scatterings. The interference effect manifests itself as the current pulse in opposite direction decaying with time *t* powerlike, in particular as $1/t$ in two-dimensional case for a film. Integrating the mean pulse over time one obtains the DC conductance L_{c}. The normal contribution is proportional to τ_0, and the counter-current, known as the electron echo, gives rise to the logarithmic term of the form $\ln(\tau_i/\tau_0)$. As a result the conductance L_{c} was obtained in the form [46, 47]

$$L_{\mathrm{c}}=\frac{n^2e^2\tau_0}{m}-\frac{e^2}{2\pi^2\hbar}\ln\left(\frac{\tau_i}{\tau_0}\right). \qquad (2.12)$$

Another remarkable peculiarity is that the conductance depends anomalously strongly on the magnetic field [48]. Such dependence appears because the magnetic field acts differently on electrons moving in opposite directions. It leads to the phase shift of two interfering waves, i.e. to the loss of coherence. As a result electric resistance decreases in the magnetic field. Thus, abnormal electric conductance and coherent backscattering arise due to the interference of

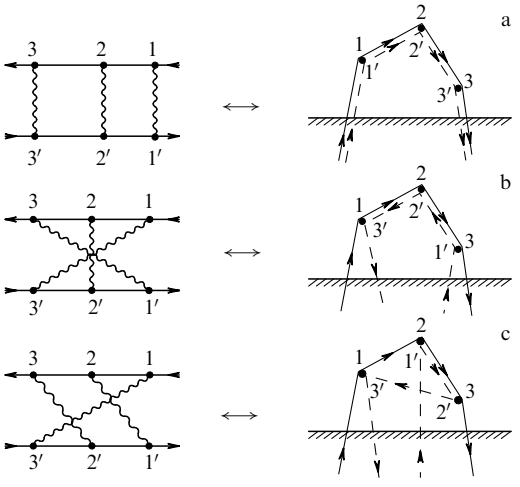

Figure 2. Triple-scattering diagrams and corresponding schemes of physical scattering processes.

waves described either by the Schrödinger equation, or by the Maxwell equation. In both cases this interference effect is caused by the contribution of cyclic diagrams.

2.3 The point-like scatterer model

The model of medium with point-like scatterers permits one to solve analytically the problem of coherent backscattering, including polarisation effects [15].

The point-like scatterer approximation means $r_c \gg \lambda$, where r_c is the correlation length. It can be presented in the form [15]

$$\langle \Delta\epsilon(\mathbf{r}_i)\, \Delta\epsilon(\mathbf{r}_j)\rangle = (4\pi)^2 g_0 \delta(\mathbf{r}_i - \mathbf{r}_j), \tag{2.13}$$

where

$$g_0 = (4\pi)^{-2} \int \mathrm{d}\mathbf{r}\, \langle \Delta\epsilon(0)\, \Delta\epsilon(\mathbf{r})\rangle. \tag{2.14}$$

The diagram vertexes connected by the wavy lines can be superposed within the point-like scatterer approximation. Then the diagrams describing the multiple scattering are presented in the form of loops. Summing the multiple scattering intensities presented by the ladder as well as cyclic diagrams one must calculate the sum of the series of loops

(2.15)

where sum $\hat{\mathbf{S}}$, called the ladder propagator of radiation transfer, is presented as the hatched oval. Along with propagator $\hat{\mathbf{S}}$ there is often introduced [20, 49] propagator $\hat{\mathbf{L}}$ which includes additionally the contribution of the single-scattering and is defined in the form

$$L_{\alpha\beta,\mu\nu}(\mathbf{r}_1, \mathbf{r}_2) = (4\pi)^2 \left[g_0 k_0^4 \delta_{\alpha\mu}\delta_{\beta\nu}\delta(\mathbf{r}_1 - \mathbf{r}_2) + g_0^2 k_0^8 S_{\alpha\beta,\mu\nu}(\mathbf{r}_1, \mathbf{r}_2)\right]. \tag{2.16}$$

The ladder diagram contribution into the scattering intensity, the single-scattering excluded, can be presented using propagator as follows

$$I^{(\mathrm{L})}_{\alpha(0)}(\mathbf{r}_0) = T_{\alpha(0)\alpha}\, T_{\alpha(0)\beta}\, g_0^2 \int \mathrm{d}\mathbf{r}_1\, \mathrm{d}\mathbf{r}_2\, S_{\alpha\beta,\mu\nu}(\mathbf{r}_1, \mathbf{r}_2) \times \exp\left[\mathrm{i}\mathbf{r}_1(\mathbf{k}_i - \mathbf{k}_i^*) - \mathrm{i}\mathbf{r}_2(\mathbf{k}_s - \mathbf{k}_s^*)\right] E_\mu\, E_\nu^*, \tag{2.17}$$

and that of the cyclic diagrams as

$$I^{(\mathrm{C})}_{\alpha(0)}(\mathbf{r}_0) = T_{\alpha(0)\alpha}\, T_{\alpha(0)\beta}\, g_0^2 \int \mathrm{d}\mathbf{r}_1\, \mathrm{d}\mathbf{r}_2\, S_{\alpha\nu,\mu\beta}(\mathbf{r}_1, \mathbf{r}_2) \times \exp\left[\mathrm{i}\mathbf{r}_1 \cdot (\mathbf{k}_i + \mathbf{k}_s^*) - \mathrm{i}\mathbf{r}_2 \cdot (\mathbf{k}_i^* + \mathbf{k}_s)\right] E_\mu\, E_\nu^*. \tag{2.18}$$

As is seen from Eqn (2.17), the ladder diagram contribution does not depend practically on scattering angle as opposed to the cyclic one. Indeed, the real parts of wave vectors $\mathbf{k}_i$ and $\mathbf{k}_s$ cancel each other out in argument of exponent in Eqn (2.17), and thus the integral is determined by their imaginary parts, i.e. by the extinction length. On the contrary the angular dependence of the cyclic diagrams is quite prominent, since the value of integral (2.18) for any scattering direction except of $\mathbf{k}_s = -\mathbf{k}_i$ is determined by the oscillating factor with the characteristic length of the wavelength order.

The loops in right-hand side (2.15) are formed by the pair of the complex-conjugated propagators

$$T_{\alpha\mu}(\mathbf{r})\, T^*_{\beta\nu}(\mathbf{r}) = \frac{k_0^4 \exp(-\sigma r)}{r^2} \left(\delta_{\alpha\mu} - \frac{r_\alpha r_\mu}{r^2}\right) \times \left(\delta_{\beta\nu} - \frac{r_\beta r_\nu}{r^2}\right) \equiv k_0^4\, \Lambda_{\alpha\beta,\mu\nu}(\mathbf{r}). \tag{2.19}$$

For simplicity summing series (2.15) one usually restricts oneself to the scalar field. Since polarisation effects appear to be essential in experiments, we describe here the solution of the problem for electromagnetic field first obtained by Stephen and Cwilich [15]. The sum of ladder diagrams can be presented in the form

$$\hat{\mathbf{S}} = \hat{\mathbf{\Lambda}} + \xi \hat{\mathbf{\Lambda}}\hat{\mathbf{\Lambda}} + \xi^2 \hat{\mathbf{\Lambda}}\hat{\mathbf{\Lambda}}\hat{\mathbf{\Lambda}} + \ldots, \tag{2.20}$$

where quantity $\xi = k_0^4 g_0$ coincides up to a numerical factor with the reciprocal extinction length in the Born approximation [50]. Summing formally series (2.20), one obtains the closed equation for the radiation transfer propagator

$$\hat{\mathbf{S}}(\mathbf{r}_1, \mathbf{r}_2) = \hat{\mathbf{\Lambda}}(\mathbf{r}_1 - \mathbf{r}_2) + \xi \int \hat{\mathbf{\Lambda}}(\mathbf{r}_1 - \mathbf{r}_3)\, \hat{\mathbf{S}}(\mathbf{r}_3, \mathbf{r}_2)\, \mathrm{d}\mathbf{r}_3. \tag{2.21}$$

The quantity $\xi \int \Lambda(\mathbf{r})\, \mathrm{d}\mathbf{r}$ is a dimensionless expansion parameter of this equation. Using an estimate $\Lambda(\mathbf{r}) \sim r^{-2} \exp(-r/l_{\mathrm{ext}})$ and definition of ξ, one concludes that this parameter is of the order of unity.

For an infinite homogeneous medium the solution is found by means of the Fourier transformation and gives an asymptotic decay law of the form $|\mathbf{r}_1 - \mathbf{r}_2|^{-1}$ for distances $|\mathbf{r}_1 - \mathbf{r}_2| \gg l_{\mathrm{ext}}$. Note that this result is not trivial since the nonintegral term decreases much faster. This solution, however, can be used only deep inside the scattering medium at distances $l \gg l_{\mathrm{ext}}$ from the boundary, where the incident field vanishes completely. Thus, for any of the problems considered, the boundary conditions appear to be essential and the propagator $\hat{\mathbf{S}}$ has to be found inside the boundary layer of depth comparable with l_{ext}.

Beginning with the classic works of Milne and Schwarzchild [51] one considers usually the problem of scattering from the half-space. One can not succeed in solving accurately the tensor equation (2.21) even for such a simple geometry. Using the resemblance between the asymptotics of the r^{-1} form and electrostatics the solution for half-space $z \geqslant 0$ was obtained by the mirror image method in the form [15]

$$\hat{\mathbf{S}}(\mathbf{r}_1, \mathbf{r}_2) = \hat{\mathbf{S}}_0(\mathbf{r}_1 - \mathbf{r}_2) - \hat{\mathbf{S}}_0(\mathbf{r}_1 - \mathbf{r}_2^{(\mathrm{s})}), \tag{2.22}$$

where $\hat{\mathbf{S}}_0(\mathbf{r})$ is the solution of Eqn (2.21) for a homogeneous medium, and $\mathbf{r}_2^{(\mathrm{s})} = (x_2, y_2, -z_2)$ is the mirror point with respect to $\mathbf{r}_2$.

Using classic results for scalar field [51] the similar approach was applied in Ref. [14, 16]. Propagator $\hat{\mathbf{S}}(\mathbf{r}_1, \mathbf{r}_2)$ was written in the form

$$\hat{\mathbf{S}}(\mathbf{r}_1, \mathbf{r}_2) = \hat{\mathbf{S}}_0(\mathbf{r}_1 - \mathbf{r}_2) - \hat{\mathbf{S}}_0(\mathbf{r}_1 - \mathbf{r}_2^{(A)}), \tag{2.23}$$

where $\mathbf{r}_2^{(A)} = (x_2, y_2, -z_2 - 2z_0)$. The value of z_0 was chosen in correspondence with the Milne solution as $z_0 = (2/3)\, l_{\mathrm{ext}}$. Taking into account the boundary conditions in the form proposed by Stephen and Cwilich [15] one obtains that

propagator $\hat{\mathbf{S}}(\mathbf{r}_1, \mathbf{r}_2) = 0$, if at least one of two points $\mathbf{r}_1, \mathbf{r}_2$ is placed at the boundary $z = 0$. Approximation [14, 16] corresponds to the similar requirement, but in the plane $z = -(2/3)\, l_{\text{ext}}$.

The image method determined either by Eqn (2.22) or by Eqn (2.23) can be verified for the propagator of the $1/r$ form, i.e. of the q^{-2} form for its Fourier-transform. One uses however such an approximation for propagator of more general form $(q^2 + \mu^2)^{-1}$ which has no pole at the origin.

Thus the problem is reduced to the homogeneous medium propagator $\hat{\mathbf{S}}_0(\mathbf{r})$. In this case performing the Fourier transformation of integral equation (2.21) one obtains a set of algebraic equations for components of tensor $\tilde{\mathbf{S}}(\mathbf{q})$

$$\tilde{S}_{\alpha\beta,\,\gamma\delta}\,(\mathbf{q}) = \tilde{\Lambda}_{\alpha\beta,\,\gamma\delta}\,(\mathbf{q}) + \xi\,\tilde{\Lambda}_{\alpha\beta,\,\mu\nu}\,(\mathbf{q})\,\tilde{S}_{\mu\nu,\,\gamma\delta}\,(\mathbf{q})\,, \tag{2.24}$$

where

$$\tilde{\mathbf{S}}(\mathbf{q}) = \int \hat{\mathbf{S}}_0(\mathbf{r})\, \exp(\mathrm{i}\mathbf{q}\cdot\mathbf{r})\, \mathrm{d}\mathbf{r} \tag{2.25}$$

is the Fourier-transform of the radiation transfer propagator, and $\tilde{\Lambda}(\mathbf{q})$ is the Fourier-transform of the priming propagator $\tilde{\Lambda}(\mathbf{r})$, given by Eqn (2.19)

$$\tilde{\Lambda}_{\alpha\beta,\,\gamma\delta}\,(\mathbf{q}) = \int \frac{\mathrm{d}\mathbf{r}}{r^2}\left(\delta_{\alpha\gamma} - \frac{r_\alpha r_\gamma}{r^2}\right)\left(\delta_{\beta\delta} - \frac{r_\beta r_\delta}{r^2}\right)\exp(-\mathrm{i}\mathbf{q}\mathbf{r} - \sigma r)\,. \tag{2.26}$$

Using the axial symmetry of this expression with respect to vector $\mathbf{q}$ the components of tensor (2.26) are easily calculated in the coordinate frame with the z axis directed along vector $\mathbf{q}$ (see, for example, Refs [52, 53]).

Assuming the initial beam to fall normally upon the boundary and backscattered beam to be observed in the (x, z) plane at small angle $\theta \geqslant 0$, counted from the backward direction, we present the cyclic diagram contributions into the scattering intensities for different initial and final polarisation states as

$$I_{\text{V}}^{(\text{C})\text{V}} = A\int_{-\infty}^{\infty} \mathrm{d}q_z f(q_z)\,\tilde{S}_{xx,\,xx}\,(\mathbf{q})\,, \tag{2.27}$$

$$I_{\text{V}}^{(\text{C})\text{H}} = I_{\text{H}}^{(\text{c})\text{V}} = A\int_{-\infty}^{\infty} \mathrm{d}q_z f(q_z)\left[\tilde{S}_{xy,\,yx}\,(\mathbf{q})\cos^2\phi + \tilde{S}_{xz,\,zx}\,(\mathbf{q})\sin^2\phi\right], \tag{2.28}$$

where

$$A = \frac{k_0^4 g_0^2 S\,|\,E\,|^2}{2\pi r_0^2}\,,$$

S is the illuminated area from which the scattered radiation is observed, $\mathbf{q} = (k_0\theta,\, 0,\, q_z)$ and $\phi = \arctan\,(k_0\theta/q_z)$. Function $f(q_z)$ results from integration over z and z_1. Its specific form depends on the kind of accounting for the boundary conditions

$$f(q) = \begin{cases} \dfrac{2q^2}{(q^2+\sigma^2)^2} & \text{for approximation (2.22),} \\ \dfrac{(\sigma^2 - q^2)[1 - \cos\,(2qz_0)]}{(q^2+\sigma^2)^2} + \dfrac{2q^2 - q\sigma\sin\,(2qz_0)}{(q^2+\sigma^2)^2} & \text{for approximation (2.23).} \end{cases} \tag{2.29}$$

The H and V indices denote polarisations parallel and perpendicular to the scattering plane, respectively, the upper index relates to the incident light, and the lower relates to the scattered one.

The respective expressions for the ladder diagram contributions can be obtained from Eqns (2.27) – (2.29) substituting $\theta = 0$ in arguments of propagator and changing component $\tilde{S}_{xy,\,yx}$ to $\tilde{S}_{xx,\,yy}$.

For small value of argument $q\sigma^{-1}$ component $\tilde{S}_{xx,\,xx}$, which defines according to Eqn (2.27) the cyclic diagram contribution into the polarised term of the scattering intensity, has the pole of the q^{-2} form. This pole corresponds physically to the long-range behaviour of the r^{-1} form in real space, causing cyclic diagram divergence at $\theta = 0$ for an infinite medium. The ladder diagrams are always divergent for an infinite medium. Keeping in the propagator $\tilde{\mathbf{S}}$ only the asymptotic term of the form of q^{-2}, we can easily calculate the integral over q_z. Taking into account the boundary conditions in form (2.22), one gets [15]

$$I_{\text{V}}^{(\text{C})\text{V}}(\theta) = \frac{8\pi^2 A}{3}\,\frac{1}{(\sigma + k_0\theta)^2}\,. \tag{2.30}$$

This formula explains the triangle-like dependence of the polarised component intensity on the scattering angle, of the form $1 - 2k_0\theta/\sigma$, discovered experimentally [1, 2].

With the boundary conditions taken in the form (2.23), the q^{-2} asymptotics produces the angular dependence of the scattering intensity in the form [14, 16]

$$I_{\text{V}}^{(\text{C})\text{V}}(\theta) \sim \frac{1}{(\sigma + k_0\theta)^2}\left\{1 + \frac{\sigma}{k_0\theta}\left[1 - \exp(-2k_0\theta z_0)\right]\right\}. \tag{2.31}$$

The components of tensor $\tilde{\mathbf{S}}$ which determine the cyclic diagram contribution into the depolarised scattering have no singularity at $q = 0$ and thus produce the Lorentzian contour at the small value of θ [15]. The $I_{\text{H}}^{(\text{C})\text{H}}$ component contains the q^{-2} pole in the integrand similarly to $I_{\text{V}}^{(\text{C})\text{V}}$ and also has the 'triangle' form.

Asymptotics q^{-2} corresponds to distance $r \gg l_{\text{ext}}$ in real space where the diffusion approximation can be used [54, 55] for the radiation transfer equation. In the case of scattering from finite size particles the diffusion approximation involves a change of the extinction length $l_{\text{ext}} = \sigma^{-1}$ entering Eqns (2.30) or (2.31) to the transport length l_{tr}, which can far exceed l_{ext}.

2.4 Measurements of coherent backscattering

Coherent backscattering is measured mostly for aqueous latex suspensions and solid systems like ceramics. A typical setup for study of the coherent backscattering is shown in Fig. 3 [56, 57]. A laser is used as the source of radiation with a beam divergence of the 0.6-mrad order. Transmitting through a polariser P_1, the beam is incident on a beam splitter BS whereby a part of the laser radiation hits the investigated system. Since the scattering angle is close to 180° the scattered radiation detected by a photomultiplier passes once more through the beam splitter. The essential feature required of this element is that it should not deviate the incident beam and increase its divergence. In particular, a plate of a 2-cm thickness was used in Ref. [57] with divergence less than 30″. A thicker slab is convenient in adjusting and makes it possible to determine with high accuracy the position of the focal

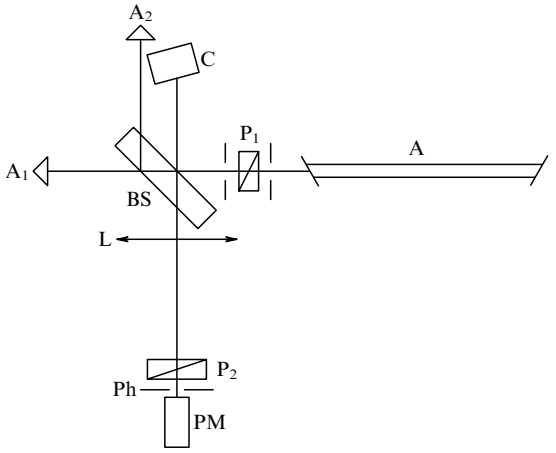

Figure 3. Schematic diagram of experimental setup for the coherent backscattering study: A, laser; C, cell; BS, beam splitter; L, lens; P_1, P_2, polarisers, Ph, pinhole; PM, photomultiplier; and A_1, A_2, light absorbing cells.

plane of a long-focused objective L. The beam reflected by the beam splitter is used for a precise adjustment of the setup as a whole. The scattered radiation passes through a polariser P_2 and a 0.2-mm-diam pinhole Ph and is detected by the photomultiplier. A reasonable backscattering experiment requires a noise caused by a diffusive reflection and scattering from elements of the setup to be analyzed and suppressed.

Van Albada and Lagendijk [1] observed backscattering enhancement in a concentrated latex suspension for various polarisations. A 5-mW He-Ne laser was used as the source of radiation. The backscattered light was measured by a detector that could be moved in the focal plane of a lens placed immediately behind the beam splitter. The angle was measured with an accuracy of 0.37 mrad. In the experiments in which no polarisers were used, background levels were well below 1% of the signal level. With the use of polarisers, the highest recorded background did not exceed 10% of the lowest recorded signal.

A 10% by weight suspension of polystyrene spheres in water was used as the scattering system. Less dense samples were prepared by dilution with water, a more concentrated sample was prepared by means of allowing the particles to settle and then decanting part of the water.

In Fig. 4 the experimental results at various latex concentrations are presented. By increasing the concentration the cone broadens and the ratio of the maximum intensity of the cone and the multiple-scattering intensity outside the cone seems to saturate at 1.4.

Outside the cone the backscattered light was completely depolarised, whereas inside the cone some polarisation remained, i.e. the depolarised component was much less than the polarised component.

Some single-scattering properties were measured and the extinction length, which is caused by a loss of light during the scattering since the polystyrene spheres do not absorb the light, was calculated. The extinction length of the $14.1 \times 10^{16}\,\mathrm{m}^{-3}$ latex suspension for light with a wavelength of 633 nm appeared to be $l_{\mathrm{ext}} = 2.6$ μm. The average $\langle \cos \Theta_s \rangle$ was equal to 0.93. Using the transport mean free path $l_{\mathrm{tr}} = l_{\mathrm{ext}}/(1 - \langle \cos \Theta_s \rangle)$ the half angle of the backscattering cone was calculated. The theoretical value of 3.3 mrad is in

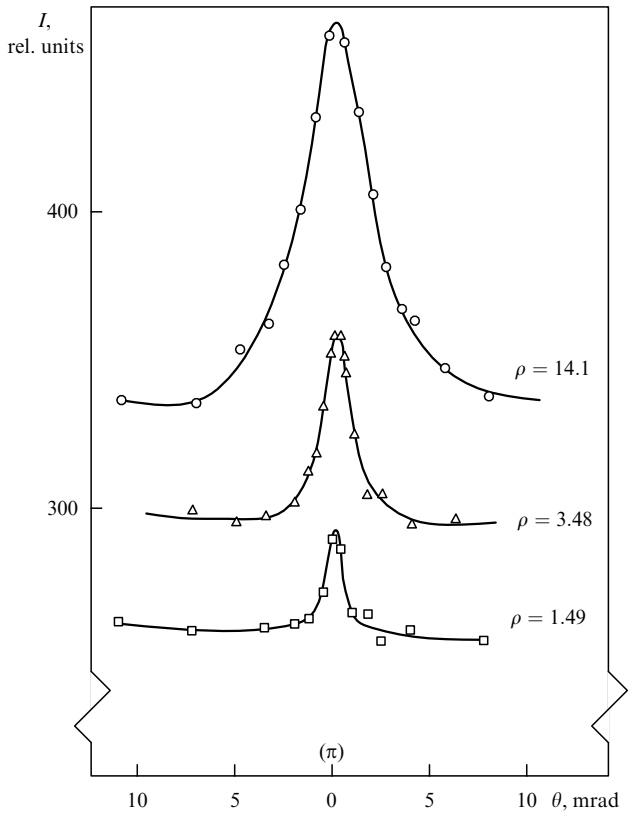

Figure 4. Backscattering intensity as the function of an angle for an aqueous 1.09-μm-diam latex sphere suspension at various densities ρ (in $10^{16}\,\mathrm{m}^{-3}$), $\lambda = 633$ nm [1].

satisfactory agreement with the experimental value of 1.6 mrad.

Wolf and Maret [2] also studied the multiple light scattering in aqueous latex suspensions. A 0.515-μm argon laser was used as a source of radiation. Beads of diameters $d = 0.109$, 0.35, 0. 46, and 0.8 μm were used, covering the crossover from pure Rayleigh scattering to strongly angle-dependent Rayleigh–Gans scattering. The initial 10% volume fraction of beads was stepwise lowered by successive dilution.

In this experiment the laser beam passes a 2-m focal distance lens, used in order to reduce the beam divergence to somewhat less than 1 mrad. A fraction of the beam is reflected onto the sample by a thin glass slide of a 0.1-mm-thickness. The sample is contained in a $10 \times 10\,\mathrm{mm}^2$ rectangular quartz cell. For all samples used, the beam diameter, about 2 mm, was much larger than the extinction length, i.e. the sample could be considered semi-infinite. The point of incidence of the beam on the sample is located at the centre of a goniometer table. Two 0.8-mm-diam pinholes mounted on the goniometer arm at distances of 0.25 and 1 m, respectively, from the cell, define the direction of detection within an angular resolution of about 3 mrad. The scattered light then passes through a linear-polarising analyzer and an interference filter, and the intensity is measured by a photomultiplier tube.

Fig. 5 shows the evolution of the backscattering peak as the volume concentration of latex beads is varied. The peak width increases linearly with latex concentration. Figure 6 shows the angular dependence of the backscattering peak for polarised and depolarised components.

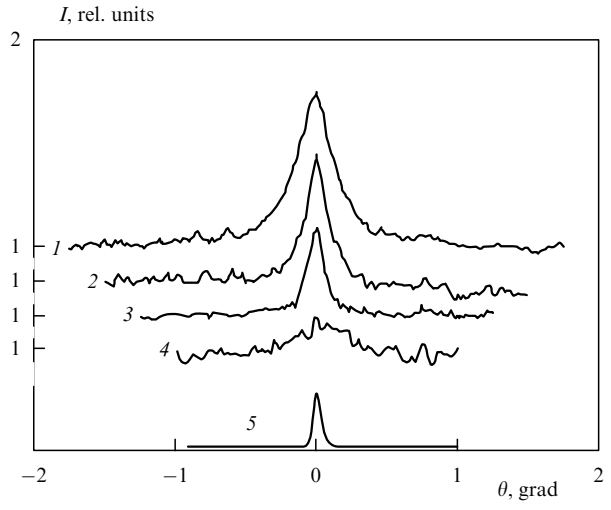

Figure 5. Angular dependence of backscattering peak of polarised component in a 0.46-μm-diam latex suspension for various volume concentrations C_L: curve *1*, $C_L = 0.11$; curve *2*, $C_L = 0.06$; curve *3*, $C_L = 0.026$; curve *4*, $C_L = 0.004$. For each curve the intensity is normalised to the intensity outside the peak. Curve *5* is the instrumental width.

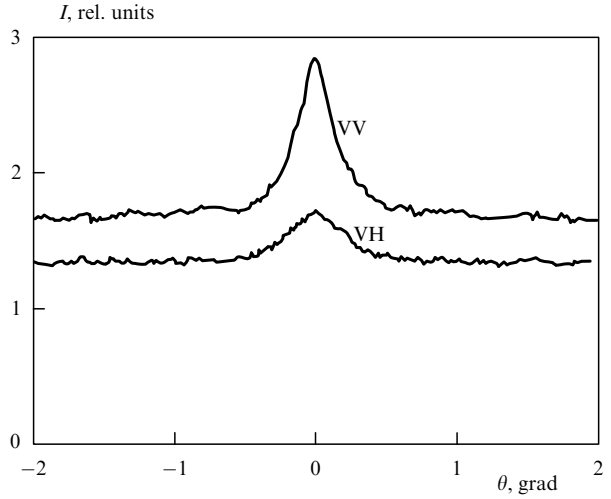

Figure 6. Polarisation dependence of the coherent backscattering for aqueous 0.46-μm-diam bead suspension at a 10% volume fraction. Polarised (VV) and depolarised (VH) components are plotted at the same scale [2].

Etemad et al. [7] carried out an experimental study on the coherent backscattering in a 'fluff' of glass SiO_2 beads in air, stabilised by a special technique. The thickness of samples varied from a few microns to a few millimetres. The size of the particles was determined with a scanning electron microscope as confined between 0.1 and 0.2 μm in diameter. The experimental setup is similar to those used in Refs [1, 2, 56].

The angular dependence exhibits very strong intensity fluctuations. They were eliminated by an ensemble averaging. This averaging was implemented either by a lateral translation of the sample, i.e. measuring in different spots, or by a very slight rotation about the point of entrance of the beam, i.e. by the measurements in different directions. This procedure uncovers a sharp peak in the backscattering direction.

Kaveh et al. [8] investigated the coherent backscattering using the Kodak White Reflectance Standard as the sample, composed of randomly oriented 1-μm-diam $BaSO_4$ particles. The 515-nm line of an argon–ion laser was used as the source of radiation. The detector–sample distance was ∼15 m. The backscattered radiation was scanned along a line which was perpendicular to and passed just above the laser beam. Similar to Ref. [7], the scattered intensity appeared to be a rapidly fluctuating angle function with a characteristic period of the λ/L order where L is the sample size. The data on the angular dependence of the backscattered intensity shown in Fig. 7a were obtained when the sample was rapidly rotated about its surface normal, equivalent to performing an ensemble average. Curves *1* and *2* correspond to the polarised and depolarised components respectively. The depolarised component does not exhibit the backscattering peak. The typical angular intensity distributions are shown in Fig. 7b for the wings ($\theta \sim 50$ mrad) and in Fig. 7c for the maximum ($\theta \approx 0$) of the peak.

The statistical properties of the scattering process are also investigated in Ref. [8]. The intensity probability $P(I)$ as function of $I/\langle I \rangle$ at the peak and in the wings was examined by processing some 3000 measurements of intensity. Within the level of experimental error the probability function appears to be the same for both the peak and the wings and

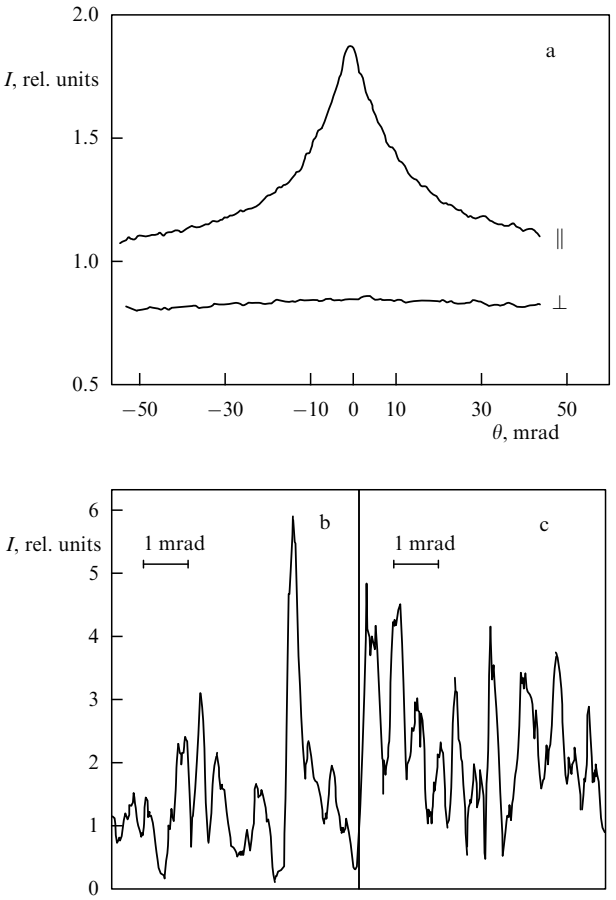

Figure 7. Backscattering peak for a reflective filter composed of randomly-oriented $BaSO_4$ microparticles: (a) data for rotating sample with analyzing polariser oriented either parallel (‖) or perpendicular (⊥) to the incident laser radiation polarisation; (b) and (c) angular distributions for stationary sample, respectively, for the wings ($\theta \sim 50$ mrad) and the maximum of the peak [8].

does not obey exponential statistics. The exponential distribution corresponds to the speckle pattern [58] which consists of well-separated bright and dark areas which exhibit a wide variation in intensity. The speckle cells observed in Ref. [8] appeared, however, as diffuse islands of light which tended both to merge and to be of similar intensity. Data were analyzed in terms of the gamma density distribution introduced into optical statistics by Mandel [59]. It takes the form

$$P(I) = \left(\frac{\mu}{\langle I\rangle}\right)^{\mu} \frac{I^{\mu-1}\exp(-\mu I/\langle I\rangle)}{\Gamma(\mu)} \tag{2.32}$$

and reverts to the exponential for $\mu = 1$. The results are well described by the gamma density distribution with $\mu = 2.5$.

Wolf et al. [60] studied the dependence of the coherent backscattering in absorbing system on the absorption coefficient. In order to study this effect, a dye which is a nearly saturated solution of Rhodamine 6G (R6G) in methanol was progressively added to a 10% solid fraction suspension of 0.46-μm-diam polystyrene spheres. The absorption mean free path L_a of a given sample was determined by measuring the transmission of an aqueous solution with identical dye concentration in the absence of particles. The largest dye concentrations were about 10%, corresponding to $L_a = 100$ μm.

The peak was found to flatten progressively as the dye concentration was increased. This is because the longer paths, which contribute only to smaller angles of the peak are eliminated. This result is consistent with the study of light scattering in slabs [61].

The statistics of photocounts was also studied in Ref. [60] for suspensions of 0.46-μm-diam polystyrene beads at the measurement time τ_0 less than 5 μs. For such a short time interval a sample can be considered practically static. In particular, the correlation function satisfies the estimate $\langle I(0)\, I(\tau_0)\rangle/\langle I\rangle^2 > 0.9$. The probability density of photocounts was taken in the form of convolution of the Poisson distribution describing photomultiplier statistics, and gamma distribution for the scattering system (the Mandel equation [59])

$$P(n) = \frac{\langle n\rangle^n \mu^{\mu}}{(\langle n\rangle + \mu)^{\mu+n}} \frac{\Gamma(n+\mu)}{n!\Gamma(\mu)}\,. \tag{2.33}$$

Experimental results were fitted by Eqn (2.33) with $\mu = 1.3$. For the $BaSO_4$ suspension the authors of Ref. [60] obtained $\mu = 1.4$.

Almamuri et al. [57] analyzed the photocount statistics inside and outside the backscattering cone for various accumulation times. The experimental setup is shown in Fig. 3. Argon and He-Ne lasers with beam divergence 0.6 mrad were used as the source of radiation. The scattered radiation passed through a 0.2-mm-diam pinhole and was measured by a photomultiplier. The statistics of photocounts were analyzed using the multi-channel analyzer with successive data processing.

For the small accumulation time, when the investigated system obeys the Gaussian statistics, function $P(n)$ is assumed to be a convolution of the Gaussian intensity distribution and the Poisson statistics of the photomultiplier, i.e. it takes the form of the Bose–Einstein distribution [62 – 64]

$$P(n) = \frac{\langle n\rangle^n}{(1+\langle n\rangle)^{n+1}}\,. \tag{2.34}$$

For larger times, when the average is taken over various realisation of the Gaussian system, $P(n)$ produces the instrumental function, i.e. it takes the form of the Poisson distribution

$$P(n) = \frac{\langle n\rangle^n}{n!}\exp(-\langle n\rangle)\,. \tag{2.35}$$

Fig. 8 illustrates the validity of these conclusions for a 1.2-μm-diam latex at the accumulation times 5×10^{-5} s and 5×10^{-2} s, respectively.

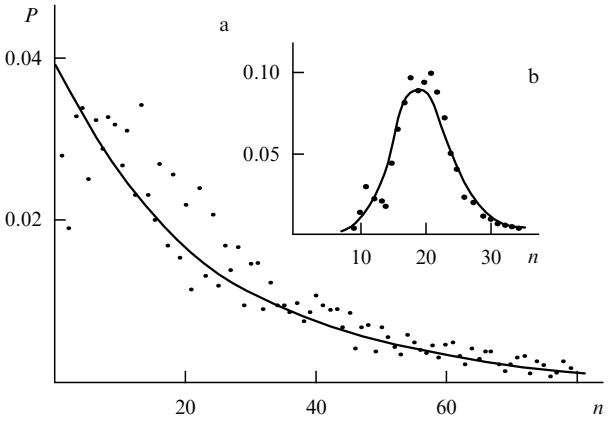

Figure 8. Probability density $P(n)$ of photocounts for the coherent backscattering from the 1.2-μm-diam latex suspension at the accumulation time (a) 5×10^{-5} s, (b) 5×10^{-2} s. Solid lines: (a) Bose–Einstein distribution, (b) Poisson distribution [57].

Lorusso et al. [65] studied the influence of multiple light scattering on the distribution function of photocounts $P(n, \tau)$, where τ is the accumulation time. The scattering system was an aqueous suspension of polystyrene spheres with variable concentration. The scattering angle was equal to 30°, so that the scattered intensity was determined by the sum of ladder diagrams. The scattered light was recorded by a cooled photomultiplier with a dark current of 10 counts per second. The suspension was confined in a flat 1.5-mm-thick cell. A single-mode He-Ne laser was used as the source of radiation. The laser beam was focused on the sample by a 150-mm focal distance lens, producing the illuminated spot with a diameter about 100 μm. The function $P(n)$, measured by a correlator, was assumed to be a superposition of coherent and stochastic signals and was presented in the form [66]

$$P(n) = \frac{N^n}{(1+N)^{n+1}}\, L_n\left[-\frac{S}{N(N+1)}\right] \exp\left(-\frac{S}{(N+1)}\right), \tag{2.36}$$

where distribution parameters S and N were understood as photon numbers of the coherent and stochastic signals, and $L_n(x)$ is the Laguerre polynomial. In the case of a purely stochastic signal this function transforms into the Bose–Einstein distribution (2.34) and for a coherent signal it transforms into the Poisson distribution (2.35). Parameters S and N are connected with the average photon number $\langle n\rangle$ and the mean square fluctuation $\langle(\delta n)^2\rangle$ by the relationships

$$\langle n\rangle = S + N,$$
$$\langle(\delta n)^2\rangle = S + N(N+1) + 2SN. \tag{2.37}$$

The function $P(n)$ was obtained for various volume concentration C_L of latex, with the $C_L = 0.74$ value corresponding to the hexagonal hard-sphere packing concentration. Eqn (2.36) describes function $P(n)$ rather well. With the latex concentration increasing the multiple scattering input increases, and $P(n)$ approaches the Poisson distribution since the scattered intensity becomes in this case weaker dependent on time, as noted by the authors.

Besides the model systems, coherent backscattering was also observed in ordinary liquids, namely in disordered liquid crystals. Disordered liquid crystals appear to be highly opalescent systems with extinction coefficient of about $10^4\ \mathrm{cm}^{-1}$. They are thought to consist of small domains with a random local ordering without sharp boundaries between them.

The coherent backscattering was studied in the BMOAB liquid crystal and the MBBA + EBBA mixture [56]. The backscattering peaks were observed in the polarised component for both systems. Moving away from the phase transition point of nematic-isotropic phase the peak height increases (Fig. 9). This increase agrees with the growth of optical anisotropy $n_o - n_e$, where n_o and n_e are the refractive indices of ordinary and extraordinary beams. The large height of peak in BMOAB mixture is likely explained by the same origin.

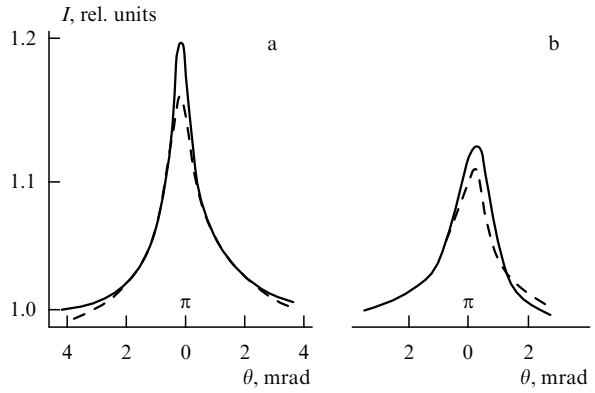

Figure 9. Angular dependence of scattering intensity near $\theta \sim 180^\circ$ for disordered liquid crystals: (a) BMOAB ($T_c = 72\,^\circ\mathrm{C}$), solid and dashed lines correspond, respectively, to $T = 41\,^\circ\mathrm{C}$ and $T = 58\,^\circ\mathrm{C}$; (b) MBBA + EBBA mixture ($T_c = 57.7\,^\circ\mathrm{C}$), solid and dashed lines correspond, respectively, to $T = 43.5\,^\circ\mathrm{C}$ and $T = 56.5\,^\circ\mathrm{C}$ [56].

2.5 Diffusion approximation

Experiments were performed mostly for systems where the size of inhomogeneity is comparable with the light wavelength. In this case the single-scattering indicatrix strongly exhibits angular dependence and the multiple scattering series can not be summed generally. Using the diffusion approximation for the radiation transfer equation an approach was outlined [16, 17] which goes beyond the framework of the point-like scatterer model.

The coherent backscattering enhancement due to the multiple scattering was anticipated for special case of a turbulent medium [67]. This effect was interpreted physically in Refs [68 – 71] as a result of a two-fold pass through the same inhomogeneities. In Ref. [72] the method of transition to the diffusion approximation was outlined permitting one to apply it to the description of the coherent backscattering which is not contained formally in the radiation transfer theory.

For simplicity, the scalar field is considered in Ref. [16, 17]. Within the weak scattering approximation, $\lambda \ll l_{\mathrm{ext}}$, the scattering intensity is presented by the ladder diagram series

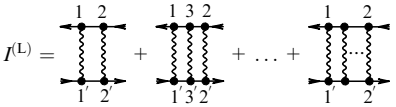

(2.38)

The single-scattering diagram is omitted here.

We separate diagram elements between the first and last scattering events

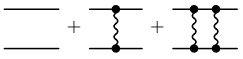

(2.39)

Series (2.39) is summed and results in the Bethe–Salpeter equation

$$\Gamma(\mathbf{r}_1, \mathbf{r}'_1, \mathbf{r}_2, \mathbf{r}'_2) = T(\mathbf{r}_1 - \mathbf{r}_2)\, T^*(\mathbf{r}'_1 - \mathbf{r}'_2) + (4\pi)^{-2} \times \int T(\mathbf{r}_1 - \mathbf{r}_3)\, T^*(\mathbf{r}'_1 - \mathbf{r}'_3)\, G(\mathbf{r}_3 - \mathbf{r}'_3) \times \Gamma(\mathbf{r}_3, \mathbf{r}'_3, \mathbf{r}_2, \mathbf{r}'_2)\, \mathrm{d}\mathbf{r}_3\, \mathrm{d}\mathbf{r}'_3\,. \quad (2.40)$$

Function $\Gamma(\mathbf{r}_1, \mathbf{r}'_1, \mathbf{r}_2, \mathbf{r}'_2)$ is called the coherence function and denotes the average of the product of two fields generated by two point sources.

Introducing the centre-of-mass coordinates

$$\mathbf{R}_j = \frac{1}{2}\,(\mathbf{r}_j + \mathbf{r}'_j),$$

and the relative ones $\mathbf{r}''_j = \mathbf{r}_j - \mathbf{r}'_j$, the product of the complex-conjugated propagator pair of the scalar field can be written within the wave zone approximation as follows

$$T(\mathbf{r}_j - \mathbf{r}_l)\, T^*(\mathbf{r}'_j - \mathbf{r}'_l) = k_0^4 R_{jl}^{-2} \exp(-\sigma R_{jl}) \exp\left[\mathrm{i}\mathbf{k}_{jl}(\mathbf{r}''_j - \mathbf{r}''_l)\right], \quad (2.41)$$

where

$$\mathbf{k}_{jl} = \frac{k\mathbf{R}_{jl}}{R_{jl}}\,, \qquad \mathbf{R}_{jl} = \mathbf{R}_j - \mathbf{R}_l\,,$$

and $\mathbf{k}_{jl}$ means the wave vector describing the propagation of wave between the j-th and l-th scattering events. Then Eqn (2.40) can be written in the form

$$\Gamma(\mathbf{R}_1, \mathbf{R}_2, \mathbf{r}''_1, \mathbf{r}''_2) = k_0^4 R_{12}^{-2} \exp\left[-\sigma R_{12} + \mathrm{i}\mathbf{k}_{12} \cdot (\mathbf{r}''_1 - \mathbf{r}''_2)\right] + \int \frac{k_0^4 \exp\left[-\sigma R_{13} + \mathrm{i}\mathbf{k}_{13} \cdot (\mathbf{r}''_1 - \mathbf{r}''_3)\right]}{(4\pi)^2 R_{13}^2} \times G(\mathbf{r}''_3)\, \Gamma(\mathbf{R}_3, \mathbf{R}_2, \mathbf{r}''_3, \mathbf{r}''_2)\, \mathrm{d}\mathbf{R}_3\, \mathrm{d}\mathbf{r}''_3\,. \quad (2.42)$$

We transform the coherence function into the Fourier integral with respect to the relative coordinates

$$\Gamma(\mathbf{R}_1, \mathbf{R}_2, \mathbf{r}''_1, \mathbf{r}''_2) = k_0^{-4} \int \frac{\mathrm{d}\mathbf{p}_1\, \mathrm{d}\mathbf{p}_2}{(2\pi)^6} \exp(\mathrm{i}\mathbf{p}_1 \cdot \mathbf{r}''_1 + \mathrm{i}\mathbf{p}_2 \cdot \mathbf{r}''_2) \times F\left(\mathbf{R}_1, \mathbf{R}_2, \frac{\mathbf{p}_1}{p_1}, \frac{\mathbf{p}_2}{p_2}\right) \delta(p_1 - k)\, \delta(p_2 - k) \quad (2.43)$$

Taking into account that the field product average is formed due to elastic scatterings, in which the absolute value of the wave vector preserves, one introduces explicitly δ-functions into the Fourier-transform (2.43) [17]. When solving Eqn (2.42) by iterations, these δ-functions arise automatically. Factor k_0^{-4} is introduced for the sake of convenience.

The contributions from the ladder as well as cyclic diagrams to the scattering intensity can be expressed through function $F(\mathbf{R}_1, \mathbf{R}_2, \mathbf{s}_1, \mathbf{s}_2)$ where $\mathbf{s}_i = \mathbf{p}_i/k$. Indeed, according to Eqns (2.38), (2.39), and (2.43), in the case of normal incidence upon the half-space $I^{(\mathrm{L})}$ can be presented in the form

$$I^{(\mathrm{L})} \sim Sk_0^8 \int_0^\infty \mathrm{d}Z_1\,\mathrm{d}Z_2 \exp\left[-\sigma(Z_1+Z_2)\right] \times \int_{-\infty}^{\infty} \mathrm{d}X_2\,\mathrm{d}Y_2 \int \mathrm{d}\mathbf{s}_1\,\mathrm{d}\mathbf{s}_2\,(4\pi)^{-2}\tilde{G}(\mathbf{p}_1+\mathbf{k}_i) \times \tilde{G}(\mathbf{p}_2-\mathbf{k}_s)\,F(\mathbf{R}_1, \mathbf{R}_2, \mathbf{s}_1, \mathbf{s}_2)\,, \tag{2.44}$$

where $\mathbf{R} = (X, Y, Z)$, and $\tilde{G}(\mathbf{q}) = \int \mathrm{d}\mathbf{r}\,G(\mathbf{r})\exp(-\mathrm{i}\mathbf{q}\cdot\mathbf{r})$ is the Fourier-transform of the correlation function $G(\mathbf{r}) = \langle \delta\epsilon(0)\,\delta\epsilon(\mathbf{r})\rangle$.

Since cyclic diagrams can be obtained from the ladder ones by rotating the lower line through 180°, their contribution to the scattering intensity takes the form [17]

$$I^{(\mathrm{C})} \sim Sk_0^8 \int_0^\infty \mathrm{d}Z_1\,\mathrm{d}Z_2 \exp\left[-\sigma(Z_1+Z_2)\right] \times \int_{-\infty}^{\infty} \mathrm{d}X_2\,\mathrm{d}Y_2 \exp(\mathrm{i}k_0\theta X_2) \int \mathrm{d}\mathbf{s}_1\,\mathrm{d}\mathbf{s}_2 \times (4\pi)^{-2}\tilde{G}(\mathbf{p}_1+\mathbf{k}_i)\,\tilde{G}(\mathbf{p}_2-\mathbf{k}_s)\,F(\mathbf{R}_1, \mathbf{R}_2, \mathbf{s}_1, \mathbf{s}_2) \tag{2.45}$$

Eqn (2.45) describes the backscattering for arbitrary scatterers. Thus the problem is reduced to the solution of the Bethe–Salpeter equation. In the case of point-like scatterers we come back to the results of Section 2.3. To take into account the finiteness of scatterers one transits from the Bethe–Salpeter equation to the radiation transfer equation.

Substituting Eqn (2.43) into Eqn (2.42) and accounting for $R_{13} \sim l_{\mathrm{ext}} \ll R_{12}$ one obtains the radiation transfer equation for the coherence function in the form [17]

$$(\mathbf{s}_1\nabla_{\mathbf{R}_1} + l_{\mathrm{ext}}^{-1})\,F(\mathbf{R}_1, \mathbf{R}_2, \mathbf{s}_1, \mathbf{s}_2) = (4\pi)^{-2}\delta(\mathbf{R}_1-\mathbf{R}_2)\,\delta(\mathbf{s}_1-\mathbf{s}_2) + (4\pi)^{-2}k_0^4 \int \mathrm{d}\mathbf{s}_3\,\tilde{G}\big(k(\mathbf{s}_3-\mathbf{s}_1)\big)\,F(\mathbf{R}_1, \mathbf{R}_2, \mathbf{s}_3, \mathbf{s}_2)\,. \tag{2.46}$$

The radiation transfer equation is solved within the diffusion approximation. It assumes [54, 55] that the angular distribution of the diffusive intensity is nearly isotropic due to the multiple scattering. Mathematically it means that expanding the scattering intensity in Legendre polynomials one can restrict oneself to the first two terms. As a result function $F(\mathbf{R}_1, \mathbf{R}_2, \mathbf{s}_1, \mathbf{s}_2)$ can be presented as follows [73]

$$F(\mathbf{R}_1, \mathbf{R}_2, \mathbf{s}_1, \mathbf{s}_2) = (4\pi)^{-2}F(\mathbf{R}_1, \mathbf{R}_2) - (4\pi)^{-2}l_{\mathrm{tr}}(\mathbf{s}_1\nabla_{\mathbf{R}_1} - \mathbf{s}_2\nabla_{\mathbf{R}_2})\,F(\mathbf{R}_1, \mathbf{R}_2). \tag{2.47}$$

Substituting the diffusion approximation (2.47) into the radiation transfer equation (2.46) one obtains

$$\nabla_{\mathbf{R}_1}F(\mathbf{R}_1, \mathbf{R}_2) = -\frac{3}{4\pi\, l_{\mathrm{tr}}}\,\delta(\mathbf{R}_1-\mathbf{R}_2)\,. \tag{2.48}$$

Here the transport length $l_{\mathrm{tr}} = l_{\mathrm{ext}}/\langle 1-\cos\theta_s\rangle$ is defined using the mean cosine of the scattering angle. The average

$$\langle 1-\cos\theta_s\rangle = \frac{\int_0^\pi (1-\cos\theta)\,\tilde{G}\,(2k\sin\theta/2)\sin\theta\,\mathrm{d}\theta}{\int_0^\theta \tilde{G}\,(2k\sin\theta/2)\sin\theta\,\mathrm{d}\theta}$$

describes the extension of the scattering indicatrix.

The diffusion equation (2.48) has to be solved for the half-space. One requires from physical considerations the diffusive intensity entering into the medium from outside to be zero on the boundary [54, 55]. In accordance with this requirement the boundary condition is written in the form [17]

$$\left(\frac{2}{3}\,l_{\mathrm{tr}}\,\gamma\,\frac{\partial F}{\partial z} - F\right)\Bigg|_{z=0} = 0\,. \tag{2.49}$$

Parameter γ is introduced to describe different kinds of accounting for boundary conditions. Choosing $\gamma = l_{\mathrm{ext}}/l_{\mathrm{tr}}$ one gets

$$\left(\frac{2}{3}\,l_{\mathrm{ext}}\,\frac{\partial F}{\partial z} - F\right)\Bigg|_{z=0} = 0\,.$$

This equation is matched to the boundary condition in the classic formulation of the Milne problem (2.23) and was used by Akkermans et al. [16]. Choosing $\gamma = 0$, one satisfies the boundary condition in the form (2.22).

Eqn (2.48) was solved in Refs [16, 17] with boundary condition (2.49). Substituting solution into Eqn (2.45) one obtains in the small angle range

$$I^{(\mathrm{C})} \sim 1 - \frac{5}{3}\,k_0\theta l_{\mathrm{tr}}\,, \tag{2.50}$$

for $\gamma = l_{\mathrm{ext}}/l_{\mathrm{tr}}$. As is seen, one obtains once more the linear dependence of intensity on the angle, i.e. the triangle form of the backscattering peak similarly to the point-like scatterer case. However, the intensity extinction due to scattering is described now by the transport length l_{tr} instead of l_{ext}. As noted previously this result agrees with experiment.

The point-like scatterer approximation implies the isotropy of the form-factor. Form-factor anisotropy arises when one accounts for the finiteness of particles or the correlation length. The condition $a \geqslant \lambda$, where a is the particle size, is fulfilled in practically all experiments. Light is scattered from such particles mostly forward. The mean square of the scattering angle is defined by the relationship [49]

$$\langle\theta_s^2\rangle \sim (ka)^{-2}\,.$$

In particular, in the Rayleigh–Gans approximation, one has $\langle\theta_s^2\rangle = 2(ka)^{-2}$. Since this value is small the scattered light maintains a definite direction even when it experiences several scattering events. For total angular randomisation the number of scattering events must satisfy the relationship [49]

$$n_r \sim 1/\langle\theta_s^2\rangle \sim \langle 1-\cos\theta_s\rangle^{-1}\,.$$

Thus the radiation occurs to be randomised over directions at distance $n_r\,l_{\mathrm{ext}} = l_{\mathrm{ext}}\langle 1-\cos\theta_s\rangle^{-1}$ of the order of l_{tr}.

There are three characteristic length parameters in the problem of light scattering from large-scale inhomogeneities: the wavelength λ, the mean free path, or extinction length l_{ext}, and transport length, or the radiation transfer length, $l_{\mathrm{tr}} > l_{\mathrm{ext}}$. These parameters are well defined in the range

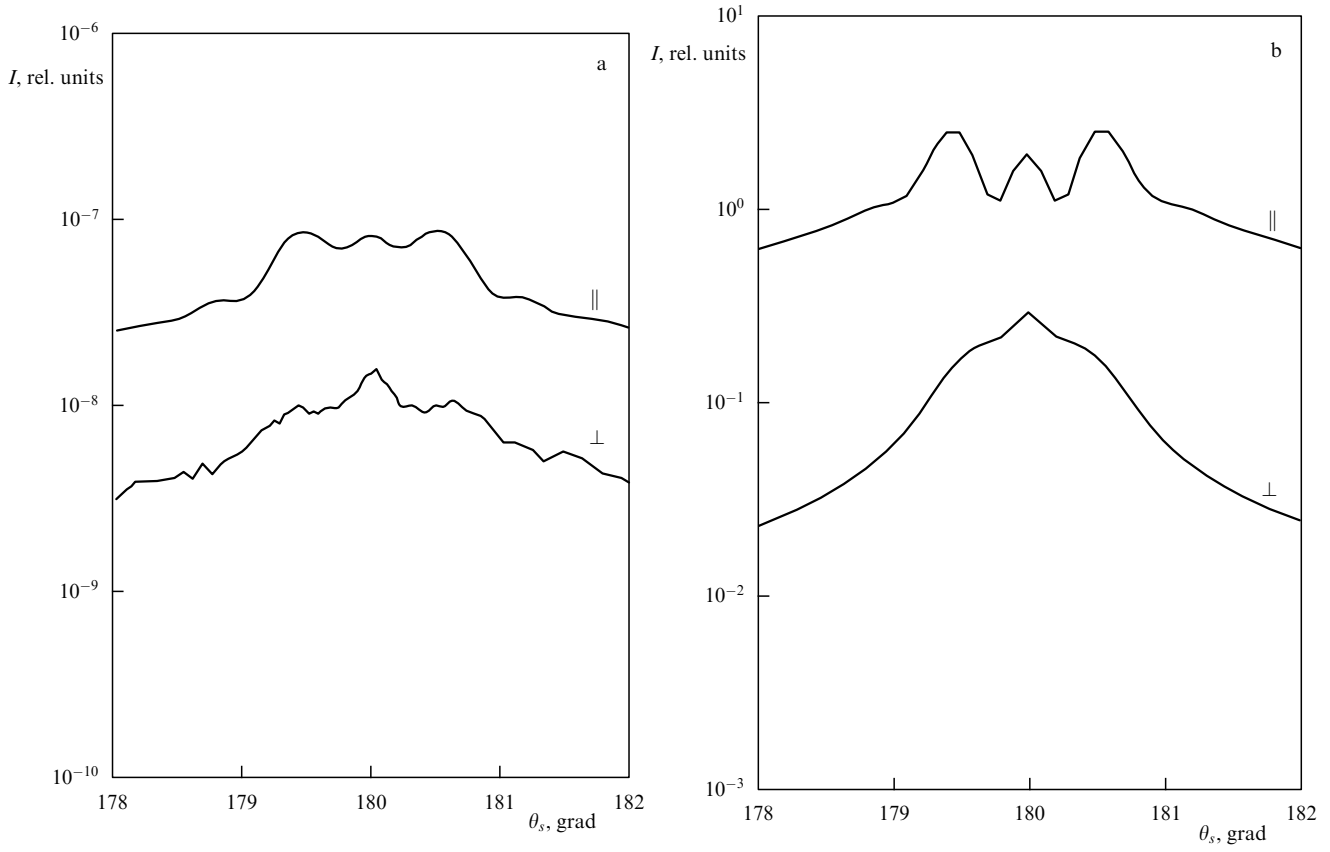

Figure 10. (a) Measured polarised (‖) and depolarised (⊥) coherent backscattering components for aqueous suspension of latex spheres with 45-μm mean diameter and standard deviation 9.9 μm, at wavelength 0.475 μm in water [79]; (b) polarised (upper curve) and depolarised (lower curve) components calculated within the double scattering approximation using the same experimental parameters [78].

$\lambda/l_{\rm ext} \ll 1$. For distances less than $l_{\rm ext}$ light propagation is described by the wave equation. At the intermediate distances between $l_{\rm ext}$ and $l_{\rm tr}$ the radiation transfer is described by the kinetic Boltzmann-like equation. And finally for distances far exceeding $l_{\rm tr}$ scattered radiation becomes isotropic and the diffusion approximation is valid [16].

The finite particle size is accounted for in the framework of the perturbation theory for $a/\lambda \ll 1$ [53]. The point-like scatterer model is used there as the zeroth order approximation. Analyzing the diagram series it was shown also that the form of the backscattering peak is described by the transport length $l_{\rm tr}$, which in this case however differs insignificantly from $l_{\rm ext}$.

Using Feynman's path integration method a new theoretical approach is proposed [74] for the description of radiation transfer in multiply scattering media. It confirms the results obtained earlier [75, 76] within the diffusion approximation.

The enhancement of backscattering from a system of finite size particles was calculated numerically in Refs [77, 78]. The case of plane wave incident upon a slab of thickness L, consisting of spherical particles was considered. The concentration of particles, was assumed to be rather dilute so that one can neglect their spatial correlations. The particles of simulated system were normally distributed over their sizes. The mean diameter of a particle was 45 μm, so that $ka = 298$. The thickness of slab was $L = 2$ cm. The scattering indicatrix was calculated by means of the Mie theory. The double-scattering intensities $I_2^{(\rm L)}$ and $I_2^{(\rm C)}$ corresponding to the ladder and cyclic diagrams were obtained. The numerical calculation was performed for the particle system which had been studied experimentally [79]. The volume particle concentration was 0.00149. The measured intensities of coherent backscattering for polarised and depolarised components are shown in Fig. 10a. Fig. 10b illustrates the results of numerical calculations for the same parameter values. As is seen, the depolarised component vanishes more rapidly than that in the experiment. The polarised component exhibits the same intermediate peaks as in experiment though their magnitudes are somewhat larger. One may conclude that the results agree rather well with the experimental ones bearing in mind that they contain the contribution of scattering of all orders.

2.6 The temporal correlation function

In previous sections we considered scattering from an idealised static system of scatterers. Since particles undergo the Brownian motion the multiply scattered fields lose their coherence with increasing time. There is a simple physical picture proposed by Maret and Wolf [18] which permits one to describe clearly the temporal damping of coherence. The temporal intensity correlation function is considered

$$C_{I^2}(t) = \langle \delta I(t)\, \delta I(0) \rangle = \langle I(t)\, I(0) \rangle - \langle I(0) \rangle^2 . \qquad (2.51)$$

It presents the fourth order correlator with respect to the scattered electric field. This correlator is factorised [26, 27, 62] in main order of parameter $\lambda\, l_{\rm ext}^{-1}$ so that the auto-correlation

function can be presented in the form

$$\langle \delta I(t)\, \delta I(0)\rangle = |\langle \delta E(t)\, \delta E^*(0)\rangle|^2 . \tag{2.52}$$

For simplicity the scalar field case is considered. Let field $\delta E(t)$ arise as a result of a sequence of scattering events occurring at moment t at points $\mathbf{r}_1(t)$, $\mathbf{r}_2(t)$, ..., $\mathbf{r}_n(t)$ with wave vectors $\mathbf{k}_1$, $\mathbf{k}_2$, ..., $\mathbf{k}_n$. Its phase is determined by the relationship

$$\delta E(t) \sim \exp \sum_j \mathrm{i}\mathbf{k}_j \cdot \mathbf{r}_j(t). \tag{2.53}$$

This field interferes with the field scattered from the same sequence of inhomogeneities at moment $t = 0$ at points $\mathbf{r}_1(0)$, $\mathbf{r}_2(0)$, ..., $\mathbf{r}_n(0)$. The time needed for the light to travel the entire path is assumed to be significantly less than the characteristic intervals of temporal change of spatial positions of scatterers. Therefore one can neglect the displacements of scatterers for the time it takes light to propagate through inhomogeneities placed at points $\mathbf{r}_1$, $\mathbf{r}_2$, ..., $\mathbf{r}_n$, and thus the temporal behaviour of the correlation function is determined as follows

$$\langle \delta E(t)\, \delta E^*(0)\rangle \sim \left\langle \exp\left\{ \mathrm{i} \sum_j \mathbf{k}_j \cdot \left[\mathbf{r}_j(t) - \mathbf{r}_j(0)\right] \right\} \right\rangle. \tag{2.54}$$

Assuming the phase shift distribution to be Gaussian one presents Eqn (2.54) in the form

$$\langle \delta E(t)\, \delta E^*(0)\rangle \sim \sum_n f(n) \exp\left(-\frac{n}{6} \langle q^2\rangle \langle r^2\rangle \right), \tag{2.55}$$

where n is the number of scattering events, $f(n)$ is a weight function dependent on the optical path, and $\langle r^2\rangle^{1/2}$ is the mean shift of scatterer during time t. In the Brownian particle model one has $\langle r^2\rangle = 6D_s t$ where D_s is the self-diffusion coefficient. Quantity $\langle q^2\rangle^{1/2}$ means the standard deviation of the wave vector transfer during a single scattering event. In the general case of anisotropic scattering, i.e. scattering from finite size particles, taking into account the definition of transport length one can write

$$\begin{aligned} \langle q^2\rangle &= 4k^2 \langle \sin^2(\theta_s/2)\rangle = 2k^2(1 - \langle \cos\theta_s\rangle) \\ &= 2k^2\, l_{\mathrm{ext}}/l_{\mathrm{tr}} . \end{aligned} \tag{2.56}$$

In the isotropic scattering case one has $l_{\mathrm{tr}} = l_{\mathrm{ext}}$ and $\langle q^2\rangle = 2k^2$. One can transit in Eqn (2.55) from summing over the discrete number of scattering events to the integration over the multiple scattering path s. The magnitude of s is obviously related to the number of scattering events through the relationship $s = nl_{\mathrm{ext}}$. The light propagator is assumed to obey to the diffusion equation [80]. In this case the weight function $P(s)$ is defined as the probability that light travels along path s from $\mathbf{r}$ to $\mathbf{r}'$

$$P(s) = \left(\frac{v}{4\pi s D} \right)^{3/2} \exp\left[-\frac{v\,|\mathbf{r} - \mathbf{r}'|^2}{4sD} \right], \tag{2.57}$$

where $D = v l_{\mathrm{tr}}/3$ is the classic diffusion coefficient of light [54, 55] and v is the radiation transfer velocity in the medium. The diffusion approximation (2.57) is valid for distances $|\mathbf{r} - \mathbf{r}'| \gg l_{\mathrm{tr}}$ [14]. Accounting for Eqn (2.55) one obtains the radiation transfer propagator $S_0(\mathbf{r}, \mathbf{r}', t)$ in the form [18, 49]

$$\begin{aligned} \mathbf{S}_0(\mathbf{r}, \mathbf{r}', t) &\sim \int_0^\infty \mathrm{d}s\, P(s) \exp\left(-\frac{2ts}{\tau_0 l_{\mathrm{tr}}} \right) \\ &= \int_0^\infty \mathrm{d}s \left(\frac{v}{4\pi s D} \right)^{3/2} \exp\left[-\frac{v\,|\mathbf{r} - r'|^2}{4sD} - \frac{2ts}{\tau_0 l_{\mathrm{tr}}} \right], \end{aligned} \tag{2.58}$$

where $\tau_0 = (D_s k^2)^{-1}$ is the characteristic time it takes a scatterer to shift at the distance of the light wavelength order. Calculating the integral by the saddle-point method one obtains

$$\mathbf{S}_0(\mathbf{r}, \mathbf{r}', t) \sim \frac{3}{4\pi} \frac{\exp(-\sqrt{6t/\tau_0}\ |\mathbf{r} - \mathbf{r}'|/l_{\mathrm{tr}})}{|\mathbf{r} - \mathbf{r}'|} . \tag{2.59}$$

This formula describes the spatial-temporal radiation transfer propagator within the diffusion approximation in a homogeneous medium, which is denoted by subscript zero.

A successive implementation of this physical picture is given by Stephen [81] starting from the scalar wave equation. The correlation function $\langle \delta E(\mathbf{r}, t)\, \delta E^*(\mathbf{r}, 0)\rangle$ is described by the diagram series similar to that of the static case, with the replacement of the equilibrium correlation functions by the spatial-temporal ones

$$G(\mathbf{r} - \mathbf{r}') \to G(\mathbf{r} - \mathbf{r}', t) = \langle \delta\epsilon(\mathbf{r}, t)\, \delta\epsilon(\mathbf{r}', 0)\rangle. \tag{2.60}$$

Note that all the vertexes of the diagram upper lines are related to moment t, and those of the lower ones are related to moment $t = 0$. Considering the point-like scatterers the Fourier-transform of the correlation function can be presented in the form

$$\tilde{G}(\mathbf{q}, t) = (4\pi)^2 g_0 \exp(-D_s q^2 t) \approx (4\pi)^2 g_0 \exp\left(-D_s \langle q^2\rangle t\right). \tag{2.61}$$

Thus the solution of the problem for the radiation transfer propagator coincides practically with that for static case considered in Section 2.3 if we take into account that parameter ξ has to be redefined as

$$\xi \to \xi \exp\left(-D_s \langle q^2\rangle t\right). \tag{2.62}$$

Since the approach described is valid for time $t \ll \tau_0$, the exponents in Eqns (2.61) and (2.62) can be expanded and as a result, for propagator $\tilde{\mathbf{L}}(\mathbf{q}, t)$, related to $\tilde{\mathbf{S}}(\mathbf{q}, t)$ by the relationship of form (2.16), one obtains

$$\tilde{L}_0(\mathbf{q}, t) = \frac{4\pi v}{l_{\mathrm{ext}}^2 \left[Dq^2 + 6(t/\tau_0)(v/l_{\mathrm{ext}}) \right]} . \tag{2.63}$$

Transition to the $\mathbf{r}$-space yields an expression similar to Eqn (2.59), which verifies the consistency of the diagram approach based on the wave equation and the probabilistic approach involving the photon random walks in a homogeneous medium. The auto-correlation function can be expressed through the radiation transfer propagator by means of formulae for the light scattering intensities (2.17) and (2.18). Thus the contribution of the cyclic diagrams takes the form

$$\begin{aligned} \langle \delta E(t)\, \delta E^*(0)\rangle \sim \int \mathrm{d}\mathbf{r}_1\, \mathrm{d}\mathbf{r}_2\, \mathbf{L}(\mathbf{r}_1, \mathbf{r}_2, t) \\ \times \exp\left[\mathrm{i}(\mathbf{k}_i + \mathbf{k}_s^*) \cdot \mathbf{r}_1 - \mathrm{i}(\mathbf{k}_i^* + \mathbf{k}_s) \cdot \mathbf{r}_2 \right] |\mathbf{E}_0|^2 , \end{aligned} \tag{2.64}$$

where

$$\mathbf{k}_i = (0, 0, k + i\sigma), \qquad \mathbf{k}_s = (k_0\theta, 0, -k - i\sigma).$$

Propagator $\mathbf{L}(\mathbf{r}_1, \mathbf{r}_2, t)$ describes the radiation transfer in the half-space. Solving the boundary problem one uses as usually the mirror image method

$$\mathbf{S}(\mathbf{r}_1, \mathbf{r}_2, t) = \mathbf{S}_0(\mathbf{r}_1 - \mathbf{r}_2, t) - \mathbf{S}_0(\mathbf{r}_1 - \mathbf{r}_2^{(b)}, t),$$

where $\mathbf{r}_2^{(b)}$ is the mirror image of point $\mathbf{r}_2$ with respect to plane $z = -z_b$ and $\mathbf{r}_2^{(b)} = (x_2, y_2, -z_2 - 2z_b)$. Choosing $z_b = 0$ and $z_b = z_0 = 2/3 l_{ext}$ one satisfies the boundary conditions in form (2.22) and in form (2.23), respectively. Accounting for the axial symmetry with respect to axis z and using Fourier-presentation (2.63), by means of the residue theorem, one obtains

$$\langle \delta E(t)\, \delta E^*(0)\rangle \sim \left(1 + \sqrt{\frac{6t}{\tau_0} + l_{ext}^2 k_0^2 \theta^2}\right)^{-2} \times \left\{1 + \left(\frac{6t}{\tau_0} + l_{ext}^2 k_0^2 \theta^2\right)^{-1} \times \left[1 - \exp\left(\frac{-2z_b}{l_{ext}} \sqrt{\frac{6t}{\tau_0} + l_{ext}^2 k_0^2 \theta^2}\right)\right]\right\}. \quad (2.65)$$

Eqn (2.65) describes the temporal correlation function for various scattering angles. It exhibits a nonanalytic dependence of correlation function on time of the $t^{1/2}$ form at $\theta = 0$ and triangle form of the peak at $t = 0$. It is worth noting the symmetry of Eqn (2.65) with respect to substitution [49]

$$\left(\frac{6t}{\tau_0}\right)^{1/2} \leftrightarrows k_0 l_{ext} \theta\,.$$

The correlation function calculated from (2.65) at $\theta = 0$ is plotted against time in Fig.11. The measured correlation function [19] is fitted to the exponential dependence of the form

$$\langle \delta E(t)\, \delta E^*(0)\rangle \sim \exp\left(-\gamma \sqrt{\frac{6t}{\tau_0}}\right),$$

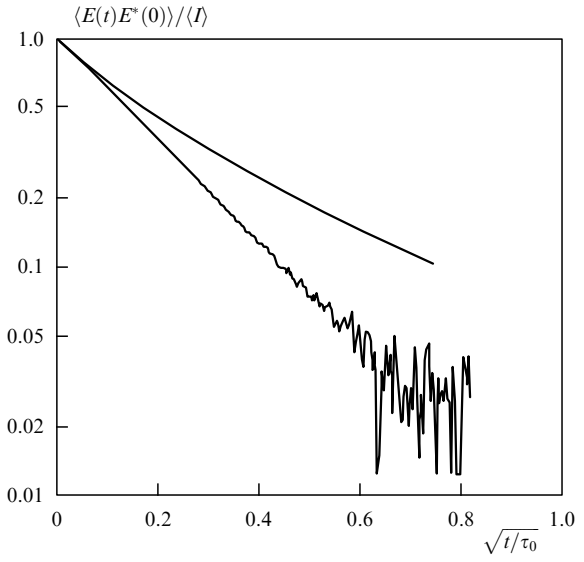

Figure 11. Normalised temporal correlation function for a 2-mm-thick slab filled with an aqueous 0.497-μm-diam latex suspension [19]. Smooth line shows the results of calculations [49].

where $\gamma \approx 2$. As is seen from Eqn (2.65) one can write for small time at $\theta = 0$

$$\langle \delta E(t)\, \delta E^*(0)\rangle \sim 1 - \gamma_{theor} \sqrt{\frac{6t}{\tau_0}}.$$

Choosing boundary conditions with $z_b = 0$ one gets $\gamma_{theor} = 2$, and for boundary condition with $z_b = (2/3)\, l_{ext}$ the result is $\gamma_{theor} \approx 2.4$. In the small time range Eqn (2.65) compares with the experiment, and for a larger time it predicts a slower decrease of the correlation function as compared with the experimental one. However, the described theoretical consideration is valid for $t \ll \tau_0$.

MacKintosh and John [49, 82] considered the auto-correlation function of electromagnetic field. They obtained formulae similar to Eqn (2.65) for the polarised and depolarised components of auto-correlation function. Their initial slopes with respect to $t^{1/2}$ turn out to be different [49]. The polarised component decays with slope $\gamma_{\parallel} \approx 1.6$, and the depolarised component decays with slope $\gamma_{\perp} \approx 2.7$. These values agree rather well with experimental values of 1.6 ± 0.1 and 2.8 ± 0.2, respectively, for scattering of $\lambda = 488$ nm light from a 0.091-μm-diam latex suspension.

Besides the plane-polarised waves, calculations of the temporal correlation function were also performed for the circular polarised waves. For coinciding directions of circular polarisation of incident and scattered light the calculated slope $\gamma_{theor} \approx 2.4$, and for the opposite circular polarisations $\gamma_{theor} \approx 1.7$.

These results are valid for particles of small size and for short time intervals. Since scattering becomes anisotropic for large-size particles, the auto-correlation function depends to a lesser extent on polarisation due to the light depolarisation in each scattering event. Such an effect was observed experimentally [83]. Namely, increasing the size of particles one gets slope $\gamma_{\parallel}$ increasing and $\gamma_{\perp}$ decreasing, resulting practically in the coincidence of these two slopes in the case of sharp anisotropic scattering. For example, at $l_{tr}/l_{ext} \geqslant 10$ slopes $\gamma_{\parallel}$ and $\gamma_{\perp}$ differ less than by 5%.

Considering the auto-correlation function in scalar case, we pointed out the symmetry between the angular and temporal dependences. Note that with the polarisation taken into account, this symmetry is only valid for the case when polarisations, linear and circular, of the incident and final waves, are the same. In the case of depolarised component, the angular dependence becomes smoother and this symmetry is violated.

Besides the temporal correlation function, also the frequency correlation function related to the former by the Fourier-transformation is studied. The low frequency part of the spectral correlation function was measured for the first time in Ref. [30]. The point source of radiation placed inside the scattering system was used. Such experimental geometry has been considered before by Stephen [20] and Shapiro [26]. The intensity–intensity correlation function $C_{I^2}(R, t)$ was obtained for the model of point-like scatterers

$$C_{I^2}(R, t) \sim \left(\frac{3}{4\pi R l_{tr}}\right)^2 \exp\left[-\frac{2R}{l_{tr}} \sqrt{\frac{6|t|}{\tau_0}}\right]. \quad (2.66)$$

This expression is in fact the square of Eqn (2.59), which is readily understood, since the radiation transfer propagator means just the point source radiation intensity inside the scattering medium. Performing the Fourier-transformation

of Eqn (2.66), one obtains the respective frequency spectrum

$$\tilde{C}_{I^2}(R,\omega) \sim \frac{1}{2\pi\omega_c}\left(\frac{\omega_c}{\omega}\right)^{3/2}\left\{\left[1-2\mathrm{C}\left(\sqrt{\frac{\omega_c}{\omega}}\right)\right]\cos\left(\frac{\omega_c}{\omega}\right) + \left[1-2\mathrm{S}\left(\sqrt{\frac{\omega_c}{\omega}}\right)\right]\sin\left(\frac{\omega_c}{\omega}\right)\right\}, \qquad (2.67)$$

where $\mathrm{C}(x)$ and $\mathrm{S}(x)$ are the integral cosine and sine, respectively, and $\omega_c = 3(R/l_{\mathrm{tr}})^2/(\pi\tau_0)$ is the characteristic frequency. The meaning of the ω_c can be easily clarified by considering $\tilde{C}_{I^2}(R,\omega)$ in two limit cases [30]. For $\omega \leqslant \omega_c$ one has

$$\tilde{C}_{I^2}(R,\omega) \sim \frac{1}{\omega_c}\left[1-\frac{15}{4}\left(\frac{\omega}{\omega_c}\right)^2 + O\left(\frac{\omega}{\omega_c}\right)^4\right], \qquad (2.68)$$

and for $\omega \gg \omega_c$

$$\tilde{C}_{I^2}(R,\omega) \sim \frac{1}{\omega_c}\left(\frac{\omega_c}{\omega}\right)^{3/2}\left[1-\left(\frac{8\omega_c}{\pi\omega}\right)^{1/2} + O\left(\frac{\omega_c}{\omega}\right)\right]. \qquad (2.69)$$

Thus ω_c appears to be a boundary frequency, which divides two frequency ranges. In the lower one, function $\tilde{C}_{I^2}$ becomes a constant, and in the upper range it decreases as $\omega^{-3/2}$ instead of ω^{-2} as it could be expected in the case of single-scattering with the Lorentzian shape of spectrum. The intermediate range appears to be quite wide, extending about two decades. Note that ω_c is, as a rule, approximately $(R/l_{\mathrm{tr}})^2$ times larger than the characteristic frequency of the single-scattering and increases with distance as $\omega_c \sim R^2$.

The He-Ne laser was used as the light source coupled to a single-mode fiber with a core diameter of 4 μm [30]. The free end of the fiber which served as a point-like source of radiation was inserted into a cylindrical sample cell of radius $a = 0.57$ cm and width $W = 0.15$ cm. The cell had been previously filled with a water suspension of 0.48-μm-diam polystyrene spheres at a volume fraction of 12%. The calculated value of the self-diffusion coefficient $D_{\mathrm{s}} = 1 \times 10^{-8}\,\mathrm{cm^2\,s^{-1}}$ at 22 °C agrees rather well with the experimental check $D_{\mathrm{s}} = 1.3\times 10^{-8}\,\mathrm{cm^2\,s^{-1}}$, measured from the single-scattering spectrum of a dilute sample. A microscope objective was used at the output of the cell. The multiply scattered light was collected by the objective and focused on a photodiode coupled to an amplifier and frequency analyzer. The distance R between the end of the fiber and the cell window was varied from $R = 50$ μm to $R = 400$ μm. In Fig. 12 spectra $\tilde{C}_{I^2}(v)$ ($v = \omega/2\pi$) are plotted for different distances from $R = 200$ μm to $R = 400$ μm. Solid lines present theoretical curves calculated by means of Eqn (2.67). The overall amplitude and frequency ω_c were used as adjustable parameters. As is seen from the figure $\tilde{C}_{I^2}(v)$ varies quite slightly with frequency at $v \ll v_c$ and decreases as $\tilde{C}_{I^2}(v) \sim 2\pi v^{-1}$ at $v \sim v_c$. It was not possible to perform measurements in the range $v \gg v_c$ where the theory predicts the $\sim v^{-3/2}$ behaviour. However the dependence of the form $\tilde{C}_{I^2}(v) \sim v^{-1.2\pm0.1}$ was found for $R = 200$ μm. Frequency v_c varies as square of distance R in agreement with the theoretical prediction. The $\omega_c \sim R^2$ dependence was also found in Ref. [19] for similar light path values, whereas the $\omega_c \sim R$ relationship is obtained for paths approximately 30 times larger [84]. The data obtained in Ref. [30] correspond to value $l_{\mathrm{tr}}\tau_0^{1/2} \approx 4.4\times$

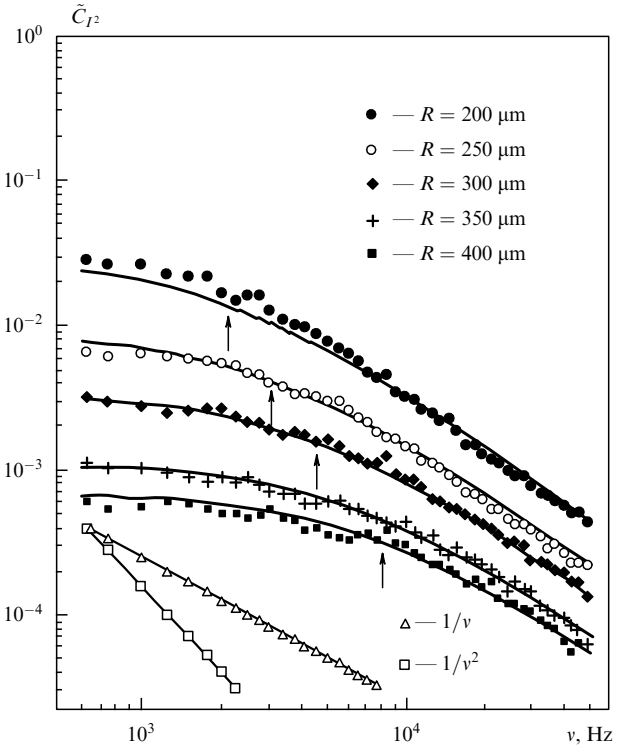

Figure 12. Comparison of experimental data (points) and theoretical fits (smooth curves) for the frequency correlation function $C_{I^2}(v)$, $v = \omega/(2\pi)$, for values of source–aperture separation R indicated. The fitting frequencies $v_c = \omega_c/(2\pi)$ are indicated as arrows. Slopes $1/v$ and $1/v^2$ are shown for comparison [30].

10^{-4} cm $\mathrm{s}^{1/2}$. It should be recalled that the theory developed is valid for the case of isotropic scatterers whereas systems consisting of sufficiently large-sized scatterers are studied experimentally, for which differences between l_{ext} and l_{tr} are large. The l_{tr} value was determined from the measured extinction length l_{ext} in highly diluted suspensions with concentration $c \sim 10^{-5}$–10^{-6} at $\lambda = 0.633$ μm. Assuming that l_{ext} varies linearly with concentration one obtains $l_{\mathrm{ext}} = 4.4$ μm for $c = 0.15$ in good agreement with the theoretical value $l_{\mathrm{ext}} = 3.9$ μm. With account taken for the known value of $\langle\cos\theta_s\rangle$, this yields $l_{\mathrm{tr}} = 23$ μm. Using the theoretical value of D_{s} one obtains $l_{\mathrm{tr}}\,\tau_0^{1/2} \approx 2 \times 10^{-4}$ cm $\mathrm{s}^{1/2}$ which is smaller than the experimental value above by a factor ~ 2. This indicates that the scattering indicatrix anisotropy is to be included in the theoretical description.

The auto-correlation function $C_{I^2}(t)$ was studied in Ref. [65] for the usual setting of an experiment with a plane wave as the source of radiation incident in a solution of 1.2-μm-diam latex particles. To consider only the ladder diagram contribution a scattering angle of 30° was used. The rate of decay of the intensity–intensity correlation function was found to increase with a rise in concentration and become nonexponential, i.e. the quantity $\ln C_{I^2}(t)$ is no more a linear function of time as it should be for dilute suspensions. The quantity $\ln\left[-\ln C_{I^2}(t)\right]$ depends now linearly on time, namely, $\ln C_{I^2}(t) \sim -t^{2/d_\omega}$ with index $d_\omega = 2$ for the single-scattering and d_ω exceeding 2 at higher concentrations. It is noteworthy that the dependence of d_ω on concentration C_L is quite similar to that of S/N (see Eqn (2.37)) ascribed by the authors of Ref. [65] to the increased contribution of multiple scattering.

The effect of short-range interparticle correlations on equilibrium and dynamic properties of multiple scattering in colloid systems has been discussed in Ref. [85]. As was noted previously, the angular dependence for noninteracting scatterers is described by the expression of the form $I^{(C)}(\theta) \sim 1 - \gamma k\theta l_{tr}$ in the vicinity of the backscattering peak, $\theta = 0$, and the temporal correlation function is presented in the form $C_{E^2} \sim 1 - \gamma(6t/\tau_0)^{1/2}$. It was shown [18, 49, 85, 86] that taking into account the interparticle correlations, one has to change l_{tr} to l'_{tr} and τ_0 to τ'_0 in the formula for $I^{(C)}(\theta)$, where l'_{tr} and τ'_0 account for the pair correlations of particles.

3. Intensity correlation functions

While studying coherent backscattering in highly inhomogeneous systems the intensity of multiply scattered light was found to exhibit strong fluctuations. They appear as temporal fluctuations in the case of colloid mixtures [57, 60] and as spatial intensity variations in that of inhomogeneous solids. Recently much interest has been paid to the study of intensity fluctuations and their correlations. These studies appear to be rather purposeful because they are the well-known quantum counterparts of these phenomena, namely the universal conductance fluctuations in disordered metals [21 – 25, 87]. The temporal correlation function considered in Section 2.6 is a particular case of such correlation functions. Along with it, spatial [26, 27, 88], angular [27, 28, 31, 89], frequency [32 – 34, 88, 90 – 92], and polarisation correlation functions are studied.

When studying intensity correlations one usually deals with the problem of light transmission through a slab of finite thickness. Considering the slab with thickness far exceeding the extinction length guarantees the light to propagate in the multiple scattering regime. This condition also guarantees the validity of the diffusion approximation. Interest in this particular problem owes its existence to the fact that despite multiple scattering the correlation effects are essentially manifested in the transmitted light due to the coherence of incident radiation. These correlation effects are also present in the reflection light but for this problem the diffusion approximation is, strictly speaking, insufficient.

3.1 Angular and frequency correlations. Memory effect

We begin our considerations with the angular correlation functions. Let two plane waves with wave vectors $\mathbf{k}_i$ and $\mathbf{k}_{i'}$ fall upon the system. We separate two plane waves with wave vectors $\mathbf{k}_s$ and $\mathbf{k}_{s'}$ in the outgoing radiation. We denote scalar fields resultant from scattering of the plane waves $\mathbf{k}_i$ and $\mathbf{k}_{i'}$ as $E(\mathbf{k}_i \to \mathbf{k}_s)$ and $E(\mathbf{k}_{i'} \to \mathbf{k}_{s'})$, and their intensities as $I(\mathbf{k}_i, \mathbf{k}_s)$ and $I(\mathbf{k}_{i'}, \mathbf{k}_{s'})$, respectively. For waves transmitting through a disordered medium in the multiple scattering regime these intensities appear to be correlated under certain conditions. We define the correlation functions as follows

$$C_{I^2}(\mathbf{k}_i, \mathbf{k}_{i'}, \mathbf{k}_s, \mathbf{k}_{s'}) = \langle \delta I_{is}\, \delta I_{i's'} \rangle = \langle I(\mathbf{k}_i, \mathbf{k}_s)\, I(\mathbf{k}_{i'}, \mathbf{k}_{s'}) \rangle - \langle I(\mathbf{k}_i, \mathbf{k}_s) \rangle \langle I(\mathbf{k}_{i'}, \mathbf{k}_{s'}) \rangle . \quad (3.1)$$

They can be factorised in the main order of parameter $\lambda/l_{ext} < 1$

$$C_{I^2}(\mathbf{k}_i, \mathbf{k}_{i'}, \mathbf{k}_s, \mathbf{k}_{s'}) = C_{I^2}(i, i', s, s') = \left| \langle E(\mathbf{k}_i \to \mathbf{k}_s)\, E^*(\mathbf{k}_{i'} \to \mathbf{k}_{s'}) \rangle \right|^2 \quad (3.2)$$

Expression (3.2) is presented graphically as the product of two disconnected diagrams

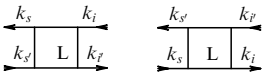

(3.3)

where L denotes the sum of all ladder diagrams. Studying the transmission correlation function one can neglect the contribution of cyclic diagrams. We consider a scalar wave propagating through the inhomogeneous medium slab with thickness L and square $S = W^2$ where W is the width of the sample.

The first diagram corresponds to the field–field correlation function in the form

$$C_{E^2}(\mathbf{k}_i, \mathbf{k}_{i'}, \mathbf{k}_s, \mathbf{k}_{s'}) = \int d\mathbf{r}_1\, d\mathbf{r}_2\, d\mathbf{r}'_1\, d\mathbf{r}'_2\, \mathbf{L}(\mathbf{r}_1, \mathbf{r}'_1, \mathbf{r}_2, \mathbf{r}'_2) \times \exp\left(i\mathbf{k}_i \cdot \mathbf{r}_1 - i\mathbf{k}_i^* \cdot \mathbf{r}'_1 - i\mathbf{k}_s \cdot \mathbf{r}_2^{(L)} + i\mathbf{k}_s^* \cdot \mathbf{r}_2^{\prime(L)}\right) \quad (3.4)$$

where superscript (L) denotes that the z component of the respective vector is measured from the $z = L$ plane. This is related to the fact that in the far zone a distance in propagators $\mathbf{T}(\mathbf{r}_2 - \mathbf{r})$ and $\mathbf{T}^*(\mathbf{r}'_2 - \mathbf{r})$, which describe the field propagation to the observation point, has to be measured from point $\mathbf{r}\,(0, 0, L)$. For simplicity the magnitude of the incident field is taken to be unity.

The integrations over $\mathbf{r}'_1$ and $\mathbf{r}'_2$ are carried out within the point-like scatterer approximation due to the δ-functions contained in the ladder operator $\mathbf{L}(\mathbf{r}_1, \mathbf{r}'_1, \mathbf{r}_2, \mathbf{r}'_2) \to \delta(\mathbf{r}_1 - \mathbf{r}'_1)\, \delta(\mathbf{r}_2 - \mathbf{r}'_2)\, \mathbf{L}(\mathbf{r}_1, \mathbf{r}_2)$.

In the case of wide sample $W \gg L$ the radiation transfer propagator is translationally invariant in plane x, y: $\mathbf{L}(\mathbf{r}_1, \mathbf{r}_2) = \mathbf{L}(\mathbf{r}_{\perp 1} - \mathbf{r}_{\perp 2},\ z_1, z_2)$ where $\mathbf{r}_\perp = (x, y)$. In this case the wave vector transversal component has to obey the 'conservation law'

$$(\mathbf{k}_i - \mathbf{k}_{i'})_\perp = (\mathbf{k}_s - \mathbf{k}_{s'})_\perp . \quad (3.5)$$

On extracting the imaginary parts of wave vectors, which are related to the extinction, Eqn (3.4) can be presented in the form

$$C_{E^2}(\mathbf{k}_i, \mathbf{k}_{i'}, \mathbf{k}_s, \mathbf{k}_{s'}) = \delta_{(\Delta\mathbf{k}_{i\perp}, \Delta\mathbf{k}_{s\perp})} S \int d^2\mathbf{r}_\perp \int_0^L dz_1 \int_0^L dz_2\, \mathbf{L}(\mathbf{r}_\perp, z_1, z_2) \times \exp\left[-\sigma\left(\frac{z_1}{\cos\theta_i} + \frac{L - z_2}{\cos\theta_s}\right) + i\mathbf{r}_\perp \cdot \Delta\mathbf{k}_{i\perp}\right], \quad (3.6)$$

where

$$\Delta\mathbf{k}_{i\perp} = (\mathbf{k}_i - \mathbf{k}_{i'})_\perp, \qquad \Delta\mathbf{k}_{s\perp} = (\mathbf{k}_s - \mathbf{k}_{s'})_\perp . \quad (3.7)$$

Correlations are usually considered between waves with close values of wave vectors. Therefore we assume $\cos\theta_i \approx \cos\theta_{i'}$ and $\cos\theta_s \approx \cos\theta_{s'}$ where θ_i and $\theta_{i'}$ are the angles of incidence and θ_s and $\theta_{s'}$ are the angles of observation of two correlated fields, respectively. The real parts of exponent describe the extinction of incident as well as outgoing beams. By complex conjugation of Eqn (3.4) one obtains the correlation function $C_{E^2}(\mathbf{k}_{i'}, \mathbf{k}_i, \mathbf{k}_{s'}, \mathbf{k}_s)$ presented by the second diagram.

In the problem considered it is necessary to satisfy the boundary conditions in planes $z = 0$ and $z = L$. This usually

requires the radiation transfer propagator to be equal to zero at these boundaries. Solving this boundary problem one uses the image method for a finite thickness slab [27, 28, 93 – 95]

$$\mathbf{L}(\mathbf{r}_\perp, z_1, z_2) = \sum_{n=-\infty}^{\infty} \big[L_0(\mathbf{r}_\perp, z_1 - z_2 + 2nL) - L_0(\mathbf{r}_\perp, z_1 + z_2 + 2nL)\big]. \quad (3.8)$$

Points $\mathbf{r}_1$ and $\mathbf{r}_2$ are located, respectively, near planes $z = 0$ and $z = L$ due to the exponentially decreasing factors in Eqn (3.6). Therefore distance $|\mathbf{r}_1 - \mathbf{r}_2| \gg l_{\text{ext}}$ and hence one can use the diffusion approximation $L_0(\mathbf{r}) = 3(l_{\text{ext}}^3 r)^{-1}$ for the homogeneous medium propagator.

Integral (3.6) can be calculated accurately. However one usually restricts oneself to an approximate estimate valid up to a numerical factor. Taking into account that regions $z_1 \sim l_{\text{ext}}$ and $z_2 \sim L - l_{\text{ext}}$ contribute mainly to the integrand due to exponential factors $\exp(-\sigma z)$ one can write $\mathbf{L}(\mathbf{r}_\perp, z_1, z_2) \approx \mathbf{L}(\mathbf{r}_\perp, l_{\text{ext}}, L - l_{\text{ext}})$ for transmission and $\mathbf{L}(\mathbf{r}_\perp, z_1, z_2) \approx \mathbf{L}(\mathbf{r}_\perp, l_{\text{ext}}, l_{\text{ext}})$ for reflection.

Performing the Fourier transformation we integrate easily over transversal variables. Integrating also by means of the residue theorem over k_z and summing the resultant geometric progression, we obtain

$$\begin{aligned} C_{E^2}(\mathbf{k}_i, \mathbf{k}_{i'}, \mathbf{k}_s, \mathbf{k}_{s'}) &= \delta_{(\Delta\mathbf{k}_{i\perp}, \Delta\mathbf{k}_{s\perp})} \frac{6\pi S}{l_{\text{ext}}^3 |\Delta\mathbf{k}_{i\perp}|} \frac{\cosh(2l_{\text{ext}}\Delta k_{i\perp}) - 1}{\sinh(\Delta k_{i\perp} L)} \\ &\times \int_0^L \mathrm{d}z_1 \int_0^L \mathrm{d}z_2 \exp\left[\left(-\frac{\sigma}{\cos\theta_i} + \mathrm{i}\Delta k_{iz}\right) z_1 + \left(-\frac{\sigma}{\cos\theta_s} + \mathrm{i}\Delta k_{sz}\right)(L - z_2)\right] \\ &\approx \delta_{(\Delta\mathbf{k}_{i\perp}, \Delta\mathbf{k}_{s\perp})} S \frac{12\pi l_{\text{ext}}}{L} \cos\theta_i \cos\theta_s F_1(\Delta k_{i\perp} L), \end{aligned} \quad (3.9)$$

where

$$F_1(x) = \frac{x}{\sinh x}. \quad (3.10)$$

This formula for the field correlation function was obtained for the first time by Feng et al. [28]. Passing to the second equality in Eqn (3.9) we neglected quantities Δk_{iz} and Δk_{sz} as compared with σ, since function $F_1(x)$ is negligibly small when $|\Delta k| > L^{-1}$.

First we note that correlation function C_{E^2} is nonzero within factorisation approximation only for $\Delta\mathbf{k}_{i\perp} = \Delta\mathbf{k}_{s\perp}$. This property was called the memory effect [28] since it means that the fields undergoing the multiple scattering remember the initial difference of the transversal wave vectors.

This memory effect can be explained physically as follows. Two waves propagating through a turbid medium and scattering from the same inhomogeneities maintain the initial phase difference originated by the different incidence directions. Then after statistical averaging only waves outgoing with the same transversal wave vector difference appear to be correlated.

We note also that correlation function C_{E^2} decays exponentially with the transversal wave vector difference increasing i.e. with increasing of the scattering angle.

Eqn (3.9) is derived for a transversally infinite slab. In this case the transversal wave vector difference can vary continuously. Feng et al. [28] considered the waveguide geometry, i.e. the slab of finite width W with a set of discrete transversal modes defined as $\Delta k_i = \pi n W^{-1}$ where n is integer. Considering function (3.10) one concludes that the memory effect is more prominent when $L \ll W$ i.e. in the case of a wide waveguide since the minimum value of argument x is $\pi L/W$. The case of a narrow waveguide $W \ll L$ was considered by Eliyahu et al. [96]. They demonstrated that the memory effect disappears for such a system.

The results of Ref. [28] on the angular dependence of correlation function were tested experimentally [31] and confirmed the existence of memory effect.

The diameter of a polarised 5 mW He-Ne laser beam with the 0.633-μm wavelength was expanded to 15 mm. The central part of the beam with a nearly flat wave front was used to study the speckle pattern. Placing a 6-mm diam mask on the sample surface ensured that the laser beam did not move across the sample during rotation. The speckle patterns were recorded with a video camera, and digitised by a computer. The sample was a thin sheet (370-μm thickness) of opal glass supported on a transparent glass substrate.

The transmission correlation function C_{I^2} is shown in Fig. 13. It represents the analysis of some 250 separate patterns each containing several hundreds speckle spots. As can be seen the data are well approximated by an exponent in agreement with the calculation results for large values of argument. Curve a in Fig. 13 shows the results obtained for light transmission through a coarsely ground glass surface corresponding to a sample with a near zero value for L. In this case C_{I^2} is nearly independent of angle $\delta\theta$. One actually has $F_1(L\Delta k_{i\perp}) \to 1$ when $L \to 0$. As is seen from the plot C_{I^2} decreases weakly with an increase in $\delta\theta$ due to the finite surface roughness, which was estimated by a microscopic measurement to be about 15 μm.

Curves b and c in Fig. 13 show the results obtained for light transmission through 370-μm- and 810-μm-thick opal glass multiple scattering samples. When fitting the experi-

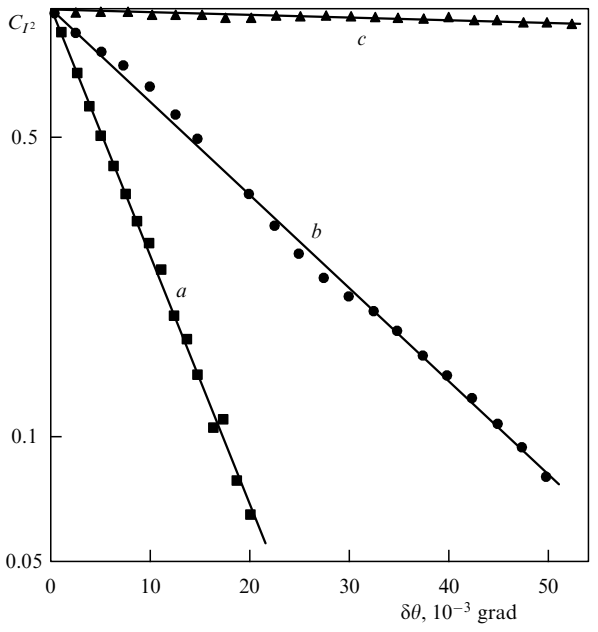

Figure 13. Angular correlation function of transmission for various samples: curve a, 370-μm-thick opal glass; curve b, 810-μm-thick opal glass; c, a coarsely ground glass surface, corresponding to a sample with a near zero value of $L \approx 0$ [31].

mental data the geometric thickness of the sample was substituted by $L - l_{\rm tr}$ since the coherent light passes at least the path of order of $l_{\rm tr}$ before it becomes diffusive. Measuring the light transmission one found $l_{\rm tr} = 100$ μm. The experimental data were fitted by the relationship

$$C_{I^2}(i,\, i',\, s,\, s') \sim \exp\left[-b\Delta k_{i\perp}\,(L - l_{\rm tr})\right],$$

where $\Delta k_{i\perp} \approx k\delta\theta$. It was established that $b = 1.07$ for both the 380-μm and the 810-μm samples. Taking into account that the experimental error could reach 10%, one can assume this parameter to be of the order of unity.

Within the factorisation approximation $C_{I^2} = |C_{E^2}|^2$, Eqn (3.10) gives

$$C_{I^2}(i,\, i',\, s,\, s') \sim \left[\frac{\Delta k_{i\perp} L}{\sinh\,(\Delta k_{i\perp} L)}\right]^2.$$

Although the experiment is performed in the open system one can use the waveguide geometry with the beam diameter taken as the wave guide width W, since the diameter exceeds significantly the sample thickness. Basically, the experiment confirms the theoretical predictions, in particular the dependence of correlation function on scale parameter $\Delta k_{i\perp} L$ and the exponential decay at large $\Delta k_{i\perp} L$.

Nevertheless, there is a significant discrepancy. The theory predicts that $C_{I^2}(\Delta k_{i\perp} L)$ always starts flat then rolls over, and finally decays exponentially. In the experiment the peak does not exhibit the flat region but shows an immediate exponential falloff. This discrepancy can be attributed to the theoretical description within the framework of the waveguide geometry, whereas the experimental system is transversally unconstrained, or to the existence of some additional mechanism for memory loss which needs to be accounted for theoretically.

Using similar consideration the intensity correlation functions were obtained for light reflected from the finite thickness slab [31, 97 – 101]. The normalised correlation function within the factorisation approximation takes the form [97]

$$C^{(R)}_{I^2}(i,\, i',\, s,\, s') = \langle R_{is}\rangle\langle R_{i',s'}\rangle\,\delta_{(\Delta k_{i\perp},\,\Delta k_{s\perp})}\,F_R^2(\Delta k_{i\perp}), \quad (3.11)$$

where $\langle R_{is}\rangle$ is the diffusive light reflection coefficient related to the transmission coefficient $\langle T_{is}\rangle$ by the relationship $\langle R_{is}\rangle + \langle T_{is}\rangle = 1$. Function F_R describing the decrease of the correlation of reflected fields is presented in the form

$$F_R(\Delta k) = \frac{L}{L - l_{\rm ext}}\,\frac{\sinh\,(\Delta k l_{\rm ext})\,\sinh\left[\Delta k(L - l_{\rm ext})\right]}{\Delta k l_{\rm ext}\,\sinh\,(\Delta k L)}. \quad (3.12)$$

With the slab thickness L increasing, $L \to \infty$, the transmission coefficient decreases as L^{-1} and reflection coefficient $\langle R_{is}\rangle \to 1$. It corresponds to the well-known fact that the light incident upon a nonabsorbing heterogeneous medium comes back totally as a diffusive radiation. Eqn (3.11) also predicts the memory effect for the reflected light. However, in this case the memory effect is nonuniversal unlike in the light transmission case. Thus, the correlation depends not only on the geometry of the sample, but also on the degree of disorder which enters Eqn (3.12) through the extinction length.

In Ref. [97] the effect of absorption on the reflection correlation was also taken into account. The absorption is shown to result in changing $\Delta k_\perp$ to $(\Delta k_\perp^2 + L_{\rm a}^{-2})^{1/2}$, where $L_{\rm a}$ is the absorption length. The correlation function decays in this case more slowly and the memory effect becomes more noticeable.

Ref. [99] shows that cyclic diagrams are to be taken into account in the reflection correlation functions. The correlation function can be presented as the sum of four diagram terms

$$C^{(R)}_{I^2}(i,i',s,s') = \begin{array}{|c|}\hline \rm L \\ \hline \rm L \\ \hline \end{array} + \begin{array}{|c|}\hline \rm L \\ \hline \rm C \\ \hline \end{array} + \begin{array}{|c|}\hline \rm C \\ \hline \rm L \\ \hline \end{array} + \begin{array}{|c|}\hline \rm C \\ \hline \rm C \\ \hline \end{array}.$$

Eqn (3.11) describes the contribution of the first term only. Taking into account all four terms one finds

$$C^{(R)}_{I^2}(i,\, i',\, s,\, s') = \text{const}\,\delta_{(\Delta\mathbf{k}_{i\perp},\,\Delta\mathbf{k}_{s\perp})} \times \frac{\left[F_R(\Delta\mathbf{k}_{i\perp}) + F_R(\Delta\mathbf{k}_{i\perp} + \mathbf{k}_{i\perp} + \mathbf{k}_{s\perp})\right]^2}{\left[1 + F_R(\mathbf{k}_{i\perp} + \mathbf{k}_{s\perp})\right]\left[1 + F_R(\mathbf{k}_{i\perp} + \mathbf{k}_{s\perp} - 2\Delta\mathbf{k}_{s\perp})\right]}. \quad (3.13)$$

A new distinctive feature of Eqn (3.13) is that the correlation function exhibits two maxima as the function of angle. The first maximum occurs when two correlating beams are almost coincident i.e. when $\Delta\mathbf{k}_{i\perp} = 0$. With account for the memory effect this corresponds to $\mathbf{k}_{i\perp} = \mathbf{k}_{i'\perp}$ and $\mathbf{k}_{s\perp} = \mathbf{k}_{s'\perp}$. The second maximum occurs around $\Delta\mathbf{k}_{i\perp} = -\mathbf{k}_{i\perp} - \mathbf{k}_{s\perp}$ corresponding to $\mathbf{k}_{i'\perp} = -\mathbf{k}_{s\perp}$, $\mathbf{k}_{s'\perp} = -\mathbf{k}_{i\perp}$. The first maximum occurs due to the ladder diagram contribution and the second one appears due to the cyclic one. Along with the transmission correlation function Freund et al. [31] also studied the reflection angular intensity correlations. Avoiding the specular reflections they used an asymmetric geometry in which the speckle pattern was measured at the reflection angle $\theta_r = 0$ (i.e. along the surface normal) while the laser beam incidence angle was $\theta_i = 30^o$. Fitting an expression of the form

$$C^{(R)}_{I^2}(\Delta k_{i\perp} l_{\rm tr}) \sim \exp(-a\Delta k_{i\perp} l_{\rm tr}),$$

to the experimental data, one again obtains $l_{\rm tr} = 100$ μm and $a = 3$ similar to the transmission case. Comparison of this fitting formula with theoretical equation (3.12) shows the same differences between theory and experiment that were found for transmission.

Besides the angular correlation the correlations of wave with different frequencies were also studied experimentally. Derivation of the frequency correlation function coincides in basically with that of the angular correlation function, however, one has to account explicitly for the frequency dependence of corresponding quantities.

The intensity–intensity correlation function with frequency ω and ω' is defined as

$$C_{I^2}(\omega,\, \omega') = \langle\delta I\,(\omega,\, \mathbf{r})\,\delta I\,(\omega',\, \mathbf{r})\rangle, \quad (3.14)$$

where $\delta I\,(\omega,\, \mathbf{r}) = I\,(\omega,\, \mathbf{r}) - \langle I\,(\omega,\, \mathbf{r})\rangle$ is the intensity fluctuation of light with frequency ω. Correlation function (3.14) approximated similarly to Eqn (3.2) is presented in the form

$$\langle\delta I\,(\omega,\, \mathbf{r})\,\delta I\,(\omega',\, \mathbf{r})\rangle = |\langle\delta E\,(\omega,\, \mathbf{r})\,\delta E^*(\omega',\, \mathbf{r})\rangle|^2, \quad (3.15)$$

where $\delta E\,(\omega,\, \mathbf{r})$ is the scattered field at point $\mathbf{r}$ with frequency ω.

Performing calculations similar to Eqns (3.6) – (3.9) one obtains the correlation function of the transmitted diffusive radiation in the form [32, 83]

$$|\langle E(\omega, \mathbf{r})\, E^*(\omega', \mathbf{r})\rangle|^2 = \\ = \text{const}\,|E_0|^4\, \frac{\cosh(\sqrt{2}\chi\, l_{\text{ext}}) - \cos(\sqrt{2}\chi\, l_{\text{ext}})}{\cosh(\sqrt{2}\chi L) - \cos(\sqrt{2}\chi L)}\,, \quad (3.16)$$

where $\chi = (\Delta\omega D^{-1})^{1/2}$.

As is seen from Eqns (3.9) and (3.16) the angular and frequency intensity correlation functions decay exponentially when the separation between the modes, correlated in frequencies or wave vectors, increases. These equations are derived under the factorisation approximation and describe the most highly fluctuating contributions to the intensity. Indeed the intensity fluctuations appear to be of the order of the intensity itself [28]

$$\frac{\langle(\delta I)^2\rangle}{\langle I\rangle^2} = 1, \quad (3.17)$$

in the case of coincident frequencies or wave vectors. This manifests itself as speckle patterns observed in the multiple light scattering in a heterogeneous medium.

3.2 Long-range intensity correlations

The considered intensity correlations are the fourth order averages of fields. Choosing for definiteness the frequency correlation function one can write

$$\langle I(\omega, \mathbf{r})\, I(\omega', \mathbf{r})\rangle = \int \mathrm{d}\mathbf{r}_1 \ldots \mathrm{d}\mathbf{r}_s\, \mathbf{T}(\omega, \mathbf{r} - \mathbf{r}_5) \\ \times \mathbf{T}^*(\omega, \mathbf{r} - \mathbf{r}_6)\, \mathbf{T}(\omega', \mathbf{r} - \mathbf{r}_7)\, \mathbf{T}^*(\omega', \mathbf{r} - \mathbf{r}_8) \\ \times \mathbf{K}(\omega, \omega'; \mathbf{r}_1, \ldots, \mathbf{r}_8)\, E_0(\omega, \mathbf{r}_1) \\ \times E_0^*(\omega, \mathbf{r}_2)\, E_0(\omega', \mathbf{r}_3)\, E_0^*(\omega', \mathbf{r}_4), \quad (3.18)$$

where function $\mathbf{K}(\omega, \omega'; \mathbf{r}_1, \ldots, \mathbf{r}_8)$ is the sum of all eight-vertex diagrams. The pairwise products of the ladder diagram sums produce the main contribution to this function:

$$\mathbf{K}(\omega, \omega'; \mathbf{r}_1, \ldots, \mathbf{r}_8) \approx \mathbf{L}(\omega, \omega; \mathbf{r}_1, \mathbf{r}_2, \mathbf{r}_5, r_6) \\ \times \mathbf{L}(\omega', \omega'; \mathbf{r}_3, \mathbf{r}_4, \mathbf{r}_7, \mathbf{r}_8) + \mathbf{L}(\omega, \omega'; \mathbf{r}_1, \mathbf{r}_4, \mathbf{r}_5, \mathbf{r}_8) \\ \times \mathbf{L}(\omega', \omega; \mathbf{r}_2, \mathbf{r}_3, \mathbf{r}_6, \mathbf{r}_7), \quad (3.19)$$

where function $\mathbf{L}(\omega, \omega; \mathbf{r}_1, \ldots, \mathbf{r}_4)$ is the sum of usual ladder diagrams and function $\mathbf{L}(\omega, \omega'; \mathbf{r}_1, \ldots, \mathbf{r}_4)$ is the sum of the same diagrams in which the upper and lower lines describe the propagation of the field with frequencies ω and ω', respectively. The first term in Eqn (3.19) leads to the product of mean intensities $\langle I(\omega)\rangle\langle I(\omega')\rangle$ and the second gives the main contribution to the correlation function described in the previous section. Note once more that both terms are equal at coincident frequencies in correspondence with Eqn (3.17).

Besides the diagrams accounted for by Eqn (3.19) one can consider connected diagrams consisting of a greater number of ladder propagators. This means physically that the interaction of different diffusion modes is taken into account in the scattering medium. Such an account produces long-range terms in correlation function [27, 28]. Earlier these diagrams were considered in the electron conduction theory of disordered metals [23, 29, 102, 103].Graphically the higher order diagrams can be obtained by connecting the ladder propagators. Such connection is performed by means of the Hikami vertex function [29]. The diagrams containing the increased number of Hikami vertex functions appear to correspond to the long-range correlations of weaker magnitude. Calculations were performed for the spatial [27] and angular [28] correlations. The contributions of the zeroth, first and second orders in the number of Hikami vertexes into the normalised angular correlation function of intensity $c_{i,i',s,s'} = C_{I^2}(i, i', s, s')/\langle I_0\rangle^2$,

$$c_{i,i',s,s'} = c^{(1)}_{i,i',s,s'} + c^{(2)}_{i,i',s,s'} + c^{(3)}_{i,i',s,s'}\,, \quad (3.20)$$

were found [28].

The number of modes for wave propagation in the waveguide with length L and transversal cross-section $S = W^2$ is $N = (2\pi/\lambda)^2 S$. Feng et al. [28] show that the expansion parameter in Eqn (3.20) is

$$g^{-1} = \left(\frac{N l_{\text{ext}}}{L}\right)^{-1}. \quad (3.21)$$

Such a waveguide randomises these modes during the multiple scattering so that the transmission coefficient $T_{is} = I_{is}/\langle I_0\rangle$ describes the share of intensity I_{is} of incoming mode i which transforms into outgoing mode s. In the case of an infinite slab with modes i and s determined, respectively, by the angles of incidence and scattering one has

$$\langle T_{is}\rangle = \frac{l_{\text{ext}}}{L}\, \cos\theta_i \cos\theta_s\,. \quad (3.22)$$

This formula can be obtained practically from Eqn (3.9) taking $\Delta k_{i\perp} = 0$. Separate terms contributing to the correlation function $c_{i,i',s,s'} = \langle \delta T_{is}\, \delta T_{i's'}\rangle$ are obtained in the form

$$c^{(1)}_{i,i',s,s'} = D_1 \langle T_{is}\rangle\langle T_{i's'}\rangle\, \delta_{(\Delta\mathbf{k}_{i\perp},\, \Delta\mathbf{k}_{s\perp})} F_1^2(\Delta k_{i\perp} L), \quad (3.23)$$

$$c^{(2)}_{i,i',s,s'} = D_2 g^{-1} \langle T_{is}\rangle\langle T_{i's'}\rangle \big[F_2(\Delta k_{i\perp} L) + F_2(\Delta k_{s\perp} L)\big], \quad (3.24)$$

$$c^{(3)}_{i,i',s,s'} = D_3 g^{-2} \langle T_{is}\rangle\langle T_{i's'}\rangle, \quad (3.35)$$

where D_j are constants of the order of unity and

$$F_2(x) = 2x^{-1}\left(\coth x - \frac{x}{\sinh^2 x}\right). \quad (3.26)$$

In the case of a wide waveguide Eqn (3.23) is derived from Eqn (3.9), which has to be squared and normalised. Function $F_1(x)$ is given by Eqn (3.10).

The first order term in g^{-1}, $c^{(2)}_{i,i',s,s'}$, describes the slowly decaying contribution to the correlation function, $c^{(2)} \sim (\Delta k_{l\perp})^{-1}$ where $l = i$ or s. The term of such a form was found for the first time by Stephen and Cwilich [27] for the spatial correlations. Despite the smallness of parameter g^{-1} this contribution turns out to be dominant if $\Delta\mathbf{k}_{i\perp} \neq \Delta\mathbf{k}_{s\perp}$. One can explain intuitively the existence of this term as follows. Falling onto the heterogeneous system under close angles, two beams travel quite close multiple-scattering paths inside the system so that outgoing from the system under different angles they become correlated in intensities, and conversely. This is manifested mathematically as two terms presented in Eqn (3.24).

The third term, $c^{(3)}_{i,i',s,s'}$, describes the uniform positive contribution to the correlations between arbitrary modes

independently of wave vector transfer in the incident or scattered radiation. This term, with an infinite correlation length, corresponds to the universal conductance fluctuations in physics of disordered metals. The magnitude of this term is rather small and its detection turns out to be a rather complicated task. However the following is noteworthy. Summing over all input and output modes (integrating over angles of incidence θ_i and scattering θ_s) one finds term $c^{(3)}$ to be dominant. Indeed, since summation over the mode number produces $\sum \sim N$, and the transmission coefficient can be evaluated as $\langle T_{is}\rangle \sim l_{\rm ext}/L$, one can write the estimates

$$\sum_{\Delta\mathbf{k}_{i\perp}}\sum_{\Delta\mathbf{k}_{s\perp}} c^{(1)} \sim \left(\frac{l_{\rm ext}}{L}\right)^2,$$

$$\sum_{\Delta\mathbf{k}_{i\perp}}\sum_{\Delta\mathbf{k}_{s\perp}} c^{(2)} \sim g^{-1}N\left(\frac{l_{\rm ext}}{L}\right)^2 \sim \frac{l_{\rm ext}}{L},$$

$$\sum_{\Delta\mathbf{k}_{i\perp}}\sum_{\Delta\mathbf{k}_{s\perp}} c^{(3)} \sim g^{-2}N^2\left(\frac{l_{\rm ext}}{L}\right)^2 \sim 1. \qquad (3.27)$$

The latter relationship means the independence of the sample size, i.e. universality of fluctuations.

Thus terms $c^{(1)}$ and $c^{(2)}$ become smaller than $c^{(3)}$ by factors $(l_{\rm ext}/L)^2$ and $l_{\rm ext}/L$ respectively. As is readily seen, summing either the input or output modes, one finds the $c^{(2)}$ term to dominate. Such estimates are valid for angular as well as frequency correlations.

Genack and Drake [32] studied the light transmission intensity for a 40 percent volume dispersion of rutile TiO_2 particles with dimensions (0.25 ± 0.15) μm in polystyrene. The sample was polished to form a wedge so that the thickness L can be varied. The pulse lasers with wave lengths of 514 nm and 581 nm and pulse duration of 90 ps and 6 ps, respectively, were used as the light source.

In Fig.14 the incident pulse and the pulse transmitted through the slab of depth $L = 543$ μm at $\lambda = 581$ nm are shown. The solid line for the transmitted pulse was obtained by convolution of the incident pulse with the transmission function $T(t, L)$. It can be presented within the diffusion approximation in the form [32, 92]

$$T(t,L) = \frac{\exp(-t/\tau_{\rm a})}{\sqrt{4\pi Dt}} \sum_{-\infty}^{\infty}\left\{\exp\left[-\frac{\left((2n-1)L - 2z_0\right)^2}{4Dt}\right] - \exp\left[-\frac{(2n-1)^2L^2}{4Dt}\right]\right\}. \qquad (3.28)$$

Function $T(t, L)$ can be obtained from a series similar to (3.8), by transforming it to the $(\mathbf{r},\ t)$ presentation [92]. Parameter $\tau_{\rm a}$ is introduced to describe the light absorption in the medium due to inelastic processes and is related to absorption length $L_{\rm a}$ with relationship $\tau_{\rm a} = L_{\rm a}^2/D$. Here D is the light diffusion coefficient. In the weak scattering limit one has $D = vl_{\rm tr}/3$. In the study considered parameters $\tau_{\rm a}$ and D were determined from the fit. Terms up to $n = 3$ are sufficient to fit the measurement data. The fit gives $D = (4.5 \pm 0.5)\times 10^5\,{\rm cm^2\,s^{-1}}$ and $\tau_{\rm a} = (243 \pm 40)$ ps for $\lambda = 581$ nm, and $D = (3 \pm 0.4) \times 10^5\,{\rm cm^2\,s^{-1}}$ and $\tau_{\rm a} = (120 \pm 20)$ ps for pulse with wave length $\lambda = 514$ nm. The pulse tail is described by a single exponential law with a characteristic time

$$\tau = \left(\tau_{\rm a}^{-1} + \frac{\pi^2 D}{L^2}\right)^{-1}. \qquad (3.29)$$

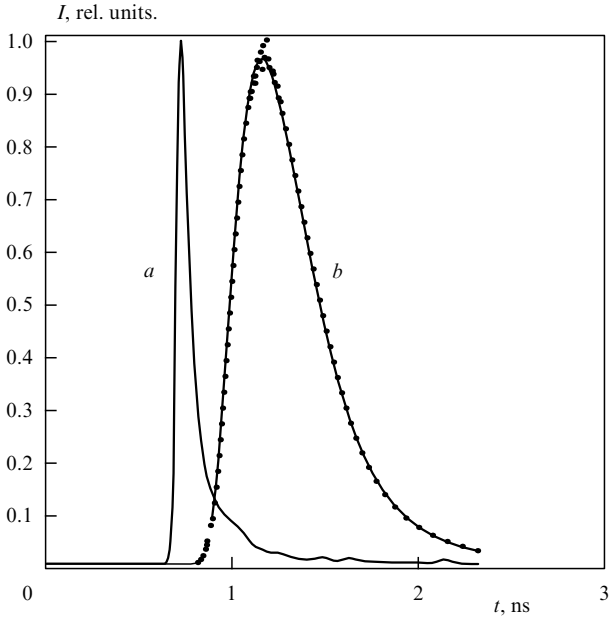

Figure 14. Distribution of time delay for: (*a*) incident pulse and (*b*) pulse transmitted through a 543-μm-thick slab of a 40 volume percent dispersion of (0.25 ± 0.15)-μm-diam TiO_2 particles; points are the measured distribution, smooth line is the convolution of the incident pulse and transmission function using values of D and $\tau_{\rm a}$ as fitting parameters [32].

Analyzing plot τ against L with Eqn (3.29) one obtains $D = (4.7 \pm 0.3) \times 10^5\,{\rm cm^2\,s^{-1}}$ and $\tau_{\rm a} = (293 \pm 40)$ ps, in good agreement with a fit to function $T(t, L)$. The transmission describing the energy transfer through the slab with thickness L is obtained integrating Eqn (3.28) over time to give

$$T(L) = \frac{\sinh(\alpha z_b)}{\sinh(\alpha L)},$$

where $\alpha = L_{\rm a}^{-1} = (D\tau_{\rm a})^{-1/2}$ is the absorption coefficient. In the case of normal incidence for $\alpha = 0$ this equation turns into Eqn (3.22). For $\lambda = 581$ nm one gets $L_{\rm a} = 105$ μm, in agreement with $L_{\rm a} = 112$ μm obtained from the $T(L)$ measurements for $L = 589$ nm [90]. Using formula $D = vl_{\rm tr}/3$ one can get the estimate $l_{\rm tr} = 1.5$ μm in agreement with the $T(L)$ measurements.

These results demonstrate that the temporal distribution and mean energy transfer are well described by diffusion approximation.

Genack and Drake [32] also measured the frequency intensity correlation function. This correlation function was presented in the form

$$C_{I^2}(\Delta\omega,\ L) = \langle \delta I(\omega)\,\delta I(\omega+\Delta\omega)\rangle \sim \left[\frac{\sinh(qz_b)}{\sinh(qL)}\right]^2, \qquad (3.30)$$

where $q = (L_a^{-2} + \Delta\omega/D)^{1/2}$. The measured half-width of correlation function turns out to be given as

$$\frac{(\Delta\omega)^*}{2\pi} = \begin{cases} \dfrac{1.46\,D}{L^2}, & \text{for } L < L_{\rm a}, \\ \dfrac{0.265\,D}{\sqrt{LL_a^3}}, & \text{for } L \gg L_{\rm a}. \end{cases}$$

The measurements were performed at $\lambda = 589$ nm using a single-frequency dye laser for a sample with width 452 μm.

The correlation function, obtained by averaging over eight different speckle spots, is in excellent agreement with the theory.

The frequency intensity–intensity correlation function for transmitted light $\langle \delta T_{is}(\omega)\, \delta T_{i's'}(\omega+\Delta\omega)\rangle$ presented similarly to the case of angular correlations as the sum of three terms (3.20) was studied by van Albada et al. [34]. Term $C^{(1)}(\Delta\omega, L)$ of zeroth order in expansion parameter g^{-1} normalised to the mean intensity of the transmitted diffusive light was written in the form [32, 34]

$$C^{(1)}(\Delta\omega, L) = \frac{x^2}{\cosh(2x) - \cos(2x)}\,, \tag{3.31}$$

where $x = (\Delta\omega/D)^{1/2}L$. It describes the short-range correlation. Eqn (3.31) can be obtained from Eqn (3.16) in the limit $(\Delta\omega/D)^{1/2} l_{\text{ext}} \ll 1$ by changing in argument 2 to $\sqrt{2}$. We retain however notations of Refs [32] and [34] since the measurement data were processed with Eqns (3.30) and (3.31). The long-range correlations are described by function $C^{(2)}(\Delta\omega, L)$ [83]

$$C^{(2)}(\Delta\omega, L) = \text{const}\, g^{-1} x^{-1}\, \frac{\sinh(2x) - \sin(2x)}{\cosh(2x) - \cos(2x)}\,. \tag{3.32}$$

Function $C^{(1)}(\Delta\omega, L)$ was measured by Freund et al.[31] and appeared to be in an excellent agreement with the theory. The same authors also confirmed the memory effect predicted in Ref. [28] .

The long-range contribution $C^{(2)}(\Delta\omega, L)$ into the frequency correlation function was studied in Refs [33, 104]. It was measured in a microwave frequency range. The scattering system presented a set of 1.27-cm-diam polystyrene spheres confined in a copper tube 7.3 cm in diameter and 150 cm in length. The spheres were packed rather densely with 58 volume percent filling fraction. When the tube was rotated new sample configurations were produced. The source frequency varied from 18 to 24 GHz when studying the dependence on the geometry of the system, and was swept from 20.6 to 21.7 GHz in 1000 steps for frequency measurements. The experimental setup scheme is shown in Fig. 15. The radiation receivers were mounted inside the sample and on the face of it provided the separation R between them, which may be.

The frequency correlation function of normalised intensities I_1 and I_2 was measured generally in various points of the sample. This function is presented as products of the frequency and spatial correlation functions

$$C_{I^2}(\Delta\omega, R) = \sum_{i=1,2} A_i\, g^{1-i}\, F_i(\Delta\omega)\, H_i(R)\,. \tag{3.33}$$

The normalised frequency functions F_i were obtained by generalising Eqns (3.10) and (3.26) to the case of the frequency correlations. They are presented in the form [33]

$$F_1(\Delta\omega) = \left(\frac{\sinh(qz_b)\sinh(\alpha L)}{\sinh(\alpha z_b)\sinh(qL)}\right)^2, \tag{3.34}$$

$$F_2(\Delta\omega) = B_1 F_1(\Delta\omega) + B_2 \bar{F}_2(\Delta\omega)\,, \tag{3.35}$$

where

$$\bar{F}_2(\Delta\omega) = \frac{(\alpha/a)\left[\coth(qL) - qL/\sinh^2(qL)\right]}{\coth(\alpha L) - \alpha L/\sinh^2(\alpha L)}\,, \tag{3.36}$$

$q^2 = \alpha^2 + \Delta\omega D^{-1}$, and coefficients A_i are parameters of the order of unity. Functions F_i and H_i are normalised to satisfy requirements $F_i = H_i = 1$ at $\Delta\omega = 0$ and $R = 0$. The spatial correlation function $H_1(R)$ was found in Refs [26, 27]:

$$H_1(R) = \left(\frac{\sin(kR)}{kR}\right)^2 \exp\left(-\frac{R}{l_{\text{tr}}}\right).$$

Function H_1 decays due to field randomisation at the scale of the wavelength order. The higher order functions decay slower and therefore contribute mainly to correlation function $C_{I^2}(\Delta\omega, R)$ at $R \gg \lambda$ and are especially large when the parameter g is small. Function $\bar{F}_2(\Delta\omega)$ decays asymptotically as $\Delta\omega^{-1/2}$.

The auto-correlation function for the 140-cm-length sample is plotted in Fig.16. The solid line is a plot of Eqn (3.34) with measured values $D = -3.1 \times 10^{10}\,\text{cm}^2\,\text{s}^{-1}$ and $L_a = 25$ cm. The high frequency part is seen to decay as $\Delta\omega^{-1/2}$.

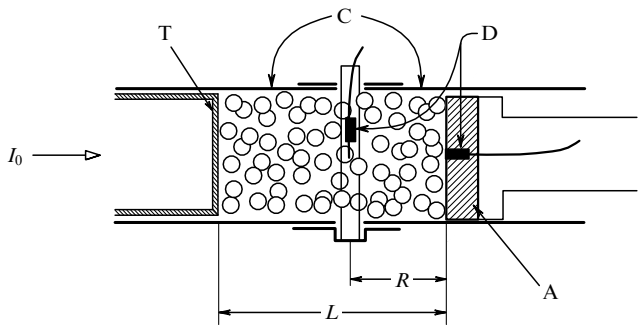

Figure 15. Schematic diagram of experimental setup for the frequency and spatial correlation function $C_{I^2}(\Delta\omega, R)$ measurements: I_0, incident radiation; T, plastic tube; C, copper cylinders; D, diode detectors; and A, absorber [33, 104].

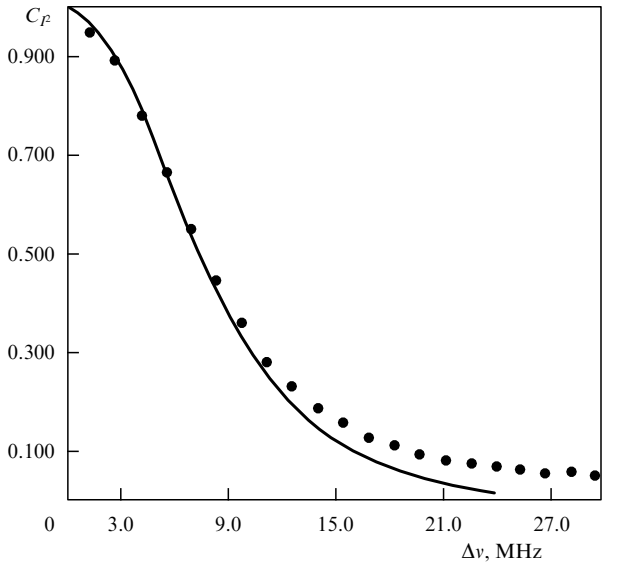

Figure 16. Frequency correlation function (points) for a 140-cm-thick sample, the solid line is a plot of Eqn (2.34) describing the short-range term of correlation function [33].

For more successive extraction of this high-frequency contribution the correlation function was measured for $R = 4$ cm and $R = 20$ cm when the term with F_1 can be neglected since the distance $R = 4$ cm exceeds by far the radiation wavelength. In the case of $R \geqslant 4$ cm the results were averaged over 1500 spectra and in the case of $R = 20$ cm the averaging was over 2800 spectra. In Fig.17 the results are plotted averaged over 11000 spectra for $R = 4, 6, 8, 10$ and 20 cm. It is seen that $C_{I^2}(\Delta\omega, R)$ does not depend on R for $4\,\text{cm} \leqslant R \leqslant 20\,\text{cm}$. The results calculated by means of Eqn (3.35) with coefficients $B_1 = 0.46$ and $B_2 = 0.54$ are shown by dots.

The auto-correlation function $C_{I^2}(\Delta\omega, R = 0)$ for $L = 150$ cm averaged over 3×10^4 spectra is described rather well by Eqn (3.33) with parameters $A_1 = 0.90$, $D = (0.30 \pm 0.2) \times 10^{10}\,\text{cm}^2\,\text{s}^{-1}$ and $A_2 g^{-1} = 0.13$. The transport length is $l_{\text{tr}} = 3D/v = (4 \pm 0, 2)$ cm. The dependence of the spatial correlation function $C_{I^2}(\Delta\omega = 0, R)$ on R is also studied there. In the case of large values of R function $C_{I^2}(R) = C^{(2)}(R)$ can be presented in the form

$$C^{(2)}(R) = g^{-1} f\left(\frac{R}{L}\right),$$

where function $f(R/L)$ means the path share of photons which achieve the output plane at distance L from the source if they have passed the plane at distance $L - R$. In the given geometry $f(R/L)$ depends linearly on R

$$f\frac{R}{(L)} = 1 - \gamma l_{\text{tr}} L^{-1} - (1 - 2\gamma l_{\text{tr}} L^{-1})\ \frac{R}{L}.$$

Function $C_{I^2}(R)$ actually appears in the experiment to be a straight line. Parameter γ was found from the slope to be $\gamma = 1.93$. For parameter g one obtains $g = 21 \pm 2$. This value corresponds rather well to the results obtained from measuring the frequency correlation function. The frequency intensity correlations were studied experimentally [34, 92] for coherent light transmitted through a disordered system. A wide frequency mode dye laser was used as the light source. The radiation frequency was varied by rotating a birefracting filter automatically connected with a computer. The total transmission intensity fluctuations for different wavelengths were measured in a sphere for summation over all output angles. Statistical data were accumulated by means of the spatial translation of the sample. The TiO_2 pigment suspended in chloroform was used as the scattering system. Such suspension was evaporated upon the transparent substrate. The sample thickness was measured after vaporisation of chloroform by a microscope. The TiO_2 volume fraction in the samples was 36%. The single scan intensity fluctuations were in the range from 0.6% to 28% of the total intensity.

Measuring the short-range part of correlation function $C^{(1)}_{I^2}(\Delta\omega)$ for samples of different thickness the diffusion coefficient D was determined. The frequency behaviour of the long-range part of correlation function $C^{(1)}_{I^2}(\Delta\omega)$ was found to be universal independently of the sample thickness.

A system of noninteracting spherical scatterers with a self-diffusion coefficient D_s was considered by Pine et al. [19]. In the case of light transmitted through a wide slab of thickness L the temporal correlation function was obtained quite similarly to the spatial and frequency ones in the form

$$C_{E^2}(t) = \frac{L}{\gamma l_{\text{tr}}}\ \frac{\sinh\left[\gamma(6t/\tau_0)^{1/2}\right]}{\sinh\left[(L/l_{\text{tr}})(6t/\tau_0)^{1/2}\right]} \approx \frac{(L/l_{\text{tr}})(6t/\tau_0)^{1/2}}{\sinh\left[(L/l_{\text{tr}})(6t/\tau_0)^{1/2}\right]}, \tag{3.37}$$

where the second holds for $t \ll \tau_0$. Quantity $z_0 = \gamma l_{\text{tr}}$ was defined in Ref. [19] as the depth where the light propagation turns to be diffusive unlike in Ref. [27], where $\gamma = 1$.

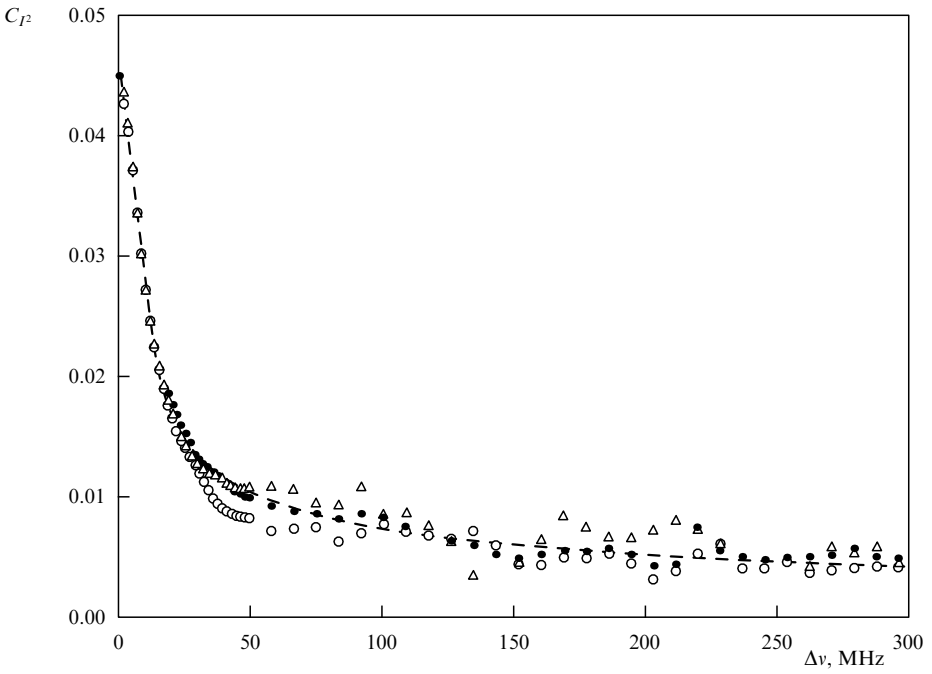

Figure 17. Frequency correlation functions of intensities between points separated by distance R: △ — $R = 4$ cm; ○ — $R = 20$ cm; •, average for $\leqslant R \leqslant$ cm [104].

Auto-correlation intensity function $C_{I^2}(t)$ was measured for a system of 0.497-μm-diam polystyrene latex spheres at a volume fraction $C = 10^{-2}$ for light transmitted through the 2-mm-thick slab. Light from a 488-nm laser was focused on a spot of ≈50-μm diam, and the scattered light was collected from a 50-μm-diam circle. The measurement data were processed using Eqn (3.37) with $\tau_0 = 3.73$ ms obtained from the single-scattering spectrum analysis at concentration $C = 10^{-5}$. Using experimental data the transport length was found to be $l_{tr} = 144$ μm. A discrepancy is admitted in Ref. [19] between the l_{tr} values obtained by means of the diffusing-wave spectroscopy method and by measuring the half-width of the coherent backscattering. In the latter case $l_{tr} = 200$ μm for the same concentration of particles of somewhat smaller size.

The auto-correlation function for diffusive light reflected by a slab in the backward direction was also studied there. The temporal correlation function for this case is as follows [19]

$$C_{E^2}^{(R)}(t) = \frac{1}{1 - \gamma l_{ext}/L} \frac{\sinh\left[(L/l_{tr})(6t/\tau_0)^{1/2}(1 - \gamma l_{tr}/L)\right]}{\sinh\left[(L/l_{tr})(6t/\tau_0)^{1/2}\right]} \approx \exp\left[-\gamma\,(6t/\tau_0)^{1/2}\right]. \quad (3.38)$$

This equation is valid for $L \gg l_{tr}$ i.e essentially for half-space. The intensity auto-correlation functions were also studied [19] for slabs of various thickness. To select the multiple scattered light the depolarised component was measured. The measurement data coincide practically with results calculated using Eqn (3.38) with $\gamma = 2$ and $l_{tr} = 143$ μm found from the transmission correlation function measurements.

The results of the frequency correlation function measurements were reported to contradict the diffusion approximation [84]. Later on these results were not confirmed [94, 105, 106], however.

The interesting results were obtained recently studying quasiperiodic structures [107, 108]. Earlier, when considering a similar problem in semiconductors the electron localisation was shown to take place not only in disordered systems but also in partially ordered quasiperiodic ones [109 – 111]. In particular, the one-dimensional Schrodinger equation was studied [109, 110] for the structure with incommensurate periods. The periods were given using the Fibonacci numbers. In this case the exponentially decaying strong localisation changes to localisation with a somewhat slower law of decay. The transmittance was measured [107, 108] for quasiperiodic multilayered dielectric consisting of thin layers of SiO_2 and TiO_2. The number of layers of specific kind were ordered by Fibonacci numbers. An elementary layer depth is chosen so that the layers become quarterwave plates for the support wave. The transmission for such layered structure was measured as a function of the wavelength for the Fibonacci sequence from S_4 to S_9. The wavelength intervals opaque for the transmitted light were found. The location of these intervals correlates with the Fibonacci numbers and agrees fairly well with the theory predictions [112].

The problem of localisation of an object placed in a heterogeneous medium was considered in Ref. [113]. The intensities of the transmitted and scattered light were measured shifting a receiver along the surface of a slab which contains 220-nm-diam TiO_2 particles suspended in glycerine. The transport length was determined from the measured extinction length using the Mie formulas. The object was a metal wire with diameter 350 μm parallel to the layer surface and perpendicular to the direction of the receiver shift. The measurement data agree fairly well with calculation results obtained within the framework of the diffusion approximation.

3.3 Frequency correlations and radiation transfer velocity

While conducting experiments on the frequency and temporal correlation functions, van Albada et al. [35] obtained for the quantity $v = v_{tr}$, entering the definition of the light diffusion coefficient $D = l_{tr}v_{tr}/3$ and having sense of the radiation transfer velocity, the result $v_{tr} \approx 0.1n^2c$, which is one order of magnitude less than light velocity c. Garcia, Genack and Lisyansky [114] found $v_{tr} = 1.86 \times 10^{10}$ cm s^{-1} which is 25% less than the phase velocity. The problem of determining v_{tr} by means of independent measurements of l_{tr} and light diffusion coefficient D was studied in Ref. [35].

The measurements were performed in a sample consisting of a fine TiO_2 powder in air with mean particle size of 220 nm. The transport length was determined by two different static techniques. The first one, which involved measuring of the cone of coherent backscattering, gave two values of l_{tr}, calculated from the half-width of the peak and from parameters of its triangle form, yielding 0.66 ± 0.03 μm and 0.58 ± 0.04 μm, respectively, at light wavelength of 633 nm. The second one invoked measurement of the energy transfer through a heterogeneous slab. For slabs of thickness L with $l_{tr} \ll L \ll L_a$, where L_a is the absorption length, the total transmission is given by $\langle T_{is}\rangle = \gamma l_{tr}/(L + \gamma l_{tr})$. Estimate $\gamma = 2.1$ was obtained by means of numerical simulation, differing somewhat from the value for scalar isotropic scattering. The total transmission $\langle T_{is}\rangle$ was measured as a function of the slab thickness at light wavelength of 633 nm. Value $l_{tr} = 0.57 \pm 0.05$ μm was found from the slope of the plot in agreement with the coherent backscattering data. Since the absorption length of about 80 μm is much larger than l_{tr}, it does not need to be taken into account.

The diffusion coefficient D and time τ of radiation transfer through a distance of the l_{tr} order, $\tau = l_{tr}^2/(3D)$, was determined measuring the frequency correlation function [35]. Using a dye laser as the source, the intensity correlation function $C_{I^2}(\Delta\omega)$ was studied over the wavelength range between 585 and 630 nm. In the backscattering geometry for $L \gg l_{tr}$ the decay of the correlation function $C_{I^2}^{(R)}(\Delta\omega)$ depends solely on time τ. In transmission geometry, the decay of $C_{I^2}(\Delta\omega, L)$ depends on values of D, L and l_{tr}. Function $C_{I^2}^{(R)}$ was written as follows [35]

$$C_{I^2}^{(R)}(\Delta\omega) = \left(\frac{B}{B - 1 - \gamma/2}\right)^2 \times \frac{\cosh\left[(B - 1 - \gamma/2)\,y\right] - \cos\left[(B - 1 - \gamma/2)\,y\right]}{\cosh(By) - \cos(By)}, \quad (3.39)$$

and $C_{I^2}(\Delta\omega, L)$ defined by Eqn (3.16) was presented at small values of argument y in the form

$$C_{I^2}(\Delta\omega, L) = \frac{B^2y^2}{\cosh(By) - \cos(By)}, \quad (3.40)$$

where $B = \gamma + L/l_{tr}$ and $y = (6\Delta\omega\tau)^{1/2}$.

As is seen from Eqn (3.40) the backscattering intensity correlation function decays at large $\Delta\omega$ values as $\exp\left[-(1 + \gamma/2)(6\Delta\omega\tau)^{1/2}\right]$. From a series of measurements using samples with L values ranging from 8 to 200 μm, one founds $\tau = (12.3 \pm 2.1)$ fs.

Using the experimental plot of half-width of the correlation function against L the diffusion coefficient is found to be $D = (11.7 \pm 1.0)\,\mathrm{m^2\,s^{-1}}$. Combining τ and D one determines the transport length $l_{\mathrm{tr}} = (3D\tau)^{1/2}$ to be within interval $0.57\ \mu\mathrm{m} \leqslant l_{\mathrm{tr}} \leqslant 0.74\ \mu\mathrm{m}$, in good agreement with the value of $l_{\mathrm{tr}} = 0.6\,\mu\mathrm{m}$ obtained from the static experiment. With these values the radiation transfer velocity turns out to be equal to $v_{\mathrm{tr}} = l_{\mathrm{tr}}/\tau = (5 \pm 1) \times 10^7\ \mathrm{m\,s^{-1}}$, with the ratio v_{tr}/c being about 0.16 ± 0.03. Thus v_{tr} coincides neither with the group, nor phase velocity.

A similar result was obtained by Kawato et al. in Ref. [115] where the radiation transfer velocity was studied in four porous glass samples with the pore radius within interval from 0.15 μm to 0.5 μm and the volume concentration of pores about 50%. The value of v_{tr} was determined from the relationship $D = v_{\mathrm{tr}} l_{\mathrm{tr}}/3$. The transport length was found measuring the angular dependence of coherent backscattering. The diffusion coefficient was obtained studying the transformation of the light pulse transmitting through a porous glass slab. As is seen from the measurements the transport length and diffusion coefficient grow approximately linearly with increase of the pore size while their ratio remains constant. The radiation transfer velocity turns out to be about 60% of the phase light velocity in glass for all four samples.

The problem of significant difference between v_{tr} and c/n is discussed in Refs [35, 116 – 120]. The authors of Refs [35, 116] start with the scalar wave equation

$$\left(\Delta - \epsilon(\mathbf{r})\ \frac{1}{c^2}\ \frac{\partial^2}{\partial t^2}\right) E(\mathbf{r}, t) = 0\,. \tag{3.41}$$

The formal solution for Green's function of this equation in the $(\Omega, \mathbf{k})$ representation can be written in the form

$$T(\Omega, \mathbf{k}) = \left[\Omega^2 c^{-2} - k^2 - \sum\,(\Omega, \mathbf{k})\right]^{-1}, \tag{3.42}$$

where $\sum(\Omega, \mathbf{k})$ is the kernel, or polarisation operator, of the respective Dyson equation.

One can write the Bethe–Salpeter equation [14, 121] for the coherence function $\langle E(\mathbf{r}_1, t_1)\, E^*(\mathbf{r}_2, t_2)\rangle$. Performing the Fourier transformation over spatial variables and Laplace transformation over temporal variables, one obtains the equation for spectrum $\Phi_{\mathbf{k}}(\mathbf{q}, \omega\,|\Omega)$ of the coherence function in the form

$$\begin{aligned}\left[-2\Omega\omega c^{-2} + 2\mathbf{q}\cdot\mathbf{k} + \sum(\Omega^+, \mathbf{k}^+) - \sum(\Omega^-, \mathbf{k}^-)\right] \\ \times\ \Phi_{\mathbf{k}}(\mathbf{q}, \omega\,|\Omega) = \Delta T(\mathbf{q}, \omega\,|\Omega, \mathbf{k}) \\ \times \left[1 + \sum_{\mathbf{k}'} U_{\mathbf{k}\mathbf{k}'}(\mathbf{q}, \omega\,|\Omega)\ \Phi_{\mathbf{k}'}(\mathbf{q}, \omega\,|\Omega)\right],\end{aligned} \tag{3.43}$$

where $U_{\mathbf{k}\mathbf{k}'}(\mathbf{q}, \omega)\,|\Omega)$ is the kernel of the Bethe–Salpeter equation, $\Delta T = T(\Omega^+, \mathbf{k}^+) - T(\Omega^-, \mathbf{k}^-)$ is the difference between the advanced and retarded Green functions, $\Omega^{\pm} = \Omega \pm \omega/2 \pm \mathrm{i}\eta$ with $\eta \to 0$, and $\mathbf{k}^{\pm} = \mathbf{k} \pm \mathbf{q}/2$. On deriving the macroscopic parameters Eqn (3.43) is to be considered as usually in limit $\mathbf{q}, \omega \to 0$. Defining the densities of energy and energy flux and relating them by the continuity equation, one introduces the energy transfer velocity. The energy density is defined as

$$\Theta(\mathbf{q}, \omega) = \frac{1}{4\pi} \int \mathrm{d}\Omega_{\mathbf{k}} \Phi_{\mathbf{k}}(\mathbf{q}, \omega\,|\Omega)\,,$$

where $\int \mathrm{d}\Omega_{\mathbf{k}}$ means integration over all directions of vector $\mathbf{k}$. The energy flux density is defined as

$$\mathbf{J}(\mathbf{q}, \omega) = v_{\mathrm{tr}} \int \frac{\mathrm{d}\Omega_{\mathbf{k}}}{4\pi}\ \frac{\mathbf{k}}{k}\ \Phi_{\mathbf{k}}(\mathbf{q}, \omega\,|\Omega),$$

where parameter v_{tr} takes the meaning of the energy transfer velocity.

Integrating Eqn (3.43) over directions of vector $\mathbf{k}$ and requiring the energy density Θ and energy flux density $\mathbf{J}$ to satisfy the continuity equation

$$\omega\Theta(\mathbf{q}, \omega) - \mathbf{q}\cdot\mathbf{J}(\mathbf{q}, \omega) = \mathrm{const},$$

one obtains for velocity v_{tr} in the lowest order of scatterer density ρ_{sc}

$$v_{\mathrm{tr}} = \frac{c^2}{v}\left[1 - \rho_{\mathrm{sc}}\ \frac{\mathrm{d}}{\mathrm{d}k^2}\ \mathrm{Re}\, f_{\mathbf{k}\mathbf{k}} + \rho_{\mathrm{sc}} \int \mathrm{d}\Omega_{\mathbf{k}'}\ \frac{\mathrm{d}\sigma}{\mathrm{d}\omega_{\mathbf{k}'}}\ \frac{\mathrm{d}\phi}{\mathrm{d}\mathbf{k}'}\right]^{-1}, \tag{3.44}$$

where $\mathrm{d}\sigma/\,\mathrm{d}\Omega_{\mathbf{k}'} = |f_{\mathbf{k}\mathbf{k}'}|^2/(4\pi)^2$ is the differential cross-section of scattering in the $\mathbf{k}$ direction and ϕ is the phase of the scattering amplitude $\phi_{\mathbf{k}\mathbf{k}'} = |f_{\mathbf{k}\mathbf{k}'}|\exp(\mathrm{i}\phi)$. Estimates obtained by means of Eqn (3.44) give [35, 116] $v_{\mathrm{tr}}/c = 0.18$, in agreement with experimental value $v_{\mathrm{tr}}/c = 0.16 \pm 0.03$.

When calculating v_{tr} within the small density approximation a similar approach was developed [118, 122] based also on the Bethe–Salpeter equation and supplemented additionally with the Ward–Takahaki identity [123]. The authors of Refs [118, 122] claimed that the radiation transfer velocity is renormalised similarly to the phase velocity. Thus, the problem of the true radiation transfer velocity remains open especially in the case of finite density of scatterers.

4. Scattering from rough surfaces

Along with the backscattering from a bulk system much attention has recently been paid to theoretical and experimental studies [38 – 42] of enhanced backscattering from very rough surfaces [36 – 42, 94, 124 – 132], whose standard deviation of surface height is of the order of the wavelength of the incident radiation or larger, and the rms surface slope is of the order of unity. Mendez and O'Donnell [36, 37] observed for the first time the backscattering enhancement from the high-sloped Gaussian rough surfaces with the rms surface height exceeding several times the wavelength. To exclude the contribution of the bulk scattering they used metallic surfaces with two-dimensional roughness distribution. One- and two- dimensional rough surfaces were studied by Kim et al. [126] and surfaces with fractured dimensionality were considered by Jordan and Moreno [132]. An exact solution of Maxwell's equations for such a surface is quite complicated [133-138]. However, significant progress has been made [38, 39, 41, 125, 139 – 142] using numerical methods. The angular dependence of the polarised light scattering from a metallic surface with a non-Gaussian roughness distribution was calculated numerically [126]. The scattering of the *s*- or *p*- polarised light incident normally upon a rough metal surface was numerically simulated [142], using various forms of a power law of the roughness height spectrum. As has been shown, a variation of the form of spectrum can significantly change the angular dependence of

scattering but cannot cancel the effect of the backscattering enhancement itself caused by multiple surface scattering.

4.1 Surface backscattering enhancement

As a rule one uses the Kirchhoff approximation [50, 143] for an analytical description of scattering from a rough surface. Under this approximation the field at some point on a surface is substituted by the field in the tangential plane passing through this point [144 – 148]. This approximation was used by Ishimaru and Chen [39] to separate the single- and double-scatterings and later was developed in Ref. [41]. Shadow function models were developed in Refs [39, 144, 146] which make it possible to successfully apply the theory to the case of high roughness.

One observes the mean scattering intensity $\langle|\delta E|^2\rangle$ which can be presented as the sum of the first and second order contributions

$$\langle|\delta E|^2\rangle = \langle|E_{\mathrm{KA1}}|^2\rangle + \langle|E_{\mathrm{KA2}}|^2\rangle\,, \tag{4.1}$$

where E_{KA1} and E_{KA2} are the fields scattered from the rough surface in the first and second orders of the Kirchhoff approximation respectively. As shown in Refs [38, 39] the cross-over terms $\langle|E_{\mathrm{KA1}}\,E_{\mathrm{KA2}}|^*\rangle$ are negligible. Quantity $\langle|E_{\mathrm{KA2}}|^2\rangle$ can thus be presented in the form [39]

$$\langle|E_{\mathrm{KA2}}|^2\rangle = S(\theta_i)\,S(\theta_s)\int \mathrm{d}k_{1z}\int \mathrm{d}k'_{1z}\langle JJ^*\rangle \times S_p(\alpha)\,S_p(\alpha'), \tag{4.2}$$

where average $\langle JJ^*\rangle$ means the radiation transfer propagator for the problem considered within the double scattering approximation. Angles α and α' determine the intermediate wave vectors between two scattering events,

$$\tan\alpha = \frac{k_{1z}}{k_{1x}}\,, \qquad \tan\alpha' = \frac{k'_{1z}}{k'_{1x}}\,,$$
$$k_{1x} = \sqrt{k^2 - k_{1z}^2}\,, \qquad k'_{1x} = \sqrt{k^2 - (k'_{1z})^2}\,.$$

Quantity $\langle JJ^*\rangle$ can be presented as the sum of the ladder and cyclic diagrams. The cyclic diagram contribution $\langle JJ^*\rangle^{(\mathrm{C})}$ is obtained in the form [39]

$$\langle JJ^*\rangle^{(\mathrm{C})} \sim \exp\left[-\frac{D^2}{8}\,(k_{ix} + k_{sx} + k'_{1x} - k_{1x})^2\right]. \tag{4.3}$$

Functions $S(\theta)$ and $S_p(\alpha)$ and parameter D are introduced to describe the shadow regions arising in the theory of wave reflection from the rough surface [143, 144, 149].The shadow function $S_p(\alpha)$ is given explicitly by Ishimaru and Chen [40]. It presents the probability that the beam with the given direction of the wave vector does not cross the surface. Thus the difference $1 - S(\alpha)$ is the probability that the beam will cross the surface hence causing double scattering to occur. For $\alpha < 0$ all reflected beams cross the surface. Parameter D is the mean distance which is travelled by the wave between scattering events. In particular from calculations it follows that $D = 11.13\lambda_R$ for a sinusoidal rough surface, where λ_R is the average wavelength of the roughness spectrum.

Eqn (4.3) describes the scattering peak in the backward direction $\mathbf{k}_i + \mathbf{k}_s = 0$. The angular width of the peak is determined approximately as follows

$$\Delta\theta \approx 2\,\frac{\sqrt{2}\lambda}{\pi D} \approx \frac{\lambda}{12\lambda_R}\,. \tag{4.4}$$

The ladder diagram contribution $\langle JJ^*\rangle^{(\mathrm{L})}$ is not written since it does not contain the backscattering peak. These results were compared with calculations performed by the Monte-Carlo method for electromagnetic wave. A good agreement between numerical and analytical results was obtained [129]. Numerical calculations predict for perfectly conducting surfaces [130] that the backscattering enhancement is to be for the TE as well as TM waves. The form of the peak depends on the incidence angle and parameters σ/λ and λ_R/λ. The same results are valid for a dielectric with a large imaginary part of permittivity. Comparative calculations were performed for the Gaussian, $W(K)$, and non-Gaussian, $W_n(K)$, roughness spectra. These distribution functions were presented in the form

$$W(K) = \frac{\sigma^2\lambda_R}{2\sqrt{\pi}}\exp\left(-\frac{K^2\lambda_R^2}{4}\right)$$

and

$$W_n(K) = \frac{\sigma^2\lambda_R}{2\sqrt{\pi}}\left[1 + \pi\left(\frac{(2n-3)!!}{(2n-2)!!}\right)^2\left(\frac{K^2\lambda_R^2}{4}\right)\right]^{-n}.$$

For comparison the spectra were normalised as follows

$$\int_{-\infty}^{\infty} W(K)\,\mathrm{d}K = \int_{-\infty}^{\infty} W_n(K)\,\mathrm{d}K = \sigma^2\,.$$

Numerical calculations predict the backscattering peak to be more prominent for the non-Gaussian spectrum. Experimental studies of backscattering were performed on the statistically one-dimensional very rough conducting surface [129]. The millimetre-wave scattering was investigated. The radiation source was placed at a distance of 50 cm away from the surface. The illuminated area presented a 9-cm-diam circle. The TE and TM polarisations were studied. The roughness spectrum was Gaussian with $\sigma/\lambda \approx \lambda_R/\lambda \approx 1$. Data were averaged over about 10^3 scans of the sample surface at three different incidence angles 0°, 20°, and 40°. The peaks manifest themselves distinctly in all cases except for the TM wave at an incidence angle of 40°.

Enhanced backscattering was experimentally studied by Jordan and Moreno [132] on multiscale surfaces whose roughness spectrum could not be described by the Gaussian with one characteristic parameter. Strongly distorted aluminium foil was used as the sample. The surface roughness is described by the height fluctuation σ, rms surface slope, and structure height function

$$S(\delta\mathbf{r}_\perp) = \left\langle\left(h\,(\mathbf{r}_\perp + \delta\mathbf{r}_\perp) - h\,(\mathbf{r}_\perp)\right)^2\right\rangle, \tag{4.5}$$

where $h(\mathbf{r}_\perp)$ is the surface deviation at point $(\mathbf{r}_\perp, z = 0)$. In general, for a fractal, function $S(\delta)$ is related to the surface parameters by

$$S(\delta) = L^{2-v}|\delta|^v - B\delta^2\,, \tag{4.6}$$

where v is the fractal dimensionality index of the surface profile and L is the horizontal distance over which the chord connecting two points on the surface has an rms unity slope. Coefficient B depends on the fractal dimensionality of the characteristic length in the roughness spectrum. The second term in Eqn (4.6) is nonessential while $v < 2$. Analyzing $\ln S$ as function of $\ln\delta$ one sees that in the range of length δ from

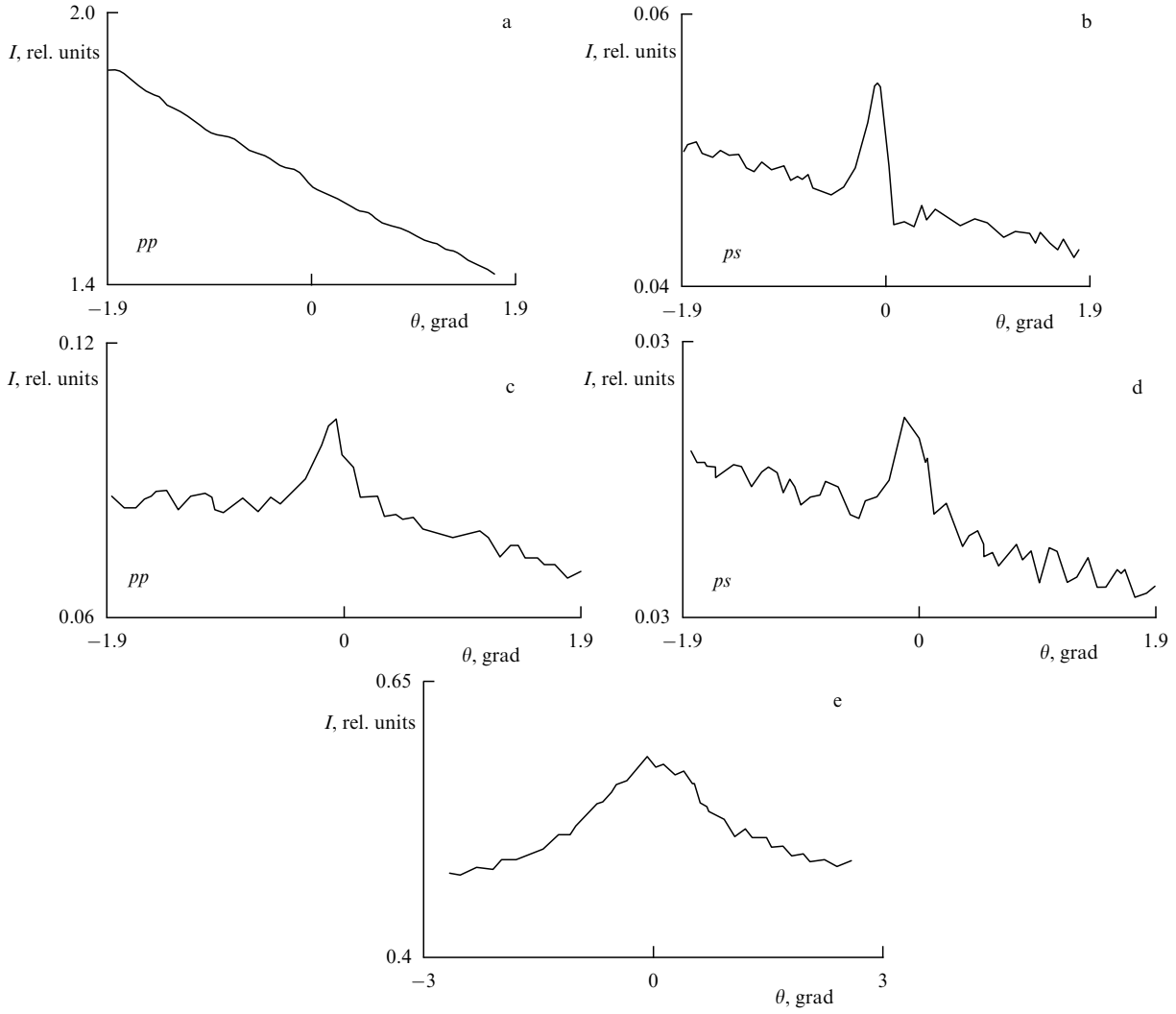

Figure 18. Angular dependence of the scattered radiation of *pp* and *ps* polarisation for the visible light ($\lambda = 0.633$ μm) at various incidence angles θ_i: (a) and (b), $\theta_i = 5°$; (c) and (d), $\theta_i = 83$. (e) is the same for a CO_2 infrared laser radiation ($\lambda = 10.6$ μm) at $\theta_i = 70°$ The scattered angle is measured from the angle of incidence [132].

1 μm to 100 μm it is linear with the slope equal to 1.94. This value differs slightly from the marginal fractal dimensionality $v = 2$. Experiments were performed with several samples each of them being characterised by the structure function index v invariable at least in the range of two decades.

The intensity of reflected light was measured using a setup similar to that shown in Fig. 3. The He-Ne laser was used as the light source. Its beam was widened up to 10 mm and passed through a half-wave plate to enable the polarisation plane to be changed. The light emerging from the splitter falls upon the rough surface. The reflected light passes once more through the splitter and reaches the detector. For sufficient angular resolution to be ensured, a 30-cm focal length lens and a 200 μm pinhole are placed between the splitter and the detector. The waves of *s*- and *p*-polarisations can be registered by the polariser. The measurements have been performed for different parts of the sample. The similar setup was used for infrared measurements with a CO_2 laser at a wavelength of 10.6 μm as the light source. Intensity as a function of angle is plotted in Figs 18, a–d, in visible region for *pp* and *ps* polarisations (the first and second indices refer to the incident and scattered waves, respectively) of light scattered from the surface with $\sigma = 50$ μm and mean slope $\Delta_q = 20°$. The angles of incidence were 5° and 83°. The enhancement of backscattering is clearly present except for the case of *pp* polarisation at 5° angle of incidence. The backscattering peaks exhibit opposite angular dependence for *pp* and *ps* polarisations. The peak for *pp* polarisation increases and peak for *ps* polarisation decreases with increase of the angle of incidence. In Fig. 18d the infrared backscattering peak is plotted for incidence angle of 70°. In this case the peak appears to be significantly wider. However this width is still two times less than that predicted by Jakeman [150, 151] who used a simple relationship between wave lengths.

4.2 Angular correlations of intensities at scattering from a rough surface

Backscattering enhancement appears to be the most obvious but not unique consequence of multiple scattering from a rough surface. There may be equally significant effects on other fundamental quantities such as the correlation functions of intensities. Knotts et al. [41, 152] measured the angular intensity correlation functions for light scattered from a one-dimensionally rough conducting surface. The

angular field correlation function can be presented in the form

$$C_{E^2}^{(\alpha,\beta)}(\theta_{i1},\theta_{s1},\theta_{i2},\theta_{s2}) = \left\langle E_\alpha(\theta_{i1}\to\theta_{s1})\, E_\beta^*(\theta_{i2}\to\theta_{s2})\right\rangle, \tag{4.7}$$

where θ_i and θ_i are the incidence angles, θ_s and θ_s are the scattering angles, and α and β are the field polarisations. Contrary to bulk multiple scattering, in the case of reflection the polarisation effects are always to be accounted for. As was shown in Refs [153, 154] the angular correlation function can be nonzero only for angles satisfying the relationship

$$\sin\theta_{i1} - \sin\theta_{s1} = \sin\theta_{i2} - \sin\theta_{s2} \tag{4.8}$$

for one-dimensionally rough surfaces. This relationship is analogous to the 'conservation law' (3.5) for the bulk scattering and thus verifies the memory effect for scattering from rough surfaces. The intensity correlation function,

$$C_{I^2}^{(\alpha,\beta)}(\theta_{i1},\theta_{s1},\theta_{i2},\theta_{s2}) = \left\langle \delta I_\alpha(\theta_{i1}\to\theta_{s1})\,\delta I_\beta(\theta_{i2}\to\theta_{s2})\right\rangle, \tag{4.9}$$

was measured [41] assuming that the factorisation theorem [26] is valid. The symmetric $\theta_{i1} = \theta_{s1}$ situation was considered. It implies, correspondingly to Eqn (4.8), that a nonzero correlation will be found only with other symmetric intensities at $\theta_{i2} = \theta_{s2}$. The incident wave was polarised at a 45° angle to the incidence plane containing thus equal s- and p-amplitudes. The scattered light could be detected in the 45° and −45° polarisation states. The intensity of light with the −45° polarisation is contributed by the single-scattering and the 45° polarisation of scattered light is produced by the multiple scattering. It permits one to separate contributions of the single- and multiple scatterings from the conducting surface. The corresponding correlation functions are denoted as follows

$$\begin{aligned} C_{I^2}^{(++)}(\theta_{i1},\theta_{s1},\theta_{i2},\theta_{s2}) &= \left\langle \delta I_+(\theta_{i1},\theta_{i1})\,\delta I_+(\theta_{i2},\theta_{i2})\right\rangle,\\ C_{I^2}^{(--)}(\theta_{i1},\theta_{s1},\theta_{i2},\theta_{s2}) &= \left\langle \delta I_-(\theta_{i1},\theta_{i1})\,\delta I_-(\theta_{i2},\theta_{i2})\right\rangle. \end{aligned} \tag{4.10}$$

Mean intensity $\langle I_+(\theta_i,\theta_i)\rangle$ and correlation function $C_{I^2}^{(++)}(\theta_{i1},\theta_{s1},\theta_{i2},\theta_{s2})$ can be easily interpreted in terms of the phase shifts occurring during the multiple scattering of beams with different wave vectors from the rough surface as shown in Fig. 19. The field correlation function is presented in the form [41]

$$C_{E^2}^{(++)}(\theta_{i1},\theta_{s1},\theta_{i2},\theta_{s2}) = \left\langle E_+(\theta_{i1}\to\theta_{s1})\, E_+^*(\theta_{i2}\to\theta_{s2})\right\rangle, \tag{4.11}$$

where $E_+(\theta_{i1}\to\theta_{s1})$ denotes the scattered field which keeps the polarisation state unchanged and hence experiences more than one scattering event. Such fields are shown in Fig. 19 and appear as a result of double-scattering. Field $E_+(\theta_{i1}\to\theta_{s1})$ describes the contribution produced by the pair of paths shown in Fig. 19a and field $E_+(\theta_{i2}\to\theta_{s2})$ contains the contribution produced by the analogous paths shown in Fig. 19b for some different pairs of the angles of incidence and scattering.

The scattering processes shown in Fig. 19 produce four contributions with phase differences $\Delta\phi_{BA,A'B'}$, $\Delta\phi_{BA,B'A'}$, $\Delta\phi_{BA,B'A'}$, $\Delta\phi_{AB,B'A'}$, to the correlation function, where for instance $\Delta\phi_{AB,B'A'}$ is the phase difference arising when the beams travel path $A\to B$ in Fig. 19a and path $B\to A$ in Fig. 19b. Accounting for the complex conjugation in Eqn (4.11), one obtains

$$\begin{aligned} \Delta\phi_{AB,A'B'} &= \frac{1}{2}\,(\Delta\phi_1 - \Delta\phi_2)\,,\\ \Delta\phi_{AB,B'A'} &= \frac{1}{2}\,(\Delta\phi_1 + \Delta\phi_2),\\ \Delta\phi_{BA,A'B'} &= \frac{1}{2}\,(-\Delta\phi_1 - \Delta\phi_2),\\ \Delta\phi_{BA,B'A'} &= 12\,(-\Delta\phi_1 + \Delta\phi_2), \end{aligned} \tag{4.12}$$

where $\Delta\phi_1 = (\mathbf{k}_{i1} + \mathbf{k}_{s1})\,\Delta\mathbf{r}$, $\Delta\phi_2 = (\mathbf{k}_{i2} + \mathbf{k}_{s2})\,\Delta\mathbf{r}$. We omit the additive term

$$\frac{1}{2}\,(\mathbf{r}_A + \mathbf{r}_B)(\mathbf{k}_{i1} - \mathbf{k}_{s1} - \mathbf{k}_{i2} + \mathbf{k}_{s2}),$$

in all four phase differences (4.12) which vanishes due to requirement (4.8).

Quantities $\Delta\phi_1$ and $\Delta\phi_2$ are the phase differences for forward and backward travelling paths in Fig. 19a and 19b, respectively. Following previous interpretations of backscattering enhancement from rough surfaces this implies that the mean intensity should be enhanced when $\Delta\phi = 0$, a depleted intensity may be seen at angles where $\Delta\phi = \pi$, and some enhancement may be observed when $\Delta\phi = \pm 2\pi$, although the strength of secondary maxima should be less due to the fluctuations in $\Delta\mathbf{r}$ occurring on a random rough surface.

The one-dimensionally rough conducting surface was fabricated by the method described in detail in Refs [37, 155]. This method leads to a surface with the nearly Gaussian height $h(\mathbf{r}_\perp)$ statistics and correlation function $\langle h(\mathbf{r}_{\perp 1})\, h(\mathbf{r}_{\perp 2})\rangle$ of Gaussian form. The surface height was found [41] to have 1.73-μm standard deviation and correlation length $r_c = 3.43$ μm. The wavelength $\lambda = 1.152$ μm laser was used as the light source. The light beam was reflected from a series of mirrors and fell upon the rough surface. The plane of incidence was kept perpendicular to the surface groove direction. Both the sample and the detector were mounted upon rotation stages. Polariser P_1 produced the +45° polarised incident beam and detector polariser P_2 could be set to ±45° polarisation positions. The intensity–intensity

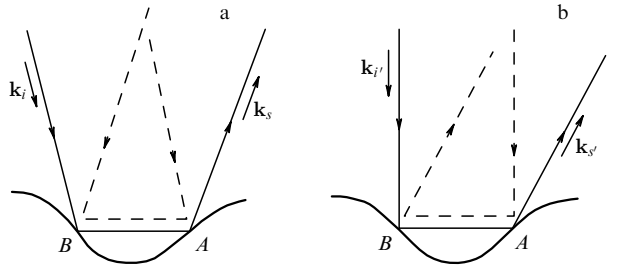

Figure 19. Double-scattering from rough surfaces: (a) fields with wave vectors $\mathbf{k}_i$ and $\mathbf{k}_s$; (b) fields with wave vectors $\mathbf{k}_{i'}$ and $\mathbf{k}_{s'}$.

correlation function was determined by measuring a set of realisations of the intensity for a particular pair of incident and scattering angles $\theta_{i1}, \theta_{s1} = \theta_{i1}$ moving the sample by an amount $\Delta x = 125$ μm in a direction parallel to the surface roughness. The data were recorded on a computer. The incident and scattered angles were then changed to new values, and the measurements were repeated for the same set of computer-controlled positions of the sample. After performing these measurements the correlation function was determined through direct computation. Of the most critical concern in this experiment was adjustment of the spatial parameters as the sample was repeatedly moved.

In Fig. 20 the mean intensities $\langle I_-(\theta_i, \theta_i)\rangle$ and $\langle I_+(\theta_i, \theta_i)\rangle$ are shown obtained from direct averaging of the data for different values of the incidence angle θ_i. There is a distinct backscattering peak in $\langle I_+(\theta_i, \theta_i)\rangle$ caused by the multiple scattering. Such a peak is not exhibited in intensity $\langle I_-(\theta_i, \theta_i)\rangle$ which is contributed mainly from the single-scattering. This peak corresponds to the phase difference $\Delta\phi = 0$. Considering the positions of minima and secondary maxima in this figure one finds that phase differences $\Delta\phi = \pm\pi$ correspond to incidence angle $\theta_i = 3.5°$, and $\Delta\phi = 2\pi$ corresponds to $\theta_i = \pm 7°$. In Fig. 21 correlation functions $C_{I^2}^{(++)}$ and $C_{I^2}^{(--)}$ are shown for different angles θ_{i1}. There are two correlation peaks instead of one for sufficiently large θ_{i1} values due to reciprocity of the multiple scattering paths.

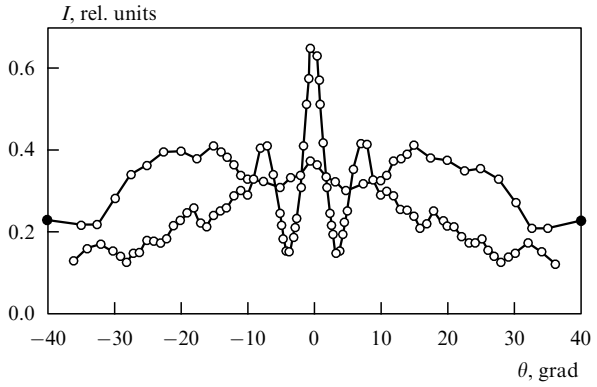

Figure 20. Averaged intensities of radiation scattered from a rough surface, as the function of angle θ_i [124]: ○ — $\langle I_-(\theta_i, \theta_i)\rangle$ (circles) and □ — $\langle I_+(\theta_i, \theta_i)\rangle$ (squares).

The phase difference analysis permits one quite simply to explain the dependence of correlation function $C_{I^2}^{(++)}$ on incidence angle θ_{i1}. For sufficiently large value $\theta_{i1} = 25°$ there are smaller correlation peaks for $\theta_{i2} = \pm\theta_{i1}$ related to the intensity auto-correlation and reciprocity condition which follows from the time-reversal symmetry of Maxwell's equations. The correlation peaks become significantly higher at $\theta_{i1} = 7°$ because for $\theta_{i2} = 7°$ the conditions of the secondary maximum $\Delta\phi_1 = 2\pi$ and $\Delta\phi_2 = 2\pi$ are fulfilled. At $\theta_{i1} = 3.5°$ and $\theta_{i2} = \pm 3.5°$ one has $\Delta\phi_1 = \pi$, $\Delta\phi_2 = \pm\pi$ correspondingly to the partial interference suppression of field. At $\theta_{i1} = 0.5°$ one has approximately $\Delta\phi_1 \approx \Delta\phi_2 \approx 0$ explaining the appearance of the strong central peak, $\theta_{i2} \approx 0$. Requirements $\Delta\phi_1 \approx 0$ and $\Delta\phi_2 \approx 2\pi$ are satisfied for $\theta_{i1} \approx 0$ and $\theta_{i2} \approx \pm 7°$, bringing the secondary maxima in $C_{I^2}^{(++)}$ into this figure.

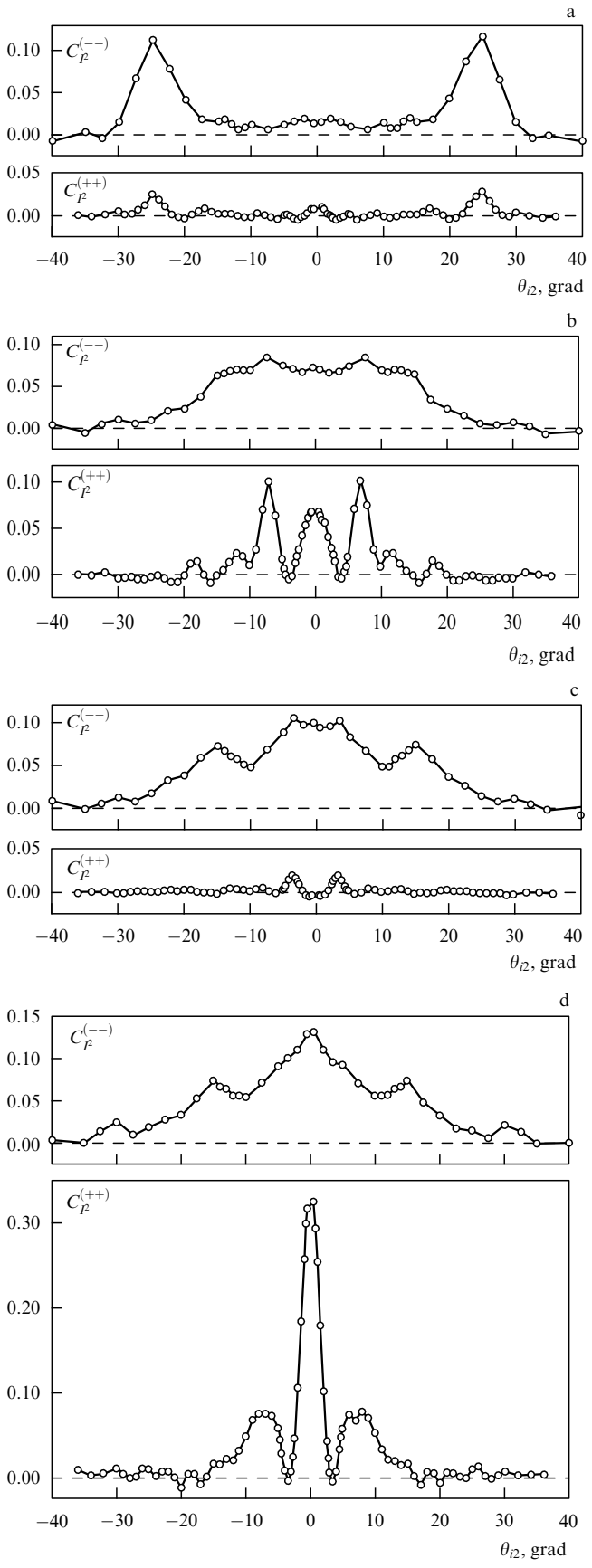

Figure 21. Angular dependences of correlation functions $C_{I^2}^{(++)}$ and $C_{I^2}^{(--)}$ for various angles θ_{i1}: 25° (a), 7° (b), 3.5° (c), and 0.5° (d) [41].

5. Conclusions

The foregoing analysis has shown that a cutting-edge area of studies has appeared in quite a classical field of physics, related to the radiation transfer in heterogeneous media, investigating the interference and coherence phenomena. These phenomena were traditionally assumed to be suppressed because of randomisation. Such development was stimulated by the discovery of quantum interference effects in metals at low temperature. It has been made possible with the modern experimental technique and above all by the use of lasers and computerised measurement units. We have outlined the achievements in the field. One observes in general a rare occurrence when theory and experiment develop simultaneously and in agreement one with another. However there are still a number of problems which demand solution. There is need in developing a theory which accounts for finite size of scatterers. In particular, in the coherent backscattering theory one has to go beyond the framework of the diffusion approximation since it is valid only far from the boundaries in the range $l \gg l_{\text{ext}}$ or l_{tr} while the effect itself occurs just within the neighbourhood of the surface region of the l_{tr} order. An example of this is a paper by Gorodnichev and Rogozkin [71] who have gone beyond the diffusion approximation scope. Studying the backscattering from solid dielectrics with rough surfaces, one faces the problem of a correct separation of contributions from the surface roughness and bulk inhomogeneities.

When investigating correlation functions a theory would seems to be desirable which takes into account the vector nature of the electromagnetic field for a more accurate description of the experiment. Bearing in mind a wide variety of practical applications it would be interesting to study a case of sample shapes different from a slab.

When investigating the coherent effects of reflection from very rough surfaces, one restricts oneself generally to double-scattering approximation. It would be worthwhile to go beyond the scope of this approximation and develop a theory of multiple scattering using the diffusion-like approximation.

Along with new results in fundamental physics, one can see in the field considered a number of possibilities for practical applications and above all for the use of the coherent effects in nontransparent medium diagnosis. Such applications range from object detection in dense smog to the study of tissue structures by means of visible light.

References

1. Van Albada M P, Lagendijk A *Phys. Rev. Lett.* **55** 2692 (1985)
2. Wolf P E, Maret G *Phys. Rev. Lett.* **55** 2696 (1985)
3. Altshuler B L et al. *v Kvantovoĭ* Teorii Tverdogo Tela (in Quantum Theory of Solids) (Ed. I M Lifshits) (Moscow: Mir, 1983)
4. Bergmann G *Phys. Rep.* **107** 1 (1984)
5. Lee P A, Ramakrishnan T V *Rev. Mod. Phys.* **57** 287 (1985)
6. Kramer B, MacKinnon A *Rep. Progr. in Physics* **56** 1469 (1993)
7. Etemad S, Thompson R, Andrejco H J *Phys. Rev. Lett.* **57** 575 (1986)
8. Kaveh M et al. *Phys. Rev. Lett.* **57** 2049 (1986)
9. Kuga Y, Ishimaru A *J. Opt. Soc. Am.* **A1** 831 (1984)
10. Kuga Y, Tsang L, Ishimaru A *J. Opt. Soc. Am.* **A2** 616 (1985)
11. Tsang L, Ishimaru A *J. Opt. Soc. Am.* **A1** 836 (1984)
12. Tsang L, Ishimaru A *J. Opt. Soc. Am.* **A2** 1331 (1985)
13. Golubentsev A A *Zh. Eksp. Teor. Fiz.* **86** 47 (1984) [*Sov. Phys. JETP* **59** 26 (1984)]
14. Akkermans E, Wolf P E, Maynard R *Phys. Rev. Lett.* **56** 1471 (1986)
15. Stephen M J, Cwilich G *Phys. Rev. B* **34** 7564 (1986)
16. Akkermans E et al. *J. Phys.* (Fr) **49** 77 (1988)
17. Barabanenkov Yu N, Ozrin V D *Zh. Eksp. Teor. Fiz.* **94** (6) 56 (1988) [*Sov. Phys. JETP* **67** (6) 1117 (1988)]
18. Maret G, Wolf P *Z. Phys. B* **65** 409 (1987)
19. Pine D J et al. *Phys. Rev. Lett.* **60** 1134 (1988)
20. Stephen M J *Phys. Rev.* **B37** 1 (1988)
21. Umbach C P et al. *Phys. Rev. B* **30** 4049 (1984)
22. Al'tshuler B L, Khmel'nitskiĭ D E *Pis'ma Zh. Eksp. Teor. Fiz.* **42** 291 (1985) [*JETP Lett.* **42** 359 (1985)]
23. Al'tshuler B L *Pis'ma Zh. Eksp. Teor. Fiz.* **41** 530 (1985) [*JETP Lett.* **41** 648 (1985)]
24. Lee P A, Stone A D *Phys. Rev. Lett.* **55** 1622 (1985)
25. Al'tshuler B L, Spivak B Z *Pis'ma Zh. Eksp. Teor. Fiz.* **42** 363 (1985) [*JETP Lett.* **42** 477 (1985)]
26. Shapiro B *Phys. Rev. Lett.* **57** 2168 (1986)
27. Stephen M J, Cwilich G *Phys. Rev. Lett.* **59** 285 (1987)
28. Feng S et al. *Phys. Rev. Lett.* **61** 834 (1988)
29. Hikami S *Phys. Rev.* **B24** 2671 (1981)
30. Rimberg A J, Westervelt R M *Phys. Rev. B* **38** 5073 (1988)
31. Freund I, Rosenbluh M, Feng S *Phys. Rev. Lett.* **61** 2328 (1988)
32. Genack A Z, Drake J M *Europhys. Lett.* **11** (4) 331 (1990)
33. Garcia N, Genack A Z *Phys. Rev. Lett.* **63** 1678 (1989)
34. Van Albada M P, de Boer J F, Lagendijk A *Phys. Rev. Lett.* **64** 2787 (1990)
35. Van Albada M P, van Tiggelen B A, Lagendijk A, Tip A *Phys. Rev. Lett.* **66** 3132 (1991)
36. Mendez E R, O'Donnell K A *Opt. Commun.* **61** 91 (1987)
37. O'Donnell K A, Mendez E R *J. Opt. Soc. Am.* **A4** 1194 (1987)
38. Chen J S, Ishimaru A *J. Acoust. Soc. Am.* **88** 1846 (1990)
39. Ishimaru A, Chen J S *J. Acoust. Soc. Am* **88** 1877 (1990); *Waves Random Med.* **1** 21 (1991)
40. Maradudin A A, Mendez E R, Michel T in *Scattering in Volumes and Surfaces*, ed. by Nieto-Vesperinas M, Dainty J C (North-Holland, Amsterdam: North-Holland, 1990)
41. Knotts M E, Michel T R, O'Donnell K A *J. Opt. Soc. Am.* **A9** 1822 (1992)
42. Nieto-Vesperinas M, Sanchez-Gil J A *J. Opt. Soc. Am.* **A10** 150 (1993)
43. Barabanenkov Yu N et al. *Progress in Optics* (Ed. E Wolf) **29** 65 (1991)
44. Langer J S, Neal T *Phys. Rev. Lett.* **16** (22) 984 (1966)
45. Kuz'min V L, Romanov V P, Kuz'min L V *Opt. Spektrosk.* **72** 227 (1992) [*Opt. Spectrosc.* **72** 125 (1992)]
46. Anderson P W, Abrahams E, Ramakrishnan T V *Phys. Rev. Lett.* **43** 718 (1979)
47. Gor'kov L P, Larkin A I, Khmel'nitskiĭ D E *Pis'ma Zh. Eksp. Teor. Fiz.* **30** 248 (1979) [*JETP Lett.* **30** 228 (1979)]
48. Altshuler B L, Khmel'nitskiĭ D, Larkin A I, Lee P A *Phys. Rev.* **B22** (11) 5142 (1980)
49. MacKintosh F C, John S *Phys. Rev. B* **40** 2383 (1989)
50. Rytov S M, Kravtsov Yu A, Tatarskiĭ V I *Vvedenie v Statisticheskuyu Radiofiziku* (Introduction to Statistical Radiophysics) (Moscow: Nauka, 1978), chast' II [Principles of statical radiophysics (Berlin: Springer, 1987)]
51. Morse P M, Feshbach H *Methods of Theoretical Physics* (New York: McGraw-Hill, 1953) [Translation into Russian; Moscow: IL, 1958]
52. Kuz'min V L, Romanov V P, Kuz'min L V *Opt. Spektrosk.* **73** 376 (1992) [*Opt. Spectrosc.* **73** (1992)]
53. Kuz'min V L, Romanov V P *Opt. Spektrosk.* **72** 1181 (1992) [*Opt. Spectrosc.* **72** (1992)]
54. Ishimaru A *Wave Propagation and Scattering in Random Media* (New York: Academic press, 1978), Vols. I and II [Translation into Russian; Moscow: Mir, 1981]
55. Apresyan L A, Kravtsov Yu A *Teoriya Perenosa Izlucheniya* (Radiation Transfer Theory) (Moscow: Nauka, 1983)
56. Vlasov D V *Pis'ma Zh. Eksp. Teor. Fiz.* **48** 86 (1988) [*JETP Lett.* **48** 91 (1988)]
57. Al'mamuri A, Vlasov D V, Zubkov L A, Romanov V P *Zh. Eksp. Teor. Fiz.* **99** 1431 (1991) [*Sov. Phys. JETP* **72** 798 (1991)]
58. Goodman J W *Proc. IEEE* **55** 1688 (1965)
59. Mandel L *Proc. Phys. Soc.* **74** Pt. 3 (477) 233 (1959)
60. Wolf P E et al. *J. Phys.* (Fr) **49** 63 (1988)
61. Van Albada M P, van der Mark M B, Lagendijk A *Phys. Rev. Lett.* **58** 361 (1987)

62. *Photon Correlation and Light Beating Spectroscopy* (Eds H Z Cummins, E R Pike) (New York: Plenum Press, 1974) [translated into Russian] (Moscow: Mir, 1978)
63. Perina J *Quantum Statistics of Linear and Nonlinear Optical Phenomena* (Dordrecht: D.Reidel Publ. Comp., 1984) [translated into Russian] (Moscow: Mir, 1987)
64. Crosignani B, Di Porto B Bertolotti M., *Statistical Properties of Scattered Light* (New York: Academic Press, 1975) [translated into Russian] (Moscow: Mir, 1980)
65. Lorusso G F, Capozzi V, Minafra A *Phys. Rev. E* **49** 3531 (1994)
66. Glauber R J, in *Laser Handbook* (Eds F T Arecchi, E O Schulz-DuBois) (Amsterdam: North-Holland, 1972) Vol. 1, p. 40
67. De Wolf D.A. *IEEE Trans. Antennas. Propag.* **19** 254 (1971)
68. Barabanenkov Yu.N., *Izv. Vyssh. Uchebn. Zaved, Radiofiz.* **16** 88 (1973)
69. Vinogradov A G, Kravtsov Yu A *Izv. Vyssh. Uchebn. Zaved, Radiofiz.* **16** 1055 (1973)
70. Kravtsov Yu A, Saichev A I *Usp. Fiz. Nauk* **137** 501 (1982) [*Sov. Phys. Usp.* **25** 494 (1982)]
71. Gorodnichev E E, Rogozkin D B *Zh. Eksp. Teor. Fiz.* **107** 209 (1995) [*JETP* **80** 112 (1995)]
72. Barabanenkov Yu N *Usp. Fiz. Nauk* **117** 49 (1975) [*Sov. Phys. Usp.* **18** 673 (1975)]
73. Case K M, Zweifel P F *Linear Transport Theory* (Massachusetts: Addison-Wesley Publ. Comp., 1967) [translated into Russian] (Moscow: Mir, 1972)
74. Perelman L T, Wu J, Itzkan I, Feld M S *Phys. Rev. Lett.* **72** 1341 (1994)
75. Patterson M S, Chance B, Wilson B C *Appl. Opt.* **28** 2331 (1989)
76. Wilson B C, Sevick E M, Patterson M C, Chance B *Proc. IEEE* **80** 918 (1992)
77. Mandt C E, Tsang L, Ishimaru A *J. Opt. Soc. Am.* **A7** 585 (1990)
78. Mandt C E, Tsang L *J. Opt. Soc. Am.* **A9** 2246 (1992)
79. Kuga Y, Ishimaru A *Appl. Opt.* **28** 2165 (1989)
80. Landau L D, Lifshitz E M *Gidrodinamika* (*Hydrodynamics*) (Moscow: Nauka, 1988)
81. Stephen M J *Phys. Lett. A* **127** 371 (1988)
82. MacKintosh F C, John S *Phys. Rev. B* **37** 1884 (1988)
83. Pine P J et al., in *Scattering and Localization of Classical Waves in Random Media* (Ed P Sheng) (Singapore: World Scientific, 1989)
84. Freund I, Kaveh M, Rosenbluh M *Phys. Rev. Lett.* **60** 1130 (1988)
85. Fraden S, Maret G *Phys. Rev. Lett.* **65** 512 (1990)
86. Wolf P E, Maret G, in *Scattering in Volumes and Surfaces* (Eds M Nieto-Vesperinas, J C Dainty) (Amsterdam: Elsevier, 1990) p. 37
87. Webb R A et al., in *Localization, Interaction and Transport Phenomena in Pure Metals* (Eds G Bergmann, Y Bruynseraede, B Kramer) (New York: Springer-Verlag, 1985)
88. Pnini R, Shapiro B *Phys. Rev. B* **39** 6986 (1989)
89. Mello P A, Akkermans E, Shapiro B *Phys. Rev. Lett.* **61** 459 (1988)
90. Genack A Z *Phys. Rev. Lett.* **58** 2043 (1987)
91. Edrei I, Kaveh M *Phys. Rev. B* **38** 950 (1988)
92. de Boer J F, van Albada M P, Lagendijk A *Phys. Rev. B* **45** 658 (1992)
93. Freund I et al. *Phys. Rev. B* **42** 2613 (1990)
94. Freund I *Waves in Random Media* **1** 245 (1991)
95. Van der Mark M B, van Albada M P, Lagendijk A *Phys. Rev. B* **37** 3575 (1988)
96. Eliyahu D, Berkovits R, Kaveh M *Phys. Rev. B* **43** 13501 (1991)
97. Berkovits R, Kaveh M, Feng S *Phys. Rev. B* **40** 737 (1989)
98. Wang L, Feng S *Phys. Rev. B* **40** 8284 (1989)
99. Berkovits R, Kaveh M *Phys. Rev. B* **41** 2635 (1990)
100. Berkovits R, Kaveh M *Europhys. Lett.* **13** 97 (1990)
101. Berkovits R, Feng S *Phys. Rev. Lett.* **65** 3120 (1990)
102. Lee P A, Stone A D *Phys. Rev. Lett.* **55** 1622 (1985)
103. Kane C L, Serota R A, Lee P A *Phys. Rev. B* **37** 6701 (1988)
104. Genack A Z, Garcia N, Polkosnik W *Phys. Rev. Lett.* **65** 2129 (1990)
105. Freund I *Opt. Commun.* **86** 216 (1991)
106. Freund I, Rosenbluh M, Berkovits R *Phys. Rev. B* **39** 12403 (1989)
107. Chow L, Guenther K H *J. Opt. Soc. Am.* **A10** 2231 (1993)
108. Gellermann W et al. *Phys. Rev. Lett.* **72** 633 (1994)
109. Kohmoto M, Kadanoff L P, Tang C *Phys, Rev. Lett.* **50** 1870 (1983)
110. Ostlund S et al. *Phys. Rev. Lett.* **50** 1873 (1983)
111. Hiramoto H, Kohmoto M *Int. J. Mod. Phys.* **B6** 281 (1992)
112. Kohmoto M, Sutherland B, Iguchi K *Phys. Rev. Lett.* **58** 2436 (1987)
113. den Outer P N, Nieuwenhuizen T M, Lagendijk A *J. Opt. Soc. Am.* **A10** 1209 (1993)
114. Garcia N, Genack A Z, Lisyansky A A *Phys. Rev. B* **46** 14475 (1992)
115. Kawato S et al. *Phys. Rev. B* **49** 90 (1994)
116. Van Tiggelen B A et al. *Phys. Rev. B* **45** 12233 (1992)
117. Kogan E, Kaveh M *Phys. Rev.* **B46** 10636 (1992)
118. Barabanenkov Yu N, Ozrin V D *Phys. Rev. Lett.* **69** 1364 (1992)
119. Van Tiggelen B A, Lagendijk A, Tip A *Phys. Rev. Lett.* **71** 1284 (1993)
120. Soukoulis C M, Datta S, Economou E N *Phys. Rev. B* **49** 3800 (1994)
121. Kirkpatrick T R *Phys. Rev. B* **31** 5746 (1985)
122. Kroha J, Soukoulis C M, Wolffe P *Phys. Rev. B* **47** 11093 (1993)
123. Mahan G D *Many-Particle Physics* (New York: Plenum press, 1981)
124. Maradudin A A, Mendez E R, Michel T *Opt. Lett.* **14** 151 (1989)
125. Michel T, Maradudin A A, Mendez E R *J. Opt. Soc. Am.* **B6** 2438 (1989)
126. Kim M-J et al. *J. Opt. Soc. Am.* **A7** 569 (1990)
127. Sanchez-Gil J A, Nieto-Vesperinas M *J. Opt. Soc. Am.* **A8** 1270 (1991)
128. Bruce N C, Dainty J C *J. Mod. Opt.* **38** 1471 (1991)
129. Ishimaru A, Chen J S, Phu P, Yoshitomi K *Waves Random Media* **3** S91 (1991)
130. O'Donnell K A, Knotts M E *J. Opt. Soc. Am.* **A8** 1126 (1991)
131. Michel T R, O'Donnell K A *J. Opt. Soc. Am.* **A9** 1374 (1992)
132. Jordan D L, Moreno F *J. Opt. Soc. Am.* **A10** 1989 (1993)
133. Vitlina R Z, Dykhne A M *Zh. Eksp. Teor. Fiz.* **99** 1758 (1991) [*Sov. Phys. JETP* **72** 983 (1991)]
134. Kuzmin V L, Romanov V P, Azbel' A Yu *Opt. Spektrosk.* **76** 447 (1994) [*Opt. Spectrosc.* **76** (1994)]
135. Bunkin F B, Samokhin A A, Fedorov M V *Zh. Eksp.Teor. Fiz.* **56** 1057 (1969) [*Sov. Phys. JETP* **29** 568 (1969)]
136. Gavrikov V K, Katz A V, Kantorovich V M *Zh. Eksp. Teor. Fiz.* **58** 1318 (1970) [*Sov. Phys. JETP* **31** 708 (1970)]
137. Vitlina R Z *Opt. Spektrosk.* **72** 660 (1992) [*Opt. Spectrosc.* **72** (1992)]
138. Kuzmin V L, Romanov V P *Phys. Rev. E* **49** 2949 (1994)
139. Maradudin A A, Michel T, McGurn A R, Mendez E R *Ann. Phys.* **203** 255 (1990)
140. Nieto-Vesperinas M, Soto-Cresp J M *Opt. Lett.* **12** 979 (1987)
141. Bruce N C, Dainty J C *J. Mod. Opt.* **38** 579 (1991)
142. Maradudin A A, Michel T, in *Wave Propagation and Scattering in Varied Media II* (Ed. V K Varadan) [*Proc. Soc. Photo-Opt. Instrum. Eng.* 1558, 233 (1991)]
143. Bass F G, Fuks I M *Wave Scattering from Statistically Rough Surface* (New York: Pergamon, 1979)
144. Jin Y *Appl. Phys* **63** 1286 (1988)
145. Liszka E G, McCoy J J *J. Acoust. Soc. Am.* **71** 1093 (1982)
146. Pavel'yev A G *Radio Eng. Electron. Phys.* **28** 5 (1983)
147. Wagner R J *J. Acoust. Soc. Am.* **41** 138 (1967)
148. Thorsos E I *J. Acoust. Soc. Am.* **83** 78 (1988)
149. Beckman P, Spizzichino L *The Scattering of Electromagnetic Wave from Rough Surfaces* (New York: Pergamon, 1963)
150. Jakeman E *J. Opt. Soc. Am.* **A5** 1638 (1988)
151. Jakeman E, Tapster P R, Weeks A R *J. Phys.* **D21** 32 (1988)
152. Knotts M E, Michel T R, O'Donnell K A *J. Opt. Soc. Am.* **A10** 928 (1993)
153. Pedersen H M *Opt. Acta* **22** 523 (1975)
154. Léger D, Perrin J C *J. Opt. Soc. Am.* **66** 1210 (1976)
155. Gray P F *Opt. Acta* **25** 765 (1978)